

CA30115



UNITED STATES
NUCLEAR REGULATORY COMMISSION
ADVISORY COMMITTEE ON REACTOR SAFEGUARDS
WASHINGTON, D. C. 20555

August 16, 2001

MEMORANDUM TO: V. Schrock, ACRS Consultant

FROM: P. Boehnert, Senior Staff Engineer 

SUBJECT: RESPONSE TO INFORMATION REQUEST - ACRS
THERMAL-HYDRAULIC PHENOMENA SUBCOMMITTEE
MEETING, JULY 17-18, 2001 - OREGON STATE
UNIVERSITY, CORVALLIS, OREGON

During the subject meeting discussions pertaining to the thermal-hydraulic research on Pressurized Thermal Shock, you requested a copy of a description document for the REMIX code. Attached, in response to your request, is a copy of the User's Manual for REMIX (NUREG/CR-6568).

A copy of this NUREG document is in our Office Files, should any Committee Members or Office Staff wish to examine it.

Attachment: As Stated

cc w/o attach (via E-mail):

ACRS Members
J. Larkins
S. Bahadur
H. Larson
R. Savio
S. Duraiswamy
ACRS Technical Staff & Fellows

V. Schrock

DRAFT

NUREG/CR-6568
BNL-NUREG-52533

APR 15 2001

**Modeling of Thermal Stratification and
Mixing Phenomena of Importance to
Pressurized Thermal Shock (PTS) Analysis
A Users' Manual for the Computer Code REMIX97**

Prepared by
H. P. Nourbakhsh and H. C. Lin

Brookhaven National Laboratory

Prepared for
U.S. Nuclear Regulatory Commission

APR 15 2001

DRAFT

NUREG/CR-6568
BNL-NUREG-52533

**Modeling of Thermal Stratification and
Mixing Phenomena of Importance to
Pressurized Thermal Shock (PTS) Analysis**

A Users' Manual for the Computer Code REMIX97

Manuscript Completed:
Date Published:

Prepared by
H. P. Nourbakhsh and H. C. Lin

Brookhaven National Laboratory
Upton, New York 11973

Chris Boyd, NRC Project Manager

Prepared for
Division of Systems Technology
Office of Nuclear Regulatory Research
U.S. Nuclear Regulatory Commission
Washington, D.C. 20555-0001
NRC JCN W-6595-6

CONTENTS

	Page
ABSTRACT	iii
FIGURES	vii
TABLES	viii
EXECUTIVE SUMMARY	
ACKNOWLEDGMENT	
NOMENCLATURE	
1. INTRODUCTION	1-1
1.1 Background	1-1
1.2 Scope and Organization of This Report	1-4
1.3 References	1-4
2. An Overview of the Regional Mixing Model and the Associated Computer Program REMIX	2-1
2.1 The Regional Mixing Model	2-1
2.2 Maximum Counter-current Flow Limited Entrainment: The NEWMIX Model	2-4
2.3 References	2-8
3. MODELING REQUIREMENTS	3-1
3.1 Technical Issue Specification	3-1
3.2 Accident Path Specification	3-2
3.3 Design and Configuration Specification	3-3
3.4 Phenomena Evaluation	3-3
3.4.1 Cold Leg	3-4
3.4.2 Vessel/Downcomer	3-6
3.4.3 Lower Plenum	3-6
3.4.4 Pump/Loop Seal	3-7
3.5 References	3-7
4. PHYSICAL MODELS	4-1
4.1 The Extended Regional Mixing Model	4-1
4.1.1 HPI Buoyant Jet Entrainment	4-8
4.1.2 Mixing Within the HPI Line	4-13
4.1.3 Counter-current Flow Limited Entrainment in the Presence of Loop Flow	4-19
4.1.4 Backflow of HPI Jet Towards the Upstream Region of the Cold Leg	4-28
4.1.5 Mixing of the Planar Plume in the Downcomer Region Below the Cold Leg	4-30
4.1.6 Heat Transfer in Structures	4-30
4.1.7 Convective Heat Transfer Coefficient	4-31
4.1.8 Equations of State	4-31
4.2 Solution Procedure	4-34
4.3 Overview of REMIX97 Code	4-34
4.4 References	4-38

CONTENTS (Cont'd.)

	Page
5. CODE VERIFICATION AND VALIDATION	5-1
5.1 Overview of the Thermal Mixing Test Facilities	5-1
5.2 Comparison of Code Predictions with CREARE 1/5-Scale Test Data	5-3
5.3 Comparison of Code Predictions with CREARE 1/2-Scale Tests Data	5-21
5.4 Comparison of Code Predictions with PURDUE 1/2-Scale Test Data	5-24
5.5 References	5-31
6. SUMMARY AND CONCLUSIONS	6-1
Appendix A A USER'S MANUAL FOR THE REMIX97 COMPUTER CODE	A-1

FIGURES

		Page
1.6	Elements of PTS risk analysis process	1-1
2.1	Conceptual definition of flow regime and the regional mixing model	2-1
2.2	Illustration of counter-current flow limited entrainment for $\rho^* = 0.8$ and $\beta = 0.5$ (The value of $Fr_{HPI, cL}$ ranges from 0.02 to 0.3, in increments of 0.02)	2-6
2.3	Illustration of counter-current flow limited entrainment for $\rho^* = 0.8$ and $\beta = 1$ (The value of $Fr_{HPI, cL}$ ranges from 0.02 to 0.3, in increments of 0.02)	2-7
3.1	Basic components of the methodology for technical issue resolution	3-1
3.2	Comparison of the theoretical stratification criterion, Eq. (3.1), with the CREARE and HDR test results (○ or ● : CREARE 1/5 scale, Δ : CREARE 1/2 scale, □ : HDR)	3-3
4.1	Conceptual definition of the flow regime and the extended regional mixing model	4-1
4.2	Specification of control volume around the injection mixing region, MRI	4-4
4.3	Coordinate system and physical dimensions for a buoyant jet	4-11
4.4	Comparison of present trajectory results with the data of Fan ^{4,15} for vertical buoyant jets discharged normal to a cross flow	4-15
4.5	Comparison of integral model and $\kappa-\epsilon-\overline{T}^{\prime 2}$ turbulence model calculations for the entrainment to axisymmetric vertical buoyant jets discharged to quiescent ambients	4-15
4.6	Effect of ambient flow on trajectory of buoyant jets	4-16
4.7	Effect of ambient flow on total entrainment to buoyant jets	4-16
4.8	Effect of injection Froude number on trajectory of buoyant jets	4-17
4.9	Effect of injection Froude number on total entrainment to buoyant jets	4-17
4.10	Effect of the initial angle of inclination from horizontal on trajectory of buoyant jets	4-18
4.11	Effect of the initial angle of inclination from horizontal on total entrainment to buoyant jets	4-18
4.12	Effective increase in plume entrainment length due to back flow in the injection line	4-19
4.13	Effect of volumetric loop flow ratio, Q_L^* , on the upstream counter-current flow limited entrainment for $\rho^* = 0.8$, $\alpha = 0.75$ and $Fr_{HPI, cL} = 0.05$	4-25
4.14	Effect of volumetric loop flow ratio, Q_L^* , on the downstream counter-current flow limited entrainment for $\rho^* = 0.8$, $\alpha = 0.75$ and $Fr_{HPI, cL} = 0.05$	4-25
4.15	Effect of $Fr_{HPI, cL}$ on the upstream counter-current flow limited entrainment for $\rho^* = 0.8$, $\alpha = 0.75$, and $Q_L^* = 2$	4-26
4.16	Effect of $Fr_{HPI, cL}$ on the downstream counter-current flow limited entrainment for $\rho^* = 0.8$, $\alpha = 0.75$, and $Q_L^* = 2$	4-26
4.17	Effect of volumetric flow ratio, Q_L^* , on the downstream counter-current flow limited entrainment for $\rho^* = 0.8$, $\alpha = 1$, and $Q_L^* = 2$	4-27
4.18	Effect of $Fr_{HPI, cL}$ on the downstream counter-current flow limited entrainment for $\rho^* = 0.8$, $\alpha = 1$, and $Q_L^* = 2$	4-27

FIGURES (Cont'd.)

		Page
4.19	Effect of density ratio, ρ^* , on the downstream counter-current flow limited entrainment for $\rho^* = 0.8$, $\alpha = 1$, and $Q_L^* = 2$	4-28
4.20	Comparison of theoretical backflow criterion, Equation (4.43) with the CREARE 1/5-scale test results	4-32
4.21	Calculated results of centerline temperature and velocity variations for a planar buoyant jet ($\kappa\text{-}\epsilon\text{-}\overline{T}^2$ turbulent jet model)	4-32
4.22	Calculated results of temperature profiles for a planar buoyant jet ($\kappa\text{-}\epsilon\text{-}\overline{T}^2$ turbulent jet model)	4-33
4.23	Calculated results of velocity profiles for a planar buoyant jet ($\kappa\text{-}\epsilon\text{-}\overline{T}^2$ turbulent jet model) ...	4-33
4.24	General solution procedure for calculating the cooldown transient, pertinent to low Froude number injections	4-36
4.25	General solution procedure for calculating the cooldown transient on the basis of maximum entrainment, pertinent to high Froude number injections	4-37
5.1	Schematic of CREARE 1/5-scale (MIX3) test facility	5-4
5.2	Schematic of CREARE 1/5-scale (MIX4) test facility	5-4
5.3	Comparison of HPI entrainment rate between code predictions and CREARE 1/5-scale data	5-6
5.4	Comparison of HPI buoyant jet flow split ratio between code predictions and CREARE 1/5-scale data	5-6
5.5	Comparison of the fluid temperature transients at the bottom of the cold leg for CREARE 1/5-scale test No. 71 with the REMIX97 prediction	5-7
5.6	Comparison of the downcomer fluid temperature transients for CREARE 1/5-scale test No. 71 with the REMIX97 prediction (for thermocouple location 7; refer to Figure 5.1)	5-8
5.7	Comparison of the downcomer fluid temperature transients for CREARE 1/5-scale test No. 71 with the REMIX97 prediction (for thermocouple location 8; refer to Figure 5.1)	5-8
5.8	Comparison of the downcomer fluid temperature transients for CREARE 1/5-scale test No. 71 with the REMIX97 prediction (for thermocouple location 12; refer to Figure 5.1)	5-9
5.9	Comparison of the downcomer fluid temperature transients for CREARE 1/5-scale test No. 71 with the REMIX97 prediction (for thermocouple location 21; refer to Figure 5.1)	5-9
5.10	Comparison of the downcomer fluid temperature transients for CREARE 1/5-scale test No. 71 with the REMIX97 prediction (for thermocouple location 24; refer to Figure 5.1)	5-10
5.11	Comparison of the fluid temperature transients at the bottom of the cold leg for CREARE 1/5-scale test No. 74 with the REMIX97 prediction	5-10
5.12	Comparison of the downcomer fluid temperature transients for CREARE 1/5-scale test No. 74 with the REMIX97 prediction (for thermocouple location 7; refer to Figure 5.1)	5-11
5.13	Comparison of the downcomer fluid temperature transients for CREARE 1/5-scale test No. 74 with the REMIX97 prediction (for thermocouple location 8; refer to Figure 5.1)	5-11
5.14	Comparison of the downcomer fluid temperature transients for CREARE 1/5-scale test No. 74 with the REMIX97 prediction (for thermocouple location 12; refer to Figure 5.1)	5-12

FIGURES (Cont'd.)

		Page
5.15	Comparison of the downcomer fluid temperature transients for CREARE 1/5-scale test No. 74 with the REMIX97 prediction (for thermocouple location 21; refer to Figure 5.1)	5-12
5.16	Comparison of the downcomer fluid temperature transients for CREARE 1/5-scale test No. 74 with the REMIX97 prediction (for thermocouple location 24; refer to Figure 5.1)	5-13
5.17	Comparison of the fluid temperature transients at the bottom of the cold leg for CREARE 1/5-scale test No. 100 with the REMIX97 prediction	5-13
5.18	Comparison of the downcomer fluid temperature transients for CREARE 1/5-scale test No. 100 with the REMIX97 prediction (for thermocouple location 7; refer to Figure 5.1)	5-14
5.19	Comparison of the downcomer fluid temperature transients for CREARE 1/5-scale test No. 100 with the REMIX97 prediction (for thermocouple location 8; refer to Figure 5.1)	5-14
5.20	Comparison of the downcomer fluid temperature transients for CREARE 1/5-scale test No. 100 with the REMIX97 prediction (for thermocouple location 12; refer to Figure 5.1)	5-15
5.21	Comparison of the downcomer fluid temperature transients for CREARE 1/5-scale test No. 100 with the REMIX97 prediction (for thermocouple location 21; refer to Figure 5.1)	5-15
5.22	Comparison of the downcomer fluid temperature transients for CREARE 1/5-scale test No. 100 with the REMIX97 prediction (for thermocouple location 24; refer to Figure 5.1)	5-16
5.23	Comparison of the lower plenum fluid temperature transients for CREARE 1/5-scale test No. 100 with the REMIX97 prediction	5-16
5.24	Comparison of the loop seal fluid temperature transients for CREARE 1/5-scale test No. 100 with the REMIX97 prediction	5-17
5.25	Comparison of the fluid temperature transients at the bottom of the cold leg for CREARE 1/5-scale test No. 106 with the REMIX97 prediction	5-17
5.26	Comparison of the downcomer fluid temperature transients for CREARE 1/5-scale test No. 106 with the REMIX97 prediction (for thermocouple location 7; refer to Figure 5.1)	5-18
5.27	Comparison of the downcomer fluid temperature transients for CREARE 1/5-scale test No. 106 with the REMIX97 prediction (for thermocouple location 8; refer to Figure 5.1)	5-18
5.28	Comparison of the downcomer fluid temperature transients for CREARE 1/5-scale test No. 106 with the REMIX97 prediction (for thermocouple location 12; refer to Figure 5.1)	5-19
5.29	Comparison of the downcomer fluid temperature transients for CREARE 1/5-scale test No. 106 with the REMIX97 prediction (for thermocouple location 21; refer to Figure 5.1)	5-19
5.30	Comparison of the downcomer fluid temperature transients for CREARE 1/5-scale test No. 106 with the REMIX97 prediction (for thermocouple location 24; refer to Figure 5.1)	5-20
5.31	Comparison of the lower plenum fluid temperature transients for CREARE 1/5-scale test No. 106 with the REMIX97 prediction	5-20
5.32	Schematic of CREARE 1/2-scale test facility	5-22
5.33	Cold leg instrument locations for CREARE 1/2-scale test facility	5-22
5.34	Downcomer instrument locations for CREARE 1/2-scale test facility	5-23
5.35	Comparison of the fluid temperature transients at the bottom of the cold leg for CREARE 1/2-scale test (May 105) with the REMIX97 prediction	5-25
5.36	Comparison of the spatial variation of the fluid temperature in the cold leg (downstream from the injector) for the CREARE 1/2-scale test (May 105) with the REMIX97 prediction	5-25

FIGURES (Cont'd.)

		Page
5.37	Comparison of the downcomer fluid temperature transients for CREARE 1/2-scale test (May 105) with the REMIX97 prediction (thermocouple location 57: 0.41 m below cold leg centerline)	5-26
5.38	Comparison of the downcomer fluid temperature transients for CREARE 1/2-scale test (May 105) with the REMIX97 prediction (thermocouple location 67: 0.77 m below cold leg centerline)	5-26
5.39	Comparison of the downcomer fluid temperature transients for CREARE 1/2-scale test (May 105) with the REMIX97 prediction (thermocouple location 77: 1.13 m below cold leg centerline)	5-27
5.40	Comparison of the lower plenum fluid temperature transients for CREARE 1/2-scale test (May 105) with the REMIX97 prediction	5-27
5.41	Comparison of the loop seal fluid temperature transients for CREARE 1/2-scale test (May 105) with the REMIX97 prediction	5-28
5.42	Schematic view of PURDUE's 1/2-scale facility (configuration B&W)	5-28
5.43	Comparison of the concentration transients in the cold leg and at the exit stream for the PURDUE 1/2-scale test B&W-IC with the REMIX97 prediction	5-29
5.44	Comparison of the spacial variation of the concentration in the cold leg for the PURDUE 1/2-scale test B&W-IC with the REMIX97 prediction	5-30

TABLES

	Page
3.1 Importance ranking of plausible phenomena related to downcomer fluid cooldown transients under low (or zero) loop flow condition	3-5
4.1 Nondimensional form of $\kappa\text{-}\epsilon\text{-}\overline{T}^2$ turbulence jet model	4-9
4.2 Nondimensional form of governing equations for a circular jet discharged into a flowing ambient (integral method)	4-11
5.1 Comparison of the world PTS thermal mixing facilities	5-2
5.2 Geometric data of CREARE 1/5-scale test facility (MIX4)	5-3
5.3 Test conditions of CREARE 1/5-scale tests used for REMIX97 code comparisons	5-5
5.4 Geometric data of CREARE 1/2-scale test facility	5-21
5.5 Geometric data of PURDUE 1/2-scale test facility (Configuration B&W)	5-24

EXECUTIVE SUMMARY

Many thermal hydraulic aspects of overcooling events, except the thermal stratification effects, can be analyzed by using system codes, such as TRAC and RELAP. The term "thermal stratification" here means nonuniformity in temperature and density in a direction transverse to the flow path. Such thermal stratification is obtained at low loop flow, and it is not represented in system codes currently used to simulate overcooling events with PTS potential.

The regional mixing model and the associated computer codes REMIX and NEWMIX, which has been previously documented, is based on a fundamentally-oriented zonal approach which integrates local stratification and mixing behavior into an overall system response. These codes are only applicable when there is no loop flow (complete loop stagnation condition). Specific versions of these codes, REMIX-S and NEWMIX-S have also been previously developed for applications to experimental simulations involving solute induced buoyancy.

A study was conducted to provide a number of modeling improvements to the REMIX code that include extending the regional mixing model to include low loop flow conditions. This improved version of the code combines REMIX, NEWMIX, REMIX-S and NEWMIX-S into a single code REMIX97.

In the original formulation of regional mixing model the thermal response (i.e., mixed mean temperature, hot stream temperature, etc.) of the upstream and the downstream of safety injection point were assumed to be identical. Although this is a good approximation under stagnated loop flow condition, its validity in the presence of loop flow may be questionable.

Therefore, in the present extension of regional mixing model, both at the global and at the local level of computation, the upstream and the downstream of the safety injection point were treated separately.

Thermal mixing in relation to pressurized thermal shock has been examined experimentally throughout the world. In order to evaluate the technical adequacy of the REMIX97 code, the code was used to predict a limited set of data that are relevant to U.S. reactors. These data were obtained under a wide range of experimental conditions including low Froude number injections of interest to Westinghouse and Combustion Engineering designed reactors and very high Froude number injections of interest to Babcock & Wilcox designed reactors. The experimental conditions also included the presence of low loop flow, solute and/or thermally induced buoyancy and concentration or temperature measurement as an indication of mixing. Excellent agreement between the REMIX97 code calculated results and experimental data was noted.

At very low loop flow, the HPI jet after some mixing at the point of injection divides into two stably stratified cold streams, one flowing downstream toward the downcomer and the other going upstream toward the pump and loop seal. However, as the loop flow increases the extent of backflow toward the upstream region of the cold leg decreases. As a part of present study a criterion for the existence of backflow toward the upstream region of the cold leg was obtained analytically. The backflow criterion was compared with the CREARE 1/5-scale data. Excellent agreement was noted.

NOMENCLATURE

A_i	= cross-sectional areas of fluid stream i
A_b	= A_c / A_{cl}
D	= diameter
D_i	= diameter of fluid stream, or system component i
d_i	= depth of fluid stream i
d_c^*	= d_c / D_{cl}
$Fr_{HPI,cl}$	= $(Q_{HPI} / A_{cl}) (g D_{cl} \Delta \rho / \rho)^{-1/2}$, superficial Froude number in the cold leg
Fr_i	= $U_i (D_i g \Delta \rho / \rho)^{-1/2}$, Froude number of stream i
Gr	= $g B L^3 (T_w - T_m) / 2 \nu^2$, Grashof number
g	= acceleration due to gravity
h	= enthalpy per unit mass or heat transfer coefficient
L	= length along downcomer
L_{off}	= equivalent length for backflow in HPI line
Nu	= Nusselt number
Q_e^*	= Q_e / Q_{HPI}
Q_s	= total heat flow into system from structures
Re	= Reynolds number
S	= streamwise coordinate
T	= temperature
t	= time
u	= velocity in the axial direction
v	= velocity in the transverse direction
V	= volume
W	= common width of contact between the two flowing streams
W^*	= $W D_{cl} / A_{cl}$
x	= horizontal Cartesian coordinate
y	= lateral Cartesian coordinate
z	= vertical Cartesian coordinate

NOMENCLATURE (Cont'd.)

Greek

α	= flow split ratio
β	= fraction of entrainment from downcomer side
$\Delta\rho$	= density difference
κ	= turbulent kinetic energy
ε	= dissipation rate of turbulence
ν	= kinematic viscosity
ρ	= density
ρ	= ρ_h / ρ_{HPI}

Subscripts

c	= cold stream
CL	= cold leg
d	= downstream region
e	= entrainment
HPI	= high pressure injection
h	= hot stream
m	= well mixed or mean
max	= maximum
o	= outflow
s	= structures
u	= upstream region

superscripts

*	= nondimensional
---	------------------

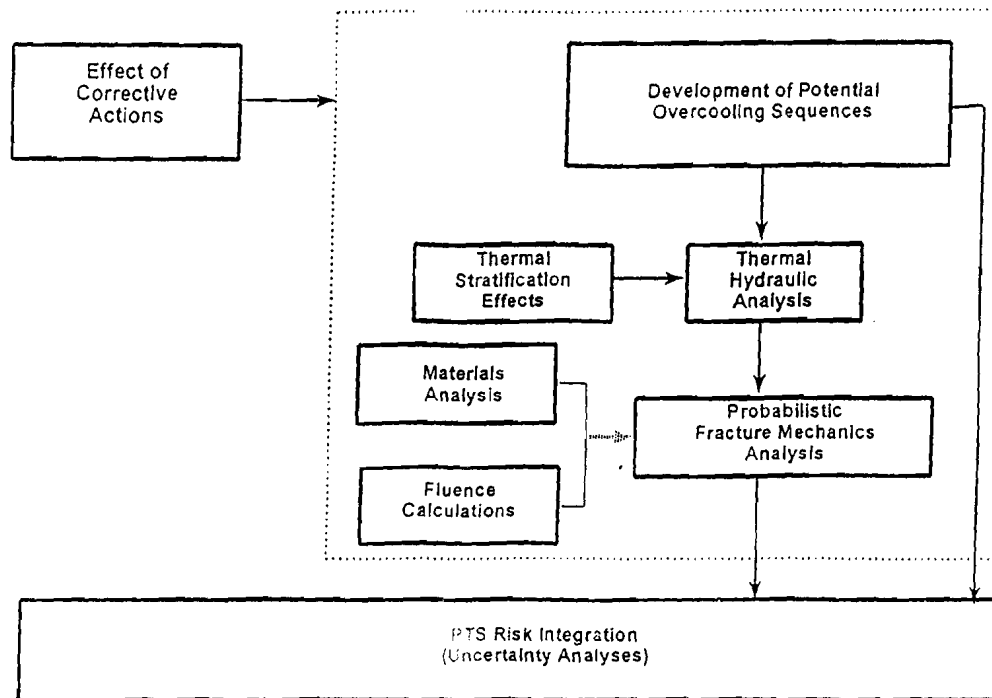


Figure 1.1 Elements of PTS risk analysis process

results applicable) were interdispersed with periods of flow stagnation (stratification). The predicted flow stagnation was due to loss of coolant inventory and the associated interruption of the natural circulation flow paths by steam bubbles. Much of the experimental and analytical efforts in quantification of stratification and associated cooldown effects, were thus focused only on stagnated loop flow conditions.

There are two general approaches for modeling turbulent flow and mixing processes: (1) Field models, and (2) lumped-parameter models. Both approaches have been applied for analysis of thermal stratification and associated cooldown effects due to high-pressure safety injection.

Field models, where equations of motion and transport are solved over domain of interest, with a variety of empirical approaches or approximations used to treat turbulence and transport properties have been developed or have been applied to PTS-related

thermal mixing problems. Parallel to the experimental research programs, great efforts were directed towards the application of existing transient multi-dimensional computer codes, such as COMMIX^{1,7} and TEMPEST,^{1,8} their extensions and improvements, as well as the development of a new special purpose code, the SOLA-PTS.^{1,9}

Field model codes provide greater detail than lumped parameter codes, since the governing conservation equations are solved for incremental region of the flow. However, due to large dimensions of the calculational domain, establishing grid independence to resolve the shear (mixing) layers is an extremely costly process. Computational expenses become even higher as the loop flow decreases because of the increase in the time constant of the cooldown transient. Therefore, these multi-dimensional code calculations for low loop flow conditions are only feasible for a limited time span of the total problem time.

There are two types of lumped parameter models which have been used to evaluate the cooldown effects due to high pressure safety injection: (1) lumped-volume models; and (2) fundamentally-orientated phenomenological zonal models. An example of a lumped-volume model is the transient cooldown model under stagnated loop flow conditions devised by Oh, et al.,^{1.10} which uses a number of well mixed volume elements (arbitrary fixed volumes) for which the transient mass and energy balance are solved. This model uses semi-empirical correlations (for the entrainment and plume spreading angle) developed on the basis of CREARE 1/5-scale and SAI experiments. This model is the basis for the Battelle-Frankfurt code VOLMIX.^{1.11} A simple empirical mixing model, based on CREARE test data, has also been developed by Chexal, et al.,^{1.12} intended for prediction of lower bound temperatures in the downcomer near the vessel wall.

Zone models are similar to lumped volume models in that they divide the flow field into well mixed regions. However, these divisions are made on the basis of flow phenomena, such as regions of buoyant plumes and stratified layers within a subsystem (e.g., cold leg), rather than fixed division of a particular system as with lumped volume methods. The needed flows and entrainments can be developed based on the available experimental data and state-of-the-art analyses for idealized geometries. Such zonal models would be more effective for treating the effects of stratification and buoyancy.

The regional mixing model (REMIX code mode) developed by Nourbakhsh and Theofanous^{1.13,1.14} is based on a fundamentally-orientated zonal approach which integrates local mixing behavior into an overall system response. The model accounts for countercurrent flow limitation between the cold and hot streams at the cold leg/downcomer junction, and incorporates plume mixing rates which are consistent with data from idealized plume geometries. The regional mixing model and associated computer code REMIX^{1.15} was intended for vertically downward,

low Froude number injections ($Fr_{HPI} \sim 1$) of interest to Westinghouse and Combustion Engineering designed reactors. Such highly buoyant plumes exhibit little, if any, inertia and thus, under stagnated loop flow conditions, the angle of HPI-nozzle inclination has very little effect on both total entrainment and the fraction of entrained flow coming from the vessel side of the horizontal cold leg.

For very high Froude number HPI injections ($Fr_{HPI} \sim 16$) of interest to Babcox & Wilcox designed reactors, forceful jet impingement on the opposite cold leg boundary result in a significant increase in local mixing and entrainment which is not depicted in the entrainment model incorporated in the REMIX code. However, since the extent of mixing in the regional mixing model is also controlled by the counter-current flow limitation at the cold leg/downcomer junction, the cooldown transient can be calculated on the basis of maximum entrainment as it was done in the NEWMIX code.^{1.15} The computer code NEWMIX is identical to REMIX except that the mixing at the point of HPI location is assumed to occur with the maximum entrainment controlled only by counter-current flow limitation (independent of HPI nozzle orientation). Specific versions of these codes, REMIX-S and NEWMIX-S have also been developed for applications to experimental simulations involving solute induced buoyancy.

The regional mixing model and the associated computer codes REMIX and NEWMIX has been successfully employed to the interpretation of all available thermal mixing experimental data obtained from system simulation tests.^{1.16} The model has also been utilized in support of the NRC PTS study.^{1.17}

The previous thermal hydraulic analysis of small-break LOCAs of PTS-potential in the Calvert Cliffs plant was revisited in 1988.^{1.18} Using a more recent version of the TRAC code (with improved condensation modeling under low flow and high vapor fraction), it was concluded that the previously envisioned fully stagnated loop flow regime at high

primary system pressure was not possible. Furthermore, it was shown that even the very low loop flows are important in moderating the cooldown transients.

It should be noted that computer codes REMIX and NEWMIX are only applicable when there is no loop flow (complete loop stagnation condition). An analytical mixing model based on the integral method has been developed by Kim.^{1,19} The model predicts mixing of the HPI buoyant jet injected from the top of the cold leg under loop flow conditions. This model, which is the basis for the Battelle-Frankfurt Code JETMIX,¹¹ can only analyze steady state flow conditions and thus cannot predict the cooldown transient.

A study was conducted at Brookhaven National Laboratory to provide a number of modeling improvements to the REMIX code that include extending the regional mixing model to include low-loop flow conditions. This improved version of the code combines REMIX, NEWMIX, REMIX-S and NEWMIX-S into a single code REMIX97. In addition to the modeling improvement, the options for input data to the code has been restructured in order to facilitate its integration with system codes (e.g., RELAP).

1.2 Scope and Organization of This Report

The objective of this document is to specify the overall structure of the computer code REMIX97. Section 2 presents a general description of the regional mixing model and the associated computer program REMIX. An integrated structure somewhat similar to the one developed for the severe accident technical issue resolution^{1,20} was adopted to assess the modeling requirements for the analysis of thermal stratification and associated cooldown effects due to safety injection under low-loop flow conditions. The basic component for this physically-based methodology and its application to the postulated overcooling accident scenarios are discussed in

Section 3. The code modeling framework including the mathematical models and their solution methods are described in Section 4. Section 5 provides an overview of the code verification and validation activities. Section 6 presents a brief summary, together with conclusions. The user manual of the REMIX97 code, which describes the code input and output, is included in Appendix A.

1.3 References

- 1.1 Regulatory Guide 1.154, "Format and Content of Plant-Specific Pressurized Thermal Shock Safety Analysis Reports for Pressurized Water Reactors," U. S. Nuclear Regulatory Commission, January 1987.
- 1.2 *Code of Federal Regulations*, Title 10, Part 50 (10CFR50), "Domestic Licensing of Production and Utilization Facilities," §50.61, 1985.
- 1.3 C. D. Fletcher, et al., "RELAP5 Thermal-Hydraulic Analysis of Pressurized Thermal Shock Sequences for the OCONEE-1 Pressurized Water Reactor," U.S. Nuclear Regulatory Commission, NUREG/CR-3761, June 1984.
- 1.4 C. D. Fletcher, et al., "RELAP5 Thermal-Hydraulic Analysis of Pressurized Thermal Shock Sequences for the H. B. Robinson Unit 2 Pressurized Water Reactor," U.S. Nuclear Regulatory Commission, NUREG/CR-3977, April 1985.
- 1.5 J. R. Ireland, et al., "TRAC Analysis of Severe Overcooling Transients for the OCONEE-1 PWR," U.S. Nuclear Regulatory Commission, NUREG/CR-3706, May 1985.
- 1.6 G. D. Springs, et al., "TRAC-PF1 Analysis of Potential Pressurized-Thermal-Shock Transients at Calvert Cliffs-1, Unit 1, U.S. Nuclear Regulatory Commission, NUREG/CR-4109, February 1985.

- 1.7 H. M. Domanus, et al., "COMMIX-1A: A 3-D, Transient Single-Phase Computer Program for Thermal Hydraulic Analysis of Single and Multicomponent Systems," U.S. Nuclear Regulatory Commission, NUREG/CR-2896, 1983.
- 1.8 L. L. Eyler and D. S. Trent, "Pressurized Thermal Shock: TEMPEST Computer Code Simulation of Thermal Mixing in the Cold Leg and Downcomer of a Pressurized Water Reactor," U.S. Nuclear Regulatory Commission, NUREG/CR-3564 (PNL-4909), April 1984.
- 1.9 B. J. Daly and M. D. Torrey, "SOLA-PTS: A Transient, Three-Dimensional Algorithm for Fluid-Thermal Mixing and Wall Heat Transfer in Complex Geometries," U.S. Nuclear Regulatory Commission, NUREG/CR-3822 (LA-101320-MS), July 1984.
- 1.10 S. Oh, J. P. Sursock, and K. H. Sun, "A Mixing Model for Transient Cooldown in a Reactor Cold Leg and Downcomer Under Stagnant Loop Flow," 21st AIChE/ASME National Heat Transfer Conference, Seattle, WA, July 24-27, 1983, ASME Paper No. 83-HT-13.
- 1.11 L. Wolf, et al., "Application of Engineering and Multi-Dimensional Finite Difference Codes to HDR Thermal Mixing Experiments TEMA," Proceedings of the 14th Water Reactor Safety Information Meeting, Gaithersburg, MD, October 27-31, 1986, Vol. 4, pp. 395-444.
- 1.12 V.K. Chexal, J. Chao, R. Nichell, and T. Griesback, "An Empirical Mixing Model for Pressurized Thermal Shock Applications," *Nuclear Technology* 69 (1985) 94.
- 1.13 H. P. Nourbakhsh and T. G. Theofanous, "Decay of Buoyancy Driven Stratified Layers with Applications to PTS, Part I: Regional Mixing Model," Nuclear Engineering and Design (in press).
- 1.14 T. G. Theofanous, H. P. Nourbakhsh, P. Gherson, and K. Iyer, "Decay of Buoyancy-Driven Stratified Layers with Applications to Pressurized Thermal Shock," NUREG/CR-3700, U. S. Nuclear Regulatory Commission, May 1984.
- 1.15 K. Iyer, H. P. Nourbakhsh, and T. G. Theofanous, "REMIX: A Computer Program for Temperature Transients Due to High Pressure Injection After Interruption of Natural Circulation," NUREG/CR-3701, U. S. Nuclear Regulatory Commission, May 1986.
- 1.16 T. G. Theofanous and H. Yan, "A Unified Interpretation of One-Fifth to Full-Scale Thermal Mixing Experiments Related to Pressurized Thermal Shock," NUREG/CR-5677, 1991.
- 1.17 T. G. Theofanous, K. Iyer, H. P. Nourbakhsh, and P. Gherson, "Buoyancy Effects in Overcooling Transients Calculated for the NRC Pressurized Thermal Shock Study," NUREG/CR-3702, U. S. Nuclear Regulatory Commission, May 1986.
- 1.18 T. G. Theofanous, J. L. LaChance, and K. A. Williams, "The Thermal Hydraulics of SBLOCAs Relative to Pressurized Thermal Shock," NUREG/CR-5135, October 1988.
- 1.19 J. H. Kim, "An Analytical Mixing Model for Buoyant Jet Injected into Pipe Flow," ASME Winter Annual Meeting, Boston, MA, November 13-18, 1984, ASME Paper No. 83-WA/HT-42; *J. Heat Transfer*, Vol. 107 (1985) 630-635.

- 1.20 U. S. Nuclear Regulatory Commission, "An Integrated Structure and Scaling Methodology for Severe Accident Technical Issue Resolution NUREG/CR-5809, Draft for Public Comment, November 1991.

2. AN OVERVIEW OF THE REGIONAL MIXING MODEL AND THE ASSOCIATED COMPUTER PROGRAM REMIX

In this section, an overview of the regional mixing model and the associated computer code REMIX, as previously documented, is presented. As a part of the present study, a number of modeling improvements to the REMIX code has been made. More detailed discussions on the regional mixing model and its improvements, including the extension of the model to include the low loop flow conditions, will be provided in Sections 3 and 4.

2.1 The Regional Mixing Model

The safety injection of relatively cold water into a stagnant loop of a PWR leads to thermal stratification accompanied by counter-current flows and recirculation. The ensuing flow regime was first established analytically by Theofanous and Nourbakhsh.^{2,1} The physical situation may be described with the help of Figure 2.1. A "cold stream" originates with the safety injection buoyant jet at the point of injection, continues towards both ends of the cold leg, and decays away as the resulting

buoyant jets fall into the downcomer and pump/loop-seal regions. A "hot stream" flows counter to this "cold stream" supplying the flow necessary for mixing (entrainment) at each location. This mixing is most intensive in certain locations identified as mixing regions (MRs). MR1 indicates the mixing associated with the buoyant, nearly axisymmetric safety injection jet. MR3 and MR5 are regions where mixing occurs because of transients (jumps) from horizontal layers into falling jets. MR4 is the region where the downcomer (planar) buoyant jet finally decays. The cold streams have special significance because they induce a global recirculating flow pattern with flow rates significantly higher than the net flow through the system (Q_{HPI}). This keeps a major portion of the system volume including the loop seals (vertical leg below the pump and bottom horizontal leg), the downcomer (excluding the region above the cold leg), and the lower plenum in a well mixed condition. The whole process may be viewed as the quasi-static decay of the cold streams within a slowly varying "ambient" temperature.

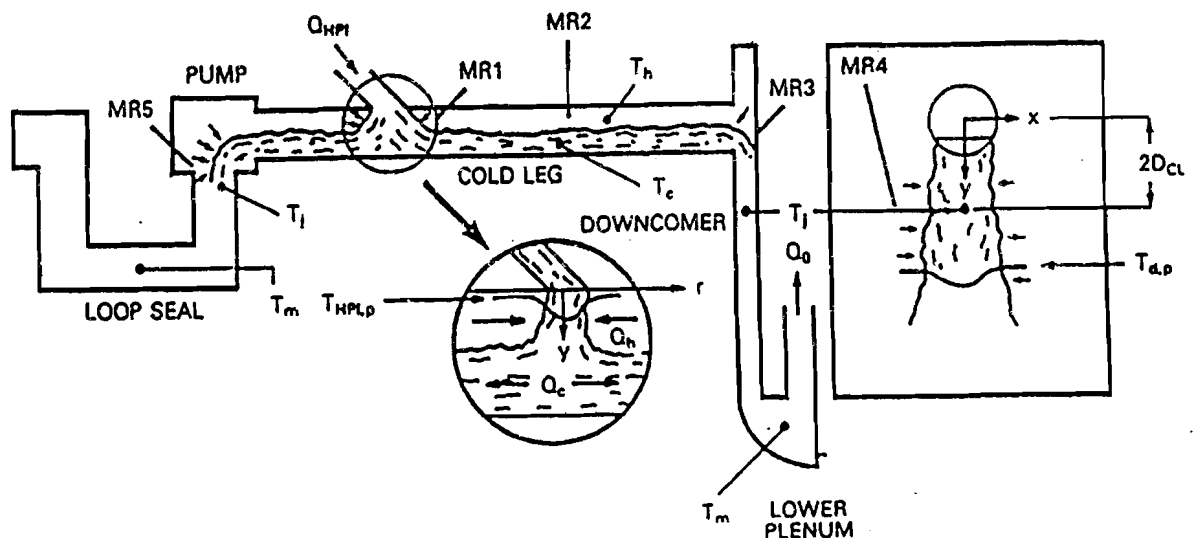


Figure 2.1 Conceptual definition of flow regime and the regional mixing model

2. An Overview of the Regional Mixing Model...

The quantitative aspects of this physical behavior were incorporated in the Regional Mixing Model developed by Nourbakhsh and Theofanous.^{2,2,2,3} The model accounts for countercurrent flow limitations between the cold and hot streams at the cold leg/downcomer junction and incorporates plume mixing rates which are consistent with data from idealized single plume geometries. The regional mixing model and the associated computer code REMIX^{2,4} Has been successfully employed to the interpretation of all available mixing experimental data obtained from the system simulation tests performed in support of the PTS study.^{2,5}

The computation proceeds at two levels. The first is global and provides a "mean" system response. The other is local and seeks to partition mass and energy into the cold and hot streams consistent with mixing (entrainment) rates and countercurrent flow requirements. The local computation provides, at arbitrary selected times, snapshots of details constructed based on the global results. The mathematical formulations can be followed with the help of Figure 2.1. Here the term "system" refers to the assembly of components shown in Figure 2.1 with the following clarifications: (a) the outer vertical leg of the loop seal and the upper region of the downcomer above the cold leg are not included; (b) the lower plenum volume is taken up to the lower edge of the core barrel; and (c) the downcomer and lower plenum volumes are partitioned equally among the available loops.

At the global level of the computation, the whole system is assumed to be well mixed. The mass and energy conservation equations for the whole system can then be expressed as:

$$V \frac{d(\rho_m h_m)}{dt} = Q_{HPI} \rho_{HPI} h_{HPI} - Q_o \rho_m h_m + Q_s \quad (2.1)$$

$$V \frac{d\rho_m}{dt} = Q_{HPI} \rho_{HPI} - Q_o \rho_m \quad (2.2)$$

where V , ρ_m and ρ_{HPI} are the volume of whole system, mixed mean density and HPI density, respectively. h_m and h_{HPI} are mixed mean enthalpy and HPI enthalpy, respectively. Q_{HPI} , Q_o and Q_s are the HPI volumetric flowrate, the outflow volumetric flowrate and the total heat transfer rate from structures, respectively.

Equations (2.1) and (2.2), together with the equation of state for water, $\rho_m = f(h_m)$, are solved numerically to obtain $Q_o(t)$, $h_m(t)$ and $\rho_m(t)$. The total heat transfer rate from structures, $Q_s(t)$, is calculated simultaneously from a numerical solution of the one-dimensional transient heat conduction equation. At solid interface, the boundary conditions are expressed in terms of prescribed heat transfer coefficients. The REMIX code can accommodate any number of such heat slab calculations.

Local calculations provide the details of the flow, energy (temperature), and the volume of the cold and hot streams. One of the more important features of the regional mixing model is that this volume partition is not chosen arbitrarily but rather is obtained as part of the solution. The mass and energy balance for a control volume around the injection mixing region, MRI (see Figure 2.1), can be expressed as:

$$Q_{HPI} \rho_{HPI} + Q_h \rho_h = Q_c \rho_c \quad (2.3)$$

$$Q_{HPI} \rho_{HPI} h_{HPI} + Q_h \rho_h h_h = Q_c \rho_c h_c \quad (2.4)$$

where Q_c and Q_h are the total cold and hot stream flow rates (going to both or coming from both directions as shown in Figure 2.1). h_c and h_h are the cold stream enthalpy and hot stream enthalpy, respectively.

The hot stream flow rate is assumed to be equal to that entrained to the falling plume. The Chen and Rodi^{2,6} Turbulence model was utilized to obtain the entrainment to a low Froude number axisymmetric

2. An Overview of the Regional Mixing Model...

vertical buoyant jets. The results have been fit by the following expression:

$$Q_h = Q_e = 0.52 Q_{HPI} \left(\frac{d_h}{D_{HPI}} \right)^{1.236} Fr_{HPI}^{-0.414} \quad (2.5)$$

where d_h is the fall height, $d_h = D_{cL} - d_c$. The injection Froude number, Fr_{HPI} , is defined as:

$$Fr_{HPI} = \frac{Q_{HPI} / A_{HPI}}{\left(g D_{HPI} \frac{\rho_{HPI} - \rho_h}{\rho_{HPI}} \right)^{1/2}} \quad (2.6)$$

where D_{HPI} and A_{HPI} are the diameter and area of injection line, respectively.

Energy is partitioned into the hot and cold stream volumes, so that the total energy remains equal to the mixed-mean value obtained from the global calculations. Thus:

$$V_c \rho_c h_c + V_h \rho_h h_h = (V_c + V_h) \rho_m h_m \quad (2.7)$$

The volume of cold stream, V_c , can be expressed in terms of cold leg length and the height of the cold stream, d_c . The hot volume, V_h , is assumed to be equal to the sum of the hot stream volume (in the cold leg) plus 25% of the pump volume plus the volume of a horizontal downcomer slice with a height equal to two cold leg diameters.

The condition of stationarity (of propagation rather than growth) of long, neutrally stable waves at the interface between the cold and hot streams is expressed as:^{2.1,2.7}

$$Fr_c^2 + Fr_h^2 = 1 \quad (2.8)$$

Equations (2.3) through (2.8) together with equation of state for water, $\rho = f(h)$, are solved numerically to obtain Q_e , Q_c , ρ_h , ρ_c , h_h , h_c , and d_h . An iterative solution procedure is used in REMIX code. First, an

initial estimate of cold stream height is chosen. Based on this initial height, the values for all other variables are determined from Equations (2.3) to (2.7). The procedure repeats until Equation (2.8) is satisfied.

The Froude numbers in Equation (2.8) should be based on the appropriate length scale (stream cross sectional area divided by the width of contact between the two streams), and the cold stream and hot stream flow rates exiting and entering the cold leg, respectively.

In the regional mixing model, the hot stream flow coming from the direction of vessel is expressed in terms of a fraction, β , of the total entrained flow to the falling buoyant jet. Therefore, the hot stream flow for use in Fr_h is βQ_e . Since the system is closed on the loop seal side, the net flow of cold stream exiting the cold leg to be used in Fr_c of Equation (2.8) should be $Q_{HPI} + \beta Q_e$. Thus, in terms of parameter β , Equation (2.8) may be written as:

$$\frac{(Q_{HPI} + \beta Q_e)^2 / A_c^2}{g \frac{A_c}{W} \frac{\rho_c - \rho_h}{\rho_c}} + \frac{(\beta Q_e)^2 / A_h^2}{g \frac{A_h}{W} \frac{\rho_c - \rho_h}{\rho_h}} = 1 \quad (2.9)$$

Where A_c , A_h and W are the cross-sectional area of cold stream, cross-sectional area of hot stream, and the common width of contact between two streams, respectively. In the REMIX code, the value of β is provided as an input parameter. For the very low Froude number of interest, the momentum effects were neglected and the symmetric behavior, i.e., $\beta = 0.5$, was assumed in the code calculations. For cases that the cold stream can flow only in one direction, such as that of the Babcock & Wilcox reactor with an elevated cold leg (e.g., Oconee) a value of $\beta = 1$ would then be appropriate.

There are two additional aspects of REMIX which, because of their complicated nature, had to be treated empirically: (a) mixing within the HPI line and (b) mixing at the cold leg downcomer junction.

2. An Overview of the Regional Mixing Model...

For low Froude number of injection, $Fr_{HPI} < 1$, the backflow of hot stream fluid into the injection line is expected. Purdue's initial half-scale experiments^{2,8} provided the basis for taking into account the contribution of this backflow to the entrainment of cold leg fluid into the HPI buoyant jet. The approach used in REMIX code is to define an effective HPI plume origin that moves into the injection line as the Fr_{HPI} decreases below the value of 0.6. In the calculations, this additional length, L_{off} , is added to the d_h value to obtain the entrainment from Equation (2.5).

A highly complicated three-dimensional mixing pattern occurs at the cold leg downcomer junction. In the original formulation of the regional mixing model, the approach was to conservatively neglect this contribution to the mixing in the downcomer. The cold stream exiting the cold leg was assumed to form smoothly into a planar plume within the downcomer and to decay according to the $\kappa\text{-}\epsilon\text{-}\theta'$ turbulence jet model predictions.^{2,1,2,2} A refinement was possible on the basis of Purdue's half-scale experiments^{2,8}. In REMIX code, the planar plume is assumed to form within a distance of twice of the cold leg diameter below the cold leg centerline and to be fed in equal volumetric flow rates by the cold stream and surrounding hot volume fluid. The resulting temperature of plume is used as initial planar plume temperature (T_j). Beyond this point, the decay is approximated to that of a planar plume of initial width equal to cold leg diameter, D_{cl} , and Froude number of equal to one.

2.2 Maximum Counter-current Flow Limited Entrainment: The NEWMIX Model

The NEWMIX model was intended for high Froude number injections ($Fr_{HPI} > 10$). The central idea is that the forceful jet impingement on the opposite cold leg boundary result in a significant increase in local mixing at the point of HPI location (MRI), reaching to the maximum level of entrainment restricted only

by the counter-current flow limitation expressed by Equation (2.9) as discussed below.

Equation (2.9) expresses the condition of stationarity (on propagation rather than growth) of long, neutrally stable waves at the interface between the two parallel flowing streams. Accordingly, any flow condition for which Equation (2.9) applies cannot be changed gradually without leading to violent disruption of the flow by an internal hydraulic jump. As the flow rates and densities of the two streams are related by mass continuity and energy conservation, Equation (2.9) expresses a single parameter family of flows with the cold stream depth being a parameter.^{2,4} An analytical expression for this parametric relationship can be derived by eliminating ρ_c , with the help of Equation (2.3), in Equation (2.9) to obtain:

$$Q_e^{*3} + aQ_e^{*2} + bQ_e^* + C = 0 \quad (2.10)$$

where

$$a = \left\{ \frac{\beta\rho^*}{(1-A^*)^3} + \frac{\beta+2\rho^*}{A^{*3}} \right\} / \beta\rho^*\delta \quad (2.11)$$

$$b = \frac{2\beta+\rho^*}{A^{*3}} / \beta^2\rho^*\delta \quad (2.12)$$

$$c = \left\{ \frac{1}{A^{*3}} - \frac{1}{W^*Fr_{HPI,CL}^2} \right\} / \beta^2\rho^*\delta \quad (2.13)$$

and

$$\delta = \frac{1}{(1-A^*)^3} + \frac{1}{A^{*3}} \quad (2.14)$$

The dimensionless quantities, Q_e^* , ρ^* , A^* , W^* , and $Fr_{HPI,CL}$ are defined as:

$$Q_e^* = \frac{Q_e}{Q_{HPI}} \quad , \quad \rho^* = \frac{\rho_h}{\rho_{HPI}} \quad ,$$

$$A^* = \frac{A_c}{A_{cl}} \quad , \quad W^* = \frac{WD_{cl}}{A_{cl}} \quad ,$$

and

$$Fr_{HPI,cl} = \frac{Q_{HPI}}{A_{cl}} \left(g D_{cl} \frac{\rho_{HPI} - \rho_h}{\rho_{HPI}} \right)^{-1/2} \quad (2.15)$$

It should be noted that the expression for a , b , and c in Equations (2.11) through (2.13) are different than those reported incorrectly in References 2.5 and 2.9.

Since W^* and A^* may be expressed in terms of dimensionless cold stream depth

$$d_c^* = \frac{d_c}{D_{cl}} \quad (2.16)$$

Equation (2.10) provides a simple relationship of the form

$$Q_e^* = \mathcal{F}(d_c^*, Fr_{HPI,cl}, \beta, \rho^*) \quad (2.17)$$

In reactor applications, ρ^* is initially at ~ 0.8 and approaches unity as the cooldown transient continues. The effect of ρ^* variation in the results of Equation (2.17) is negligible. The $Fr_{HPI,cl}$ typically begins at the value of ~ 0.02 and increases gradually through the cooldown transient. The relevant values of the parameter β are 0.5 and 1.0. The functional dependence of Equation (2.17) may be visualized, for the appropriate ranges of these parameters, in Figures 2.2 and 2.3. For each value of $Fr_{HPI,cl}$, a maximum possible entrainment ($Q_{e,max}$) and a corresponding depth of the cold stream ($d_{c,max}$) are obtained.

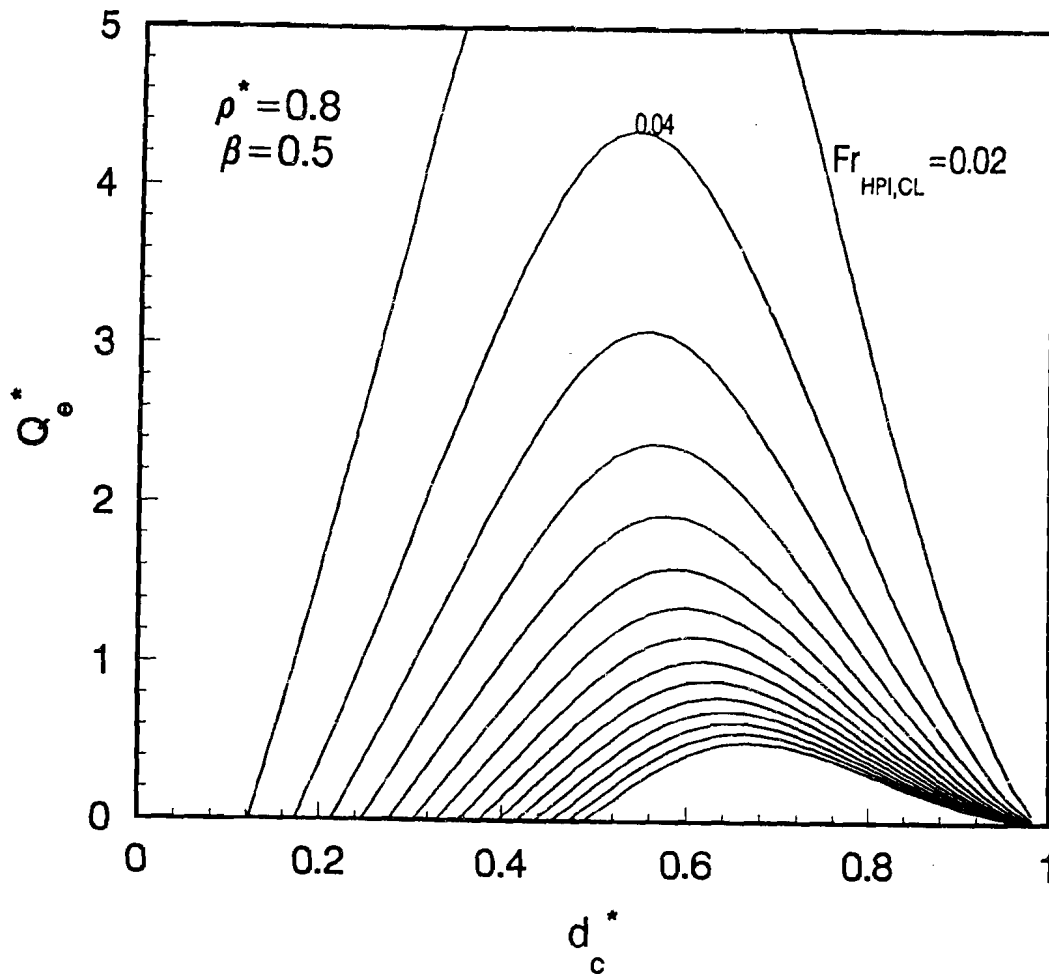


Figure 2.2 Illustration of counter-current flow limited entrainment for $\rho^* = 0.8$ and $\beta = 0.5$ (The value of $Fr_{HPI,cl}$ ranges from 0.02 to 0.3, in increments of 0.02).

2. An Overview of the Regional Mixing Model...

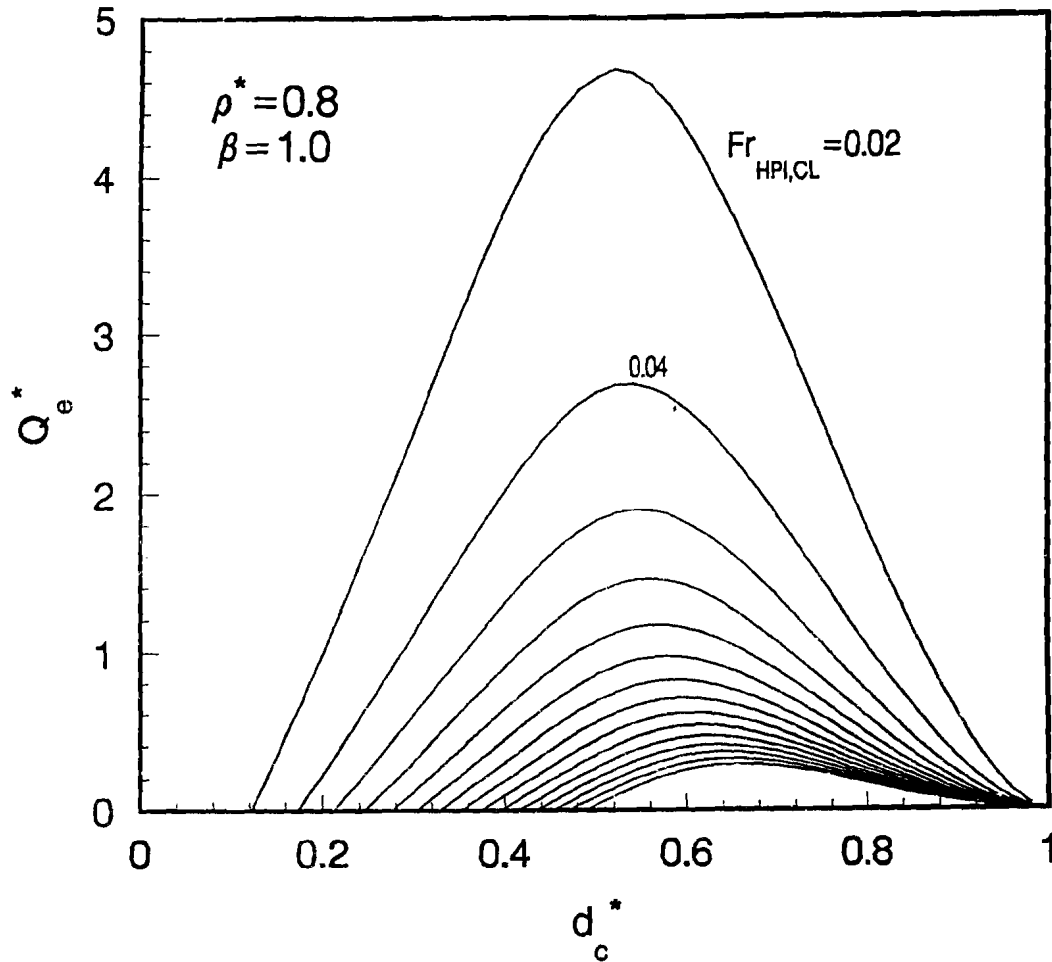


Figure 2.3 Illustration of counter-current flow limited entrainment for $\rho^* = 0.8$ and $\beta = 1$ (The value of $Fr_{HPI,CL}$ ranges from 0.02 to 0.3, in increments of 0.02).

The computer code NEWMIX is identical to REMIX except that the mixing at the point of HPI location is assumed to occur with the maximum entrainment, $Q_{e, max}$, controlled only by counter-current flow limitation.

2.3 References

- 2.1 T. G. Theofanous and H. P. Nourbakhsh, "PWR Downcomer Fluid Temperature Transients Due to High Pressure Injection at

Stagnated Loop Flow," Proc. Joint NRC/ANS Meeting on Basic Thermal Hydraulic Mechanisms in LWR Analysis, September 14, 15, 1982, Bethesda, Maryland, NUREG/CP-0043, 583-613, 1983.

- 2.2 H. P. Nourbakhsh and T. G. Theofanous, "Decay of Buoyancy-Driven Stratified Layers with Application to Pressurized Thermal Shock, Part I: The Regional Mixing Model," Nucl. Eng. & Design, (in press).

- 2.3 T. G. Theofanous, K. Iyer, H. P. Nourbakhsh, and P. Gerson, "Buoyancy Effects in Overcooling Transients Calculated for the NRC Pressurized Thermal Shock Study," NUREG/CR-3702, U.S. Nuclear Regulatory Commission, May 1986.
- 2.4 K. Iyer, H. P. Nourbakhsh, and T. G. Theofanous, "REMIX: A Computer Program for Temperature Transients Due to High Pressure Injection After Interruption of Natural Circulation," U.S. Nuclear Regulatory Commission, NUREG/CR-3701, May 1986.
- 2.5 T. G. Theofanous and H. Yan, "A Unified Interpretation of One-Fifth to Full-Scale Thermal Mixing Experiments Related to Pressurized Thermal Shock," U. S. Nuclear Regulatory Commission, NUREG/CR-5677, 1991.
2. An Overview of the Regional Mixing Model....
- 2.6 Chen, C.J. and W. Rodi, "A Mathematical Model for Stratified Turbulent Flows and Its Application to Buoyant Jets," XVIth Congress, International Association for Hydraulic Research, San Paulo, 1975.
- 2.7 J. S. Turner, *Buoyancy Effects in Fluids*, Cambridge University Press, 1979.
- 2.8 G. C. Gardner, "Motion of Miscible and Immiscible Fluids in Closed Horizontal and Vertical Ducts," *Int. J. Multiphase Flow*, Vol. 3, pp. 305-318, 1977.
- 2.9 K. Iyer and T. G. Theofanous, "Flooding-Limited Thermal Mixing: The Case of High Froude Number Injection," *Nucl. Sci. Eng.*, **108**, pp. 198-207, 1991.

3. MODELING REQUIREMENTS

To provide a framework for assessment of modeling requirements (improvements to the REMIX code) for predicting the downcomer fluid temperature transients due to safety injection at low loop flow conditions, an integrated methodology somewhat similar to the one developed for severe accident technical issue resolution³¹ was adopted. The basic components for this physically based methodology is illustrated in Figure 3.1. The integration is achieved by specifying the technical issue and prioritizing the physical processes which need to be considered to resolve an issue (Component I) and by expressing them in terms of specification for: (a) code development/modeling improvement (Component II), (b) experimentation

(Component III), and (c) assessment of existing codes (Component IV). Technical issue resolution is achieved by means of code calculations and their uncertainty quantification (Component V). This approach assures that the analytical methods used to resolve a technical issue is comprehensive, systematic, auditable and traceable.

As illustrated in Figure 3.1. Component I (phenomena evaluation) provides the foundation for code development and the entire technical issue resolution process and, therefore, its application to overcooling scenarios with pressurized thermal shock (PTS) potential is discussed in detail in this section.

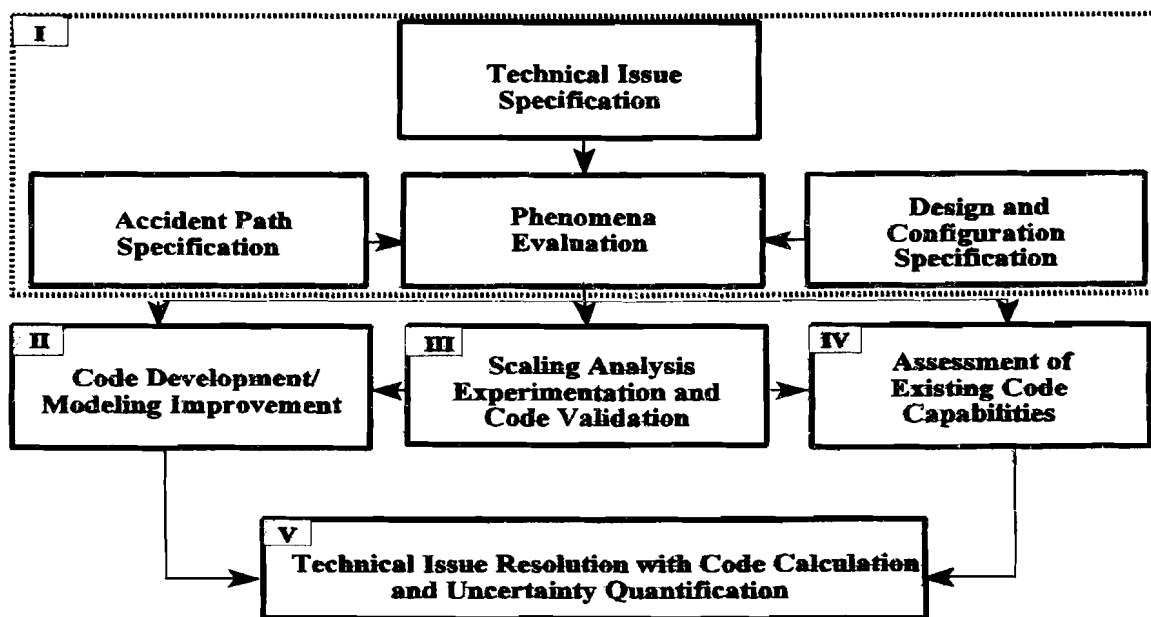


Figure 3.1 Basic components of the methodology for technical issue resolution

3. Modeling Requirements

3.1 Technical Issue Specification

A statement of the technical issue provides the focus of the subsequent work. The issue here is to predict the downcomer fluid temperature transients due to safety injection at low (and zero) loop flow conditions. The thermal stratification, obtained at low (and zero) loop flow, is not represented in system codes (e.g., TRAC and RELAP) currently used to simulate overcooling events with PTS potential.

3.2 Accident Path Specification

The physical processes important to one accident path may not have the same relevance to another path. Consequently, it is necessary to identify the specifications of the scenarios and the accident paths that need to be evaluated.

System codes such as RELAP and TRAC are employed for evaluation of all thermal hydraulic aspects of overcooling transients except for thermal stratification effects. In most cases, system code simulation turns out to be adequate because the predicted natural circulation flows are sufficiently large to eliminate any tendency toward stratification. The need for evaluation of thermal stratification effects arises from a rather specialized set of transients for which system code results indicate low loop flow or complete loop flow stagnation condition. Under such conditions, the whole process is governed by stratification/mixing phenomena.

Nourbakhsh and Theofanous^{3,2} used the stability boundary and developed a criterion for the existence of stratification in the presence of loop flow. Their stratification/mixing boundary is expressed by

$$Fr_{HPI,cL} = \left[1 + \frac{Q_L}{Q_{HPI}} \right]^{-7/5} \quad (3.1)$$

where Q_{HPI} and Q_L are the volumetric flow rates of the high pressure injection (HPI) and the loop, respectively. The Froude number, $Fr_{HPI,cL}$ is defined as:

$$Fr_{HPI,cL} = \frac{Q_{HPI}}{A_{cL}} \left\{ g D_{cL} \frac{(\rho_{HPI} - \rho_L)}{\rho_{HPI}} \right\}^{-1/2} \quad (3.2)$$

where A_{cL} and D_{cL} are the flow area and the diameter of cold leg, respectively.

The predicted stratification/mixing boundary expressed by Equation (3.1) has been shown to be in excellent agreement with the experimental results of different thermal mixing tests (see Figure 3.2).

The present code/model development effort focuses only on predicting cooldown under stratified conditions. The conditions leading to thermal stratification and the associated reactor coolant system pressure level and the duration of the low loop flow (or stagnation) periods are obtained from the thermal hydraulic analysis of potential overcooling sequences.

It should also be noted that the present study deals only with a water filled system. The physical processes of interest for low water level in the downcomer (i.e., water level below the upper edge of the cold leg nozzle) is different^{3,3} and has not been considered in the development of REMIX code.

3.3 Design and Configuration Specification

The PWR downcomer fluid temperature transients will be affected by the plant specific parameters such as loop seal/pump/cold leg/downcomer/lower plenum configuration and the size and orientation of the safety injection nozzle.

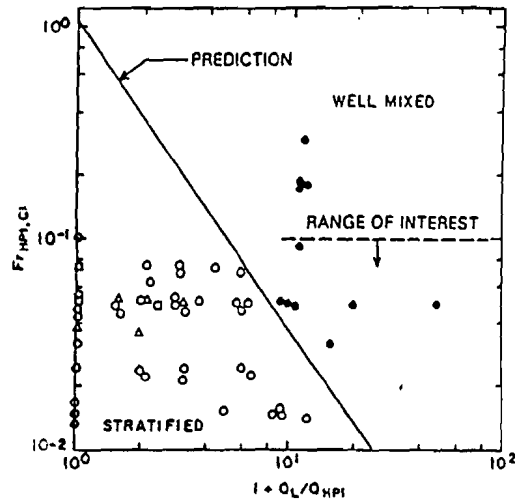


Figure 3.2 Comparison of the theoretical stratification criterion, Eq. (3.1), with the CREARE and HDR test results (○ or ● : CREARE 1/5 scale, Δ : CREARE 1/2 scale, □ : HDR)^{3,2}

In the present study, the modeling requirements are assessed considering only the diversity in design and configurations of U.S. PWRs (i.e., geometries typical of Westinghouse, Combustion Engineering, and Babcock & Wilcox designed reactors).

3.4 Phenomena Evaluation

Phenomena evaluation provides a comprehensive framework to identify and prioritize the physical processes which need to be modeled in a code so as to ensure its capability to address the downcomer fluid cooldown transients under low (or zero) loop flow condition.

In order to identify and rank the processes important to downcomer fluid cooldown, an approach similar to that discussed and developed in References 3.1 and 3.4 will be followed. The system is decomposed into components. For each component, plausible physical processes and phenomena are identified, and are differentiated as to their cause and effects. This

physically based decomposition of the downcomer fluid cooldown progression in a cause and effect sequence, ensures that all aspects are considered and examined (albeit qualitatively). Subsequent to identification of the plausible phenomena, a ranking procedure is used since it is neither practical nor necessary to evaluate all phenomena in detail.

The ranking technique is designed to direct the subsequent model improvement/code development work to those phenomena having the most significant effect on the question of concern (i.e., cooldown of the downcomer fluid due to safety injection).

To facilitate the phenomena identification, the system was partitioned into four components:

1. cold leg
2. vessel/downcomer
3. lower plenum
4. pump/loop seal

3. Modeling Requirements

A review of existing experimental and analytical studies of thermal mixing related to PTS, together with the basic knowledge about heat transfer, mixing, and stratified flow in confined systems, was used to determine plausible phenomena and to judge their relative importance to cooldown progression of the downcomer fluid. The importance ranking of plausible phenomena is summarized in Table 3.1. Three ranking categories were utilized for this screening:

1. High: The phenomenon in question could have a significant impact on the downcomer fluid cooldown.
2. Medium: The phenomenon in question is expected to have at least a measurable impact on the downcomer fluid cooldown.
3. Low: The phenomenon in question does not have significant impact on the downcomer fluid cooldown.

The ranking justification and references, where possible, together with the description of the phenomena in the context of their conceptualization by authors is presented in the following subsections.

3.4.1 Cold Leg

The question of existence of stratified regime in the cold leg is one of fundamental significance and is ranked as highly important. The importance of thermal stratification in the cold leg may be appreciated by considering the consequences of a perfectly mixed behavior. Considering that all forced agitation takes place in a well mixed control volume around the point of injection, a rapid cooldown in this volume is predicted. This cold fluid would enter the downcomer region as a highly buoyant plume, exposing any critical welds on the vessel wall to rather low temperatures. A stratified regime, on the

other hand, would allow a local mixing of safety injection jet with the fluid continuously drawn in from the vessel (downcomer and lower plenum) and loop seal along the cold leg in a counter-current flow with the cold, stratified layer beneath. This behavior is fundamentally different from that of a perfectly mixed cold-leg regime because a much larger volume of warm fluid now has access to mix with the safety injection jet and thus a slower cooldown behavior is predicted.

The mixing at the safety injection point is considered to be highly important, owing to its direct effect on the temperature of the cold stratified layer flowing into the downcomer. For a very low Froude number of injection, backflow of the hot stream fluid into the injection line is expected. The mixing within the injection line, which is physically possible only for $Fr_{HPJ} < 1$, is ranked as medium importance.

Mixing between stratified layers in the cold leg is ranked as low importance. The mixing between horizontal stratified layers is characterized by the pipe Richardson number, Ri_p . Minimal entrainment was found experimentally for horizontal stratified layers for $Ri_p > 0.01$.^{3,4} For typical reactor conditions Richardson number would be greater than 2^{3,6} and thus a clearly stable stratified regime with negligible entrainment is indicated.

The passive heat sources such as stored energy in structures is an important factor in moderating the global fluid cooldown behavior. However, the cold leg wall contributes only to less than 6% of total thermal capacitance of the system structures and, therefore, the stored energy in the cold leg wall is ranked as low importance. The heat losses to outside air is also ranked as low importance. In view of potential importance of both stored energy in the cold leg wall and heat losses to outside air for some thermal mixing experiments, these processes may need to be modeled in the code.

Table 3.1 Importance ranking of plausible phenomena related to downcomer fluid cooldown transients under low (or zero) loop flow condition

Component/Phenomenon	Relative Importance ^(a)
Cold Leg:	
— Thermal stratification in the cold leg	H
— Mixing at the safety injection point	H
— Backflow of the hot stream fluid and mixing within the injection line	M ^(b)
— Mixing between stratified layers	L
— Stored energy in the cold leg wall	L
— Heat losses from cold leg wall to outside air	L
Vessel/downcomer:	
— Mixing at the cold leg-downcomer junction	H
— Mixing in the downcomer region below the cold leg	H
— Mixing in the downcomer region above the cold leg	L
— Stored energy in structures (i.e., vessel wall, thermal shield and core barrel)	H
— Heat losses to outside air	L
— Convective heat transfer between structures and water flow in downcomer	H
Lower Plenum:	
— Thermal stratification in the lower plenum	L
— Stored energy in structures (i.e., vessel wall and internal structures)	H
— Heat losses to outside air	L
Pump/Loop Seal:^(c)	
— Mixing within the pump	H
— Mixing in the vertical leg of the loop seal below the pump	H
— Thermal stratification in the bottom horizontal leg of loop seal	L
— Mixing in the outer vertical leg of the loop seal	L
— Stored energy in structures (i.e., pump internal structures and loop seal wall)	H
— Heat losses to outside air	L

(a) L = Low importance, M = Medium importance, H = High Importance

(b) Physically possible only for $Fr_{HPI} < 1$

(c) Not important for Babcock and Wilcox designed reactors with an inclined cold leg

3. Modeling Requirements

3.4.2 Vessel/Downcomer

The mixing at the cold leg-downcomer junction is ranked as high importance owing to its direct impact on the temperature of resulting planar plume within the downcomer. A highly complicated 3-dimensional mixing pattern occurs at this junction. In view of the facts that there are no welds and the level of neutron irradiation is very low, the stress analysis in this entrance region is not of any significance to PTS analysis. Therefore, the knowledge of the detailed temperature distribution in this region may not be necessary and an integral mixing model, based on an empirically determined entrainment at the junction should be adequate.

Mixing in the downcomer below the cold leg entrance region is ranked as high importance. The prediction of fluid temperature distribution in this region is the focus of the present code development effort. Mixing in the downcomer region above the cold leg nozzle is negligible and is ranked as low importance.

The stored energy in downcomer structures (i.e., vessel wall, thermal shield, and core barrel) is ranked as high importance. The heat losses to outside air is ranked as low importance. However, as it was discussed earlier, due to potential importance of heat losses to outside air for some thermal-mixing experiments, this process needs to be modeled in the code.

Convective heat transfer between structures and water flow in downcomer is ranked as highly important. However, for reasonable choices in heat transfer coefficient, the heat transfer resistance of the metal structure is much larger^{3.7} (i.e., conduction controls). Thus, the uncertainties in the details of heat transfer coefficient has a negligible impact on the prediction of the reactor pressure vessel wall temperature.

3.4.3 Lower Plenum

Thermal stratification in lower plenum is ranked as

low importance. The cold stream entering the lower plenum, because of entrainment, carries a flow that is significantly higher than the net flow through-put ($Q_{HPI} + Q_L$). Thus, it induces an intense recirculating flow pattern that keeps a major portion of the system including lower plenum in a well-mixed condition.

Stored energy in the lower head and internal structures in lower plenum is ranked as high importance. The heat losses to outside air is ranked as low importance. However, due to its potential importance for some thermal-mixing experiments, the heat losses need to be modeled in the code.

3.4.4 Pump/Loop Seal

At very low loop flow conditions, a cold stream, which originates with the safety injection buoyant jet at the point of injection, also flows upstream (pump side of cold leg) and decays away as the resulting buoyant jet falls into pump/loop seal region. However, as the loop flow increases, the extent of the "cold stream" flowing from the point of injection towards the pump/loop seal region decreases. It should also be noted that certain geometries, such as that of the B&W plants (e.g., Oconee) with an inclined cold leg, preclude any flow towards pump/loop seal region.

Mixing within the pump and the vertical leg of loop seal below the pump are ranked as high importance.

Thermal stratification in the bottom horizontal leg of loop seal is negligible and is ranked as low importance. Mixing in the outer vertical leg of the loop seal is also negligible and is ranked as low importance.

It should be noted that the recirculating flow pattern in pump/loop seal keeps a major portion of pump/loop-seal region in a well-mixed condition. Furthermore, the details of temperature distribution in this region does not have any relevance to PTS analysis. Therefore, an integral mixing model for this region should be adequate.

3.5 References

- 3.1 U.S. Nuclear Regulatory Commission, "An Integrated Structure and Scaling Methodology for Severe Accident Technical Issue Resolution," NUREG/CR-5809, Draft for Public Comment, November 1991.
- 3.2 H. P. Nourbakhsh and T. G. Theofanous, "A Criterion for Predicting Thermal Stratification Due to High Pressure Injection in a Circulating Reactor Loop," Nuclear Science and Engineering, Vol. 94, 77-79, 1986.
- 3.3 H. P. Nourbakhsh, "Analysis of the Thermal-Hydraulic Mixing Task of the CSNI PTS International Comparative Assessment Study," presented at RPV PTS ICAS Workshop, Orlando, FL, February 25-27, 1998.
- 3.4 R. A. Shaw, et al., "Development of a Phenomena Identification and Ranking Table (PIRT) for Thermal-Hydraulic Phenomena During a PWR Large-Break LOCA," NUREG/CR-5047, 1988.
- 3.5 T. H. Ellison and J. S. Turner, "Mixing of Dense Fluid in Turbulent Pipe Flow," Journal of Fluid Mechanics, Vol. 8, pp. 514-540, 1960.
- 3.6 T. G. Theofanous and H. P. Nourbakhsh, "PWR Downcomer Fluid Temperature Transients Due to High Pressure Injection at Stagnated Loop Flow," Proc. Joint NRC/ANS Meeting on Basic Thermal-Hydraulic Mechanisms in LWR Analysis, September 14-15, 1982, Bethesda, MD, NUREG/CP-0043, 583-613, 1983.
- 3.7 T. G. Theofanous, K. Iyer, H. P. Nourbakhsh, and P. Gherson, "Buoyancy Effects in Overcooling Transients Calculated for the NRC Pressurized Thermal Shock Study," NUREG/CR-3702, U.S. Nuclear Regulatory Commission, May 1986.

4. PHYSICAL MODELS

The physically based methodology discussed in chapter 3 provides a valuable framework for a number of modeling improvements to the REMIX code that includes extending the regional mixing model to include low-loop flow conditions. To conserve resources, the improved version of the code, REMIX97, has been structured to well simulate the most important phenomena and processes, with lesser attention given to peripheral effects. Both an initial and subsequent interaction with the phenomena evaluation process discussed in chapter 3 assisted in focusing the modeling improvements on the key processes and phenomena required for technical issue resolution.

This chapter describes the mathematical models and their solution methods for predicting the downcomer

fluid temperature transients due to safety injection at low (or zero) loop flow conditions.

4.1 The Extended Regional Mixing Model

At very low loop flow condition, the thermal stratification and mixing behavior is similar to the one discussed for stagnated loop flow condition (refer to chapter 2). The physical situation may be described with the help of Figure 4.1. In the presence of low loop flow, the relevant portions of the system include, as illustrated, the loop seal, pump, cold leg (and safety injection line), downcomer, and lower plenum.

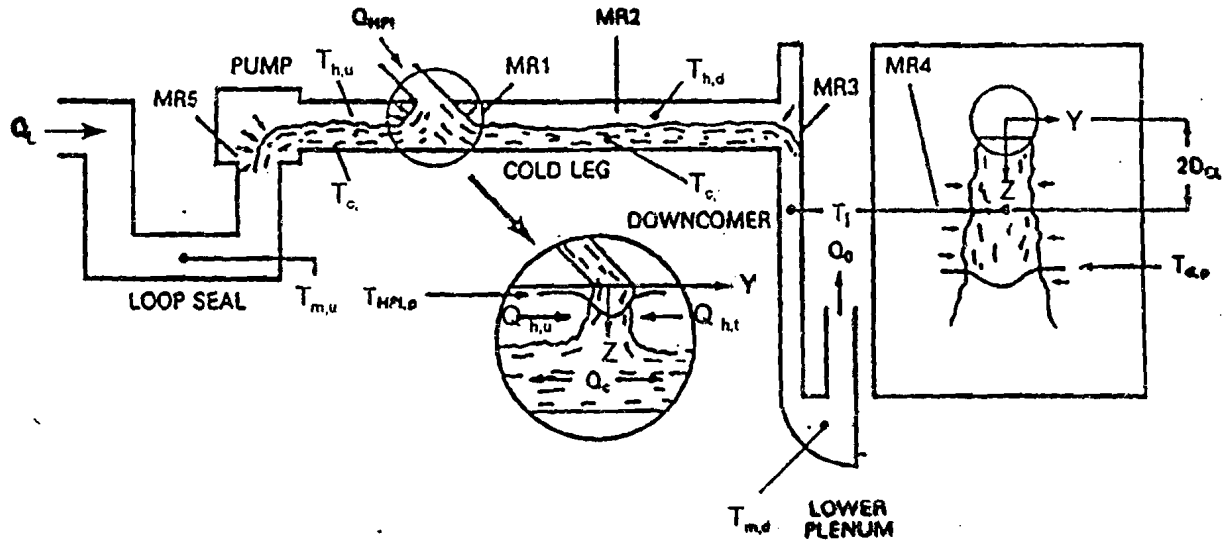


Figure 4.1 Conceptual definition of the flow regime and the extended regional mixing model

4. Physical Models

Initially, this whole portion of the primary system is filled with coolant (water) at a high temperature while the hot loop flow is circulated through the system. The cooldown transient is initiated by the safety injection of the cold coolant jet into the hot loop flow. The jet, after some mixing at the point of injection, divides into two cold streams, one flowing downstream and the other going upstream. The portion that travels downstream forms a stably stratified layer that spills over into the downcomer. The other portion of the jet that flows upstream enters the pump/loop seal region and eventually mixes with the oncoming flow. Hot streams flow counter to these cold streams supplying the flow necessary for mixing (entrainment) at each location. This mixing is quantified at different locations identified as mixing regions (MRs), as shown in Figure 4.1. MR1 indicates the mixing associated with the buoyant, nearly axisymmetric safety injection jet. MR2 is the mixing associated with the stratified cold stream flowing towards both ends of cold leg. MR3 and MR5 are the regions where mixing occurs because of transients (jumps) from horizontal layers into falling jets. MR4 is the region where the downcomer (planar) buoyant jet finally decays.

The quantitative aspect of this physical behavior is modeled somewhat similar to the regional mixing model developed for stagnated loop flow condition.^{4.1,4.2} In the original formulation of regional mixing model the thermal response (i.e., mixed mean temperature, hot stream temperature, etc.) of the upstream and the downstream of safety injection point were assumed to be identical. Although this is a good approximation under stagnated loop flow condition, its validity in the presence of loop flow may be questionable. Therefore, in the present extension of regional mixing model, both at the global and at the local level of computation, the upstream and the downstream of the safety injection point are treated separately.

The mathematical formulation can be followed with the help of Figure 4.1. Here the terms "downstream region" and "upstream region" refer to assembly of

the system components in downstream and upstream of the safety injection point, respectively.

The global mass and energy conservation equations for the downstream region can be expressed as:

$$V_d \frac{d\rho_{m,d}}{dt} = Q_{c,d} \rho_c - Q_{h,d} \rho_{h,d} - Q_o \rho_{m,d} \quad (4.1)$$

$$V_d \frac{d(\rho_{m,d} h_{m,d})}{dt} = Q_{c,d} \rho_c h_c - Q_{h,d} \rho_{h,d} h_{h,d} - Q_o \rho_{m,d} h_{m,d} + \dot{Q}_{s,d} \quad (4.2)$$

where V_d , $\rho_{m,d}$, $\rho_{h,d}$, and ρ_c are the volume of downstream region, the downstream mixed mean density, hot stream density, and cold stream density, respectively. $h_{m,d}$, $h_{h,d}$ and h_c are the downstream mixed mean enthalpy, hot stream enthalpy, and cold stream enthalpy, respectively. $Q_{c,d}$, $Q_{h,d}$, Q_o and $\dot{Q}_{s,d}$ are the cold stream volumetric flow rate, the hot stream volumetric flow rate, the outflow volumetric flow rate and the total heat transfer rate from structures in the downstream region, respectively.

Likewise, the global mass and energy conservation equations for the upstream region can be expressed as:

$$V_u \frac{d\rho_{m,u}}{dt} = Q_{c,u} \rho_c - Q_{h,u} \rho_{h,u} - Q_L \rho_L \quad (4.3)$$

$$V_u \frac{d(\rho_{m,u} h_{m,u})}{dt} = Q_{c,u} \rho_c h_c - Q_{h,u} \rho_{h,u} h_{h,u} + Q_L \rho_L h_L + \dot{Q}_{s,u} \quad (4.4)$$

where V_u , $\rho_{m,u}$, and $\rho_{h,u}$ are the volume of upstream region, the upstream mixed mean density and hot stream density, respectively. $h_{m,u}$, $h_{h,u}$, and h_L are the upstream mixed mean enthalpy, hot stream enthalpy and loop flow enthalpy, respectively. $Q_{c,u}$, $Q_{h,u}$, Q_L and $\dot{Q}_{s,u}$ are the cold stream volumetric flow rate, the hot stream volumetric flow rate, the loop volumetric flow rate and the total heat transfer rate from structures in the upstream region, respectively.

The mass and energy balance for a control volume around the injection mixing region, MRI (see Figure 4.2) can be expressed as:

$$Q_c \rho_c = Q_{HPI} \rho_{HPI} + Q_{h,u} \rho_{h,u} + Q_{h,d} \rho_{h,d} \quad (4.5)$$

$$Q_c \rho_c h_c = Q_{HPI} \rho_{HPI} h_{HPI} + Q_{h,u} \rho_{h,u} h_{h,u} + Q_{h,d} \rho_{h,d} h_{h,d} \quad (4.6)$$

Q_{HPI} and ρ_{HPI} are the HPI volumetric flow rate and HPI density, respectively. where Q_c is the total cold stream volumetric flow rate, $Q_c = Q_{c,u} + Q_{c,d}$.

Likewise, the mass and energy balance for a control volume enclosing the jet boundaries can be expressed by:

$$Q_c \rho_c = Q_{HPI} \rho_{HPI} + Q_e \rho_a \quad (4.7)$$

$$Q_c \rho_c h_c = Q_{HPI} \rho_{HPI} h_{HPI} + Q_e \rho_a h_a \quad (4.8)$$

Where Q_e is the rate of entrainment to the jet, ρ_a and h_a are the ambient density and the ambient enthalpy around the jet, respectively. Here, the ambient

density and enthalpy (temperatures) around the jet is assumed to be uniform. This is a reasonable assumption because the jet does not block the cold leg and the hot streams can go around the jet.

As a part of the present study, an integral method solution was utilized to quantify the mixing associated with a buoyant, nearly axisymmetric circular jet issuing into a flowing ambient (refer to section 4.1.1). The results for jet entrainment have been fit by the following expression:

$$Q_e = \frac{0.52 Q_{HPI} \left[\frac{d_h}{D_{HPI}} \right]^{1.236} Fr_{HPI}^{-0.414} (1 + 8.4 Fr_{HPI}^{0.854} R^{1.14})}{\sin \theta_0 + 0.31 Fr_{HPI}^{-0.139} \left[\frac{d_h}{D_{HPI}} \right]^{0.098} \cos \theta_0} \quad (4.9)$$

where θ_0 and d_h are the initial angle of inclination (HPI-nozzle inclination) from horizontal and the fall height, respectively. R is the ambient flow ratio (i.e., loop flow velocity divided by HPI flow velocity). The injection Froude number, Fr_{HPI} , is defined as:

$$Fr_{HPI} = \frac{Q_{HPI} / A_{HPI}}{g D_{HPI} \frac{\rho_{HPI} - \rho_a}{\rho_{HPI}}} \quad (4.10)$$

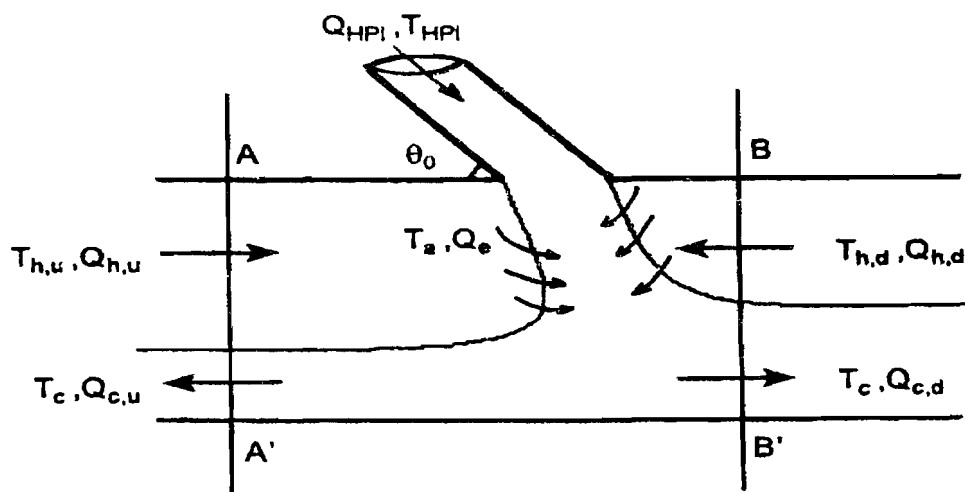


Figure 4.2 Specification of control volume around the injection mixing region, MRI

4. Physical Models

The height of the jet exposed to the hot stratum may not be uniform around the jet. In evaluating the jet entrainment, it is assumed that half of the jet is exposed to a hot stratum of a depth equal to the depth of hot stream in downstream region while the other half is exposed to a hot stratum of a depth equal to the depth of hot stream in upstream region. Thus,

$$Q_e = 0.5 \left(Q_e \Big|_{d_h = d_{h,d}} + Q_e \Big|_{d_h = d_{h,u}} \right) \quad (4.11)$$

where the $d_{h,d}$ and $d_{h,u}$ are the depths of hot streams in downstream and upstream regions, respectively.

It should be noted that under stagnated loop flow conditions ($R = 0$) and assumption of symmetry (i.e., $d_{h,u} = d_{h,d}$) the entrainment correlation (Equation 4.9) for vertically downward jets ($\theta_0 = \frac{\pi}{2}$) will be reduced to the one used in the original regional mixing model^{4,2} and associated code REMIX^{4,3} (Equation 2.5).

As discussed earlier in Chapter 3, for very low Froude number injections, the backflow of hot stream into the safety injection line is expected. In order to take into account the additional entrainment into the safety injection jet due to this backflow, an approach similar to the one used in previous REMIX calculations (refer to section 4.1.2) is adopted here. As the Froude number decreases below a critical value of 0.6, an effective safety injection plume origin that moves into the injection line is defined. In the calculations, this additional length, which is a function of the Froude number of injection, is added to the value of the fall height, d_h , to obtain the entrainment from Equation (4.9).

Energy is partitioned into the hot and cold stream volumes in both the upstream and downstream regions, so that the total energy for each region remains equal to their corresponding mean values obtained from the global calculations. Thus:

$$\begin{aligned} V_{c,d} \rho_c h_c + V_{h,d} \rho_{h,d} h_{h,d} = \\ (V_{c,d} + V_{h,d}) \rho_{m,d} h_{m,d} \end{aligned} \quad (4.12)$$

$$V_{c,u} \rho_c h_c + V_{h,u} \rho_{h,u} h_{h,u} = (V_{c,u} + V_{h,u}) \rho_{m,u} h_{m,u} \quad (4.13)$$

The volume of the cold streams, $V_{c,d}$ and $V_{c,u}$, can be expressed in terms of the cold leg length and the depth of the cold stream in the downstream and in the upstream region, respectively. The hot volume in downstream region, $V_{h,d}$, is assumed to be equal to the sum of the hot stream volume (in the downstream portion of the cold leg) plus the volume of a horizontal downcomer slice with a height equal to two cold leg diameters. Likewise, the hot volume in the upstream region, $V_{h,u}$, is assumed to be equal to the sum of the hot stream volume (in the upstream portion of the cold leg plus 25% of the pump volume. These assumptions are consistent with the assumptions used in previous REMIX code calculations under stagnated loop flow condition.^{4,2,4,4}

The condition of stationarity of long, neutrally stable waves at the interface between the cold and hot streams is expressed as:^{4,5}

$$Fr_c^2 + Fr_h^2 = 1 \quad (4.14)$$

In the original regional mixing model and the associated computer code REMIX, Equation (4.14) was applied only at the vessel junction of cold leg (i.e., downstream region). However, in the present extension of the model, the simplifying assumption of symmetry has been removed and Equation (4.14) is applied to both ends of the cold leg, i.e.,

$$\frac{(Q_{c,u}/A_{c,u})^2}{g \frac{A_{c,u}}{W_u} \frac{\rho_c - \rho_{h,u}}{\rho_c}} + \frac{(Q_{h,u}/A_{h,u})^2}{g \frac{A_{h,u}}{W_u} \frac{\rho_c - \rho_{h,u}}{\rho_{h,u}}} = 1 \quad (4.15)$$

$$\frac{(Q_{c,d}/A_{c,d})^2}{g \frac{A_{c,d}}{W_d} \frac{\rho_c - \rho_{h,d}}{\rho_c}} + \frac{(Q_{h,d}/A_{h,d})^2}{g \frac{A_{h,d}}{W_d} \frac{\rho_c - \rho_{h,d}}{\rho_{h,d}}} = 1 \quad (4.16)$$

where $A_{c,u}$, $A_{h,u}$ and W_u are the cross-sectional areas of cold stream, cross-sectional area of hot stream, and the common width of contact between two streams in upstream region, respectively. Likewise $A_{c,d}$, $A_{h,d}$ and W_d are the cross-sectional areas of cold stream, cross-sectional area of hot stream, and the common width of contact between two streams in the downstream region, respectively.

The cold stream volumetric flow rate in the downstream region $Q_{c,d}$, is expressed in terms of the flow split ratio, α , defined as the fraction of the jet flow that flows downstream toward the downcomer. Thus:

$$Q_{c,d} = \alpha Q_c \quad (4.17)$$

and

$$Q_{c,u} = (1 - \alpha) Q_c \quad (4.18)$$

In the presence of low loop flow, the loop flow accommodates a portion of the total entrainment to the safety injection jet. The hot stream flow coming from the direction of vessel is expressed in terms of a fraction, β , of the remaining entrained flow to the jet, $Q_e - Q_L$. Therefore, the net flow of cold stream in the downstream cold leg region should be $Q_{HPI} + Q_L + \beta(Q_e - Q_L)$. Thus, the flow split ratio can be expressed in terms of parameter β as:

$$\alpha = \frac{Q_{HPI} + Q_L + \beta(Q_e - Q_L)}{Q_{HPI} + Q_e} \quad (4.19)$$

For the very low Froude number of interest, the value of β is assumed to be equal to the fraction of the total entrainment obtained from the portion (one-half) of the jet exposed to hot stratum in downstream region, i.e.:

$$\beta = \frac{0.5 (Q_e |_{d_h = d_{h,d}})}{Q_e} \quad (4.20)$$

It should be noted that using Equations (4.20) and (4.11) together with the assumption of symmetry, a value of $\beta = 0.5$, assumed in the original REMIX code calculations, will be obtained.

As the loop flow increases, the extent of the cold stream flowing upstream towards the pump/loop seal region decreases. As a part of the present study a criterion for the existence of backflow towards the upstream region in the presence of loop flow has been developed (refer to section 4.1.4).

It should also be noted that certain geometries, such as that of Babcock and Wilcox reactor with an inclined cold leg (e.g., Oconee), preclude any backflow towards pump/loop seal region and a value of $\alpha = \beta = 1$ would then be appropriate.

Equations (4.1) through (4.20) together with equations of the state for water are solved numerically (refer to section 4.2) to obtain all variables including the transient temperature and flow rate of the cold stream entering the downcomer.

A highly complicated 3-dimensional mixing pattern occurs at the cold leg-downcomer junction. As discussed earlier in section 3.4.2, the knowledge of the detailed temperature distribution in this region is not necessary for PTS analysis. Therefore, an empirical approach, used in previous REMIX code calculations, is also adopted here to quantify the mixing at this junction. A planar plume is assumed to form with a distance twice that of the cold leg diameter below the cold leg centerline and to be fed in equal volumetric flow rates by the cold stream and surrounding hot volume fluid. The resulting temperature of plume is used as the initial planar plume temperature (T_j). Below this point the downcomer fluid temperature distribution is predicted based on the calculated results of the Chen and Rodi, $\kappa - \epsilon - \bar{T}^2$, turbulence model^{4,6} for a planar plume with initial width equal to D_{cl} , $Fr = 1$, and ambient temperature of $T_{m,d}$ (Refer to section 4.1.5).

4. Physical Models

As pointed out earlier in section 2.2, for very high Froude number injections the forceful jet impingement on the opposite cold leg boundary result in a significant increase in local mixing at the point of HPI location which is not depicted in the entrainment model discussed earlier. However, since the extent of mixing is also controlled by flow limitations expressed by Equations (4.15) and (4.16), the cooldown transient can be calculated on the basis of maximum entrainment (refer to section 4.1.3).

4.1.1. HPI Buoyant Jet Entrainment

The regional mixing model requires the prediction of the entrainment for the HPI buoyant jet.

The REMIX code was intended for vertically downward low Froude number injections ($Fr_{HPI} \sim 1$) of interest to Westinghouse and Combustion Engineering designed reactors. Such highly buoyant jets exhibit little inertia and thus, under stagnated loop flow conditions, the angle of HPI-nozzle inclination has very little effect on total entrainment to the jet. In the original regional mixing model,^{4,1} the jet model of Chen and Rodi^{4,6} was adopted to obtain the entrainment for the low Froude number axisymmetric vertical buoyant jets. The model utilizes the standard equations for natural convection boundary layer type flows with a vertically oriented buoyancy force and a κ - ϵ - $\overline{T'^2}$ differential turbulence model to evaluate the transport terms in the equations. With the choice of appropriate scales these equations may be put in nondimensional form such that only one main parameter, the Froude number, appears. The resulting system of equations is summarized in Table 4.1, where $i = 1$ for axisymmetric and $i = 0$ for planar geometry.

The following dimensionless quantities were used in the nondimensionalization of the governing equations:

$$\begin{aligned} z^* &= \frac{z}{D} & y^* &= \frac{y}{D} \\ u^* &= \frac{u}{u_{0,cl}} & v^* &= \frac{v}{u_{0,cl}} \\ T^* &= \frac{T_1 - T_a}{T_{0,cl} - T_a} & \epsilon^* &= \frac{\epsilon}{u_{0,cl}^3 / D} \\ \kappa^* &= \frac{\kappa}{U_{0,cl}^2} & \overline{T'^2}^* &= \frac{\overline{T'^2}}{(T_{0,cl} - T_a)^2} \end{aligned} \quad (4.21)$$

where Z and Y are the axial and transverse direction, respectively; u and v are the jet mean velocities in the axial and transverse direction, respectively; T is the mean jet temperature; T' is the fluctuating jet temperature; κ is the turbulent kinetic energy $\left(\frac{\overline{U_i U_i}}{2}\right)$; and ϵ is the dissipation rate of the turbulent kinetic energy.

The integration was carried out using the Patankar and Spalding method with 35 radial nodes for the half-jet.^{4,7} In order to achieve high computational efficiency, this method invokes a coordinate transformation, which utilizes a normalized Von Mises variable; and thus instead of y coordinate, a nondimensional stream function is used in the transverse coordinate.

The following boundary conditions were used in the calculations:

$$\begin{aligned} \kappa^* > 0 \quad Y^* \rightarrow \infty, \quad T^* = u^* = \kappa^* = \epsilon^* = \overline{T'^2}^* = 0 \\ \kappa^* > 0 \quad Y^* = 0, \quad \frac{\partial}{\partial y^*} [T^*, u^*, \kappa^*, \epsilon^*, \overline{T'^2}^*] = 0 \\ \text{at } \kappa^* = 0 \quad T^* = 1, \quad u^* = 1 \quad \kappa_0^*, \epsilon^* = \epsilon_0^* \quad \overline{T'^2}^* = \overline{T'^2}_0^* \end{aligned} \quad (4.22)$$

where the initial values for the dimensionless turbulence properties, κ_0^* , ϵ_0^* and $\overline{T'^2}^*$ were set at 0.0125 following the suggestion of Chen and Nikitopoulos.^{4,8}

Table 4.1 Nondimensional form of κ - ε - \bar{T}^{*2} turbulence jet model

Continuity	$\frac{\partial u^*}{\partial z^*} + \frac{1}{y^{*i}} \frac{\partial}{\partial y^*} (y^{*i} v^*) = 0$
Momentum	$u^* \frac{\partial u^*}{\partial z^*} + v^* \frac{\partial u^*}{\partial y^*} = \frac{1}{y^{*i}} \frac{\partial}{\partial y^*} (-y^{*i} \overline{uv}^{*'}) + \frac{T^*}{Fr^2}$
Energy	$u^* \frac{\partial T^*}{\partial z^*} + v^* \frac{\partial T^*}{\partial y^*} = \frac{1}{y^{*i}} \frac{\partial}{\partial y^*} (-y^{*i} \overline{vT}^{*'})$
Turbulent kinetic energy	$u^* \frac{\partial \kappa^*}{\partial z^*} + v^* \frac{\partial \kappa^*}{\partial y^*} = \frac{1}{y^{*i}} \frac{\partial}{\partial y^*} \left(y^{*i} C_\kappa \frac{\kappa^* v^{*2}}{\varepsilon^*} \frac{\partial \kappa^*}{\partial y^*} \right) - \overline{uv}^{*'} \frac{\partial u^*}{\partial y^*} + \frac{\overline{uT}^{*'}}{Fr^2} - \varepsilon^*$
Dissipation rate of turbulence	$u^* \frac{\partial \varepsilon^*}{\partial z^*} + v^* \frac{\partial \varepsilon^*}{\partial y^*} = \frac{1}{y^{*i}} \frac{\partial}{\partial y^*} \left(y^{*i} c_\varepsilon \frac{\kappa^* \overline{v^2}}{\varepsilon^*} \frac{\partial \varepsilon^*}{\partial y^*} \right) + c_{\varepsilon 1} \frac{\varepsilon^*}{\kappa^*} \left(-\overline{uv}^{*'} \frac{\partial u^*}{\partial y^*} + \frac{\overline{uT}^{*'}}{Fr^2} \right) - c_{\varepsilon 2} (1 - 0.035G)^i \frac{\varepsilon^{*2}}{\kappa^{*2}}$
Fluctuating temperature	$u^* \frac{\partial \bar{T}^{*2}}{\partial z^*} + v^* \frac{\partial \bar{T}^{*2}}{\partial y^*} = \frac{1}{y^{*i}} \frac{\partial}{\partial y^*} \left(y^{*i} c_T \frac{\kappa^{*2}}{\varepsilon^*} \frac{\partial \bar{T}^{*2}}{\partial y^*} \right) - 2 \overline{vT}^{*'} \frac{\partial T^*}{\partial y^*} - c_{T1} \varepsilon^* \frac{\bar{T}^{*2}}{\kappa^*}$

where:

$$\overline{uv}^{*'} = \frac{1 - c_0}{c_1} \frac{\overline{v^2}^*}{\kappa^*} \left[1 + \frac{\kappa^* \frac{\partial T^*}{\partial y^*}}{Fr^2 c_H \varepsilon^* \frac{\partial u^*}{\partial y^*}} \right] \frac{\kappa^*}{\varepsilon^*} \frac{\partial u^*}{\partial y^*} (1 - 0.465G)^i$$

$$\overline{v^2}^* = c_2 \kappa^*, \quad \overline{vT}^{*'} = -\frac{1}{c_H} \frac{\overline{v^2}^* \kappa^{*2}}{\kappa^* \varepsilon^*} \frac{\partial T^*}{\partial y^*}$$

$$\overline{uT}^{*'} = \frac{\kappa^*}{c_H \varepsilon^*} \left[-\overline{uv}^{*'} \frac{\partial T^*}{\partial y^*} - \overline{vT}^{*'} (1 - c_{H1}) \frac{\partial u^*}{\partial y^*} + \frac{(1 - c_{H1})}{Fr^2} T^{*2} \right]$$

$$G = \left[\frac{y_{0.5u}^*}{2u_{cL}^*} \left(\frac{du_{cL}^*}{dz^*} - \left| \frac{du_{cL}^*}{dz^*} \right| \right) \right]^{0.2}$$

and

$$\begin{array}{llllll} c_0 = 0.55 & c_1 = 2.2 & c_2 = 0.53 & c_\varepsilon = 0.15 & c_{\varepsilon 1} = 1.43 & c_{\varepsilon 2} = 1.92 \\ c_\kappa = 0.225 & c_T = 0.13 & c_{T1} = 1.25 & c_H = 3.2 & c_{H1} = 0.5 & \end{array}$$

4. Physical Models

The results of the turbulence model calculations for the entrainment to low Froude number axisymmetric vertical buoyant jets was fit by the following expression:

$$\frac{Q_e}{Q_o} = 0.52 \left[\frac{z}{D} \right]^{1.236} Fr^{-0.414} \quad (4.23)$$

which was utilized, for convenience, in the computation. It should be noted that the entrainment function (Equation 4.23) is valid for $0.2 < Fr < 1$ and $0.5 < \frac{z}{D} < 4$.

The general adequacy of the $\kappa\text{-}\epsilon\text{-}\overline{T'^2}$ turbulent jet model has been demonstrated by Chen, Rodi, and co-workers^{4,6, 4.8, 4.9} by comparison of model predictions, in terms of decay and growth, with the principal data available for $Fr > 1$. The results of turbulence model calculations was also shown to be in agreement with the axisymmetric plume decay data obtained at $Fr < 1$.^{4.10}

As a part of the present study, an integral method solution somewhat similar to the one used by Hirst^{4.11} was also utilized to quantify the mixing associated

with buoyant circular jets injected at arbitrary angles to flowing ambients.

The coordinate system to describe the trajectory and physical dimensions of a jet is shown in Figure 4.3. The streamwise coordinate, S , is measured along the direction of the mean centerline of the jet. The local angle between S and y , the inclination of the jet from the horizontal is θ . Here any ambient motion is assumed to be horizontal, that is, in the direction of y .

The basic partial differential equations governing the development of a buoyant jet, using the entrainment mixing concept, were derived in a coordinate system which moves with the jet centerline. The resulting equations were simplified by assuming the flow to be axisymmetric and then integrating these equations over a cross section of the jet. Assuming that the velocity and temperature profiles are both Gaussian and invoking Boussinesq approximation with constant value of volumetric coefficient of thermal expansion, β , yields a set of ordinary differential equations with the streamwise coordinate as the single independent variable. With the choice of appropriate scales these equations may be put in a nondimensional form presented in Table 4.2.

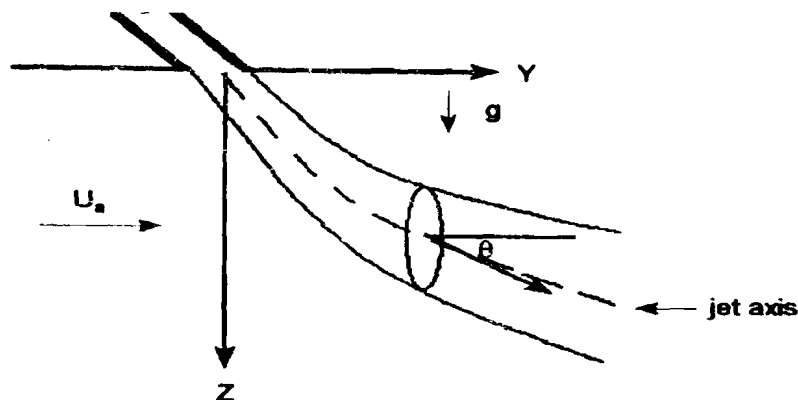


Figure 4.3 Coordinate system and physical dimensions for a buoyant jet

Table 4.2 Nondimensional form of governing equations for a circular jet discharged into a flowing ambient (integral method)

Continuity	$\frac{d}{ds^*} (u_m^* b^{*2}) = 2\alpha \left(\left u_m^* - R \cos \theta \right + a R \sin \theta \right)$
Horizontal momentum	$\frac{d}{ds^*} (u_m^{*2} b^{*2} \cos \theta) = 4 R \alpha b^* \left(\left u_m^* - R \cos \theta \right + a R \sin \theta \right)$
Vertical momentum	$\frac{d}{ds^*} (u_m^{*2} b^{*2} \sin \theta) = T_m^* \frac{2\lambda^2 b^{*2}}{Fr^2}$
Energy	$\frac{d}{ds^*} \left(u_m^* T_m^* \frac{\lambda^2 b^{*2}}{(\lambda^2 + 1)} \right) = 0$
Horizontal trajectory	$\frac{dy^*}{ds^*} = \cos \theta$
Vertical trajectory	$\frac{dz^*}{ds^*} = \sin \theta$

The following dimensionless quantities were used in the nondimensionalization of the governing equations:

$$\begin{aligned}
 s^* &= \frac{S}{D} & b^* &= \frac{b}{D} \\
 u_m^* &= \frac{u_m}{u_o} & T_m^* &= \frac{T_m - T_o}{T_o - T_a} \\
 R &= \frac{u_a}{U_o} & &
 \end{aligned}
 \tag{4.24}$$

where u_m , T_m are the local streamwise centerline velocity and centerline temperature, respectively. b is a characteristic jet width defined as the radial distance at which u is equal to $\frac{1}{e}$ times the mean centerline value, u_m .

It should be noted that the integral turbulent jet model presented in Table 4.1 apply only in the zone of established flow which begins when turbulent mixing

reaches the jet centerline. Therefore, the initial conditions at the end of the zone of flow establishment (at S_e) should be specified in terms of the jet discharge conditions (at $s = 0$).

The length of the initial region of flow development, S_e , is taken from Abraham,^{4,12} to be:

$$\begin{aligned}
 \frac{S_e}{D} &= 6.2 & Fr^2 &\geq 40 \\
 \frac{S_e}{D} &= 3.9 + 0.057 Fr^2 & 5 &\leq Fr^2 < 40 \\
 \frac{S_e}{D} &= 2.075 + 0.425 Fr^2 & 1 &\leq Fr^2 < 5 \\
 \frac{S_e}{D} &= 0 & 0 &\leq Fr^2 < 1
 \end{aligned}
 \tag{4.25}$$

The initial conditions at S_e , based on the analytical

4. Physical Models

development by Hirst,^{4.11} are taken to be:

$$\begin{aligned}
 u_{m,e}^* &= 1 \\
 b_e^* &= \frac{1}{\sqrt{2(1+\cos\theta_0)}} \\
 T_{m,e}^* &= \frac{\lambda^2 + 1}{2\lambda^2} \frac{1 + \cos\theta_0}{1 + \lambda^2 \cos\theta_0}
 \end{aligned}
 \quad (4.26)$$

where λ is the relative radial spreading ratio between velocity and temperature. Abraham^{4.12} recommended $\lambda = 1.16$, which was used in the present analysis.

The resulting coupled system of first order differential equations were integrated numerically using a library program (based on the gear method) available at Brookhaven National Laboratory.

Various entrainment coefficients, based on experimental data for $Fr > 1$, have been proposed in literature. An excellent review of submerged jet modeling techniques and experimentation have been published by Gebhart, et al.^{4.13} For the low Froude number of interest to the present study, a constant "coflow" entrainment coefficient, $\alpha = 0.082$, proposed by List and Imberger^{4.14} for simple buoyant plumes discharged into quiescent ambients ($R = 0$), was used in the analysis. The value of the coefficient for the entrainment contribution arising from crossflow, $\alpha = 9.0$, suggested by Hirst,^{4.11} was used in the calculations.

Figure 4.4 presents the comparisons between Fan's^{4.15} trajectory measurements for buoyant jets discharged to a flowing ambient and the present integral method predictions.

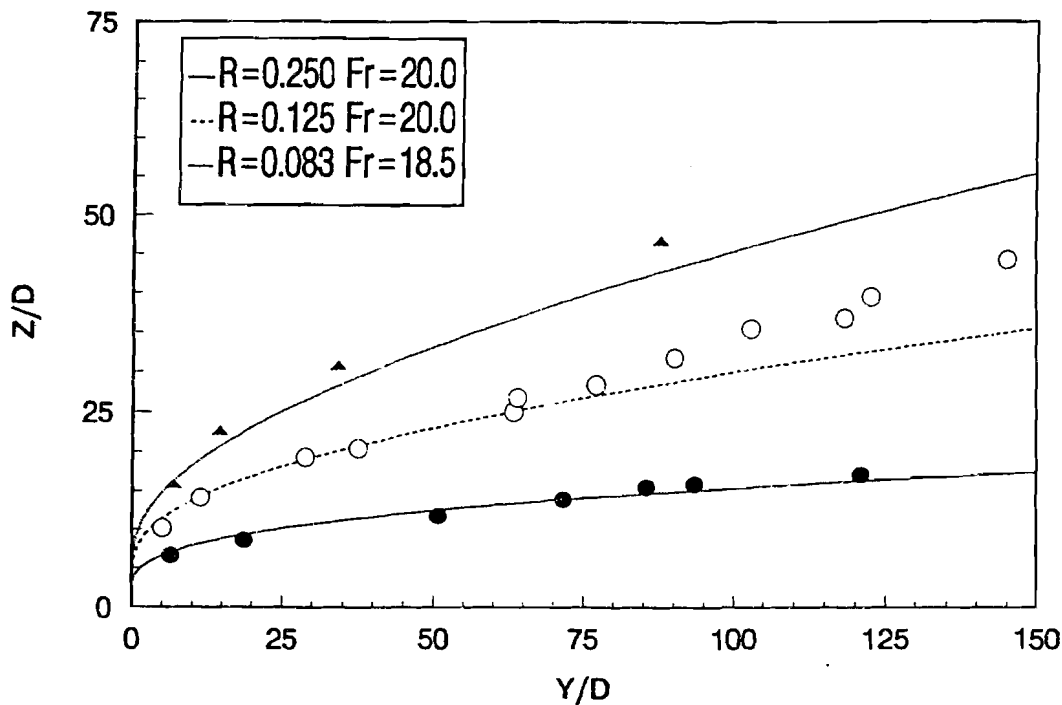


Figure 4.4 Comparison of present trajectory results with the data of Fan^{4.15} for vertical buoyant jets discharged normal to a cross flow

There have been no experimental studies on the behavior of low Froude number ($Fr < 1$) buoyant jets discharged to flowing ambients reported in literature. In order to assess the validity of the present integral model for low Froude number buoyant jets, the newly calculated entrainments for vertical buoyant jets discharged to quiescent ambients were compared with the results of $\kappa\text{-}\epsilon\text{-}\overline{T}^{\prime 2}$ model. As shown in Figure 4.5 the disagreement between the two is relatively small especially for the range of interest ($\frac{z}{D} < 3$) to the present application.

A systematic study of the present integral model predictions, in terms of trajectory and entrainment were performed. Typical sensitivities of the results to the ambient flow ratio, the initial angle of inclination from horizontal and the Froude number of injection is presented in Figures 4.6 through 4.11.

The results for the entrainment to low Froude number buoyant jets have been fit by the following expression:

$$\frac{Q_e}{Q_0} = \frac{0.52 \left[\frac{z}{D} \right]^{1.236} Fr^{-0.414} (1 + 8.4 Fr^{0.854} R)}{\sin \theta_0 + 0.32 Fr^{-0.139} \left(\frac{z}{D} \right)^{0.098} \cos \theta_c} \quad (4.27)$$

which is utilized in REMIX97 computation.

The form of expression for entrainment was chosen such that for vertically downward buoyant jets ($\theta_0 = \frac{\pi}{2}$) discharged in to quiescent ambients ($R = 0$), it would be reduced to the one used in the original REMIX code calculations (Equation 4.23).

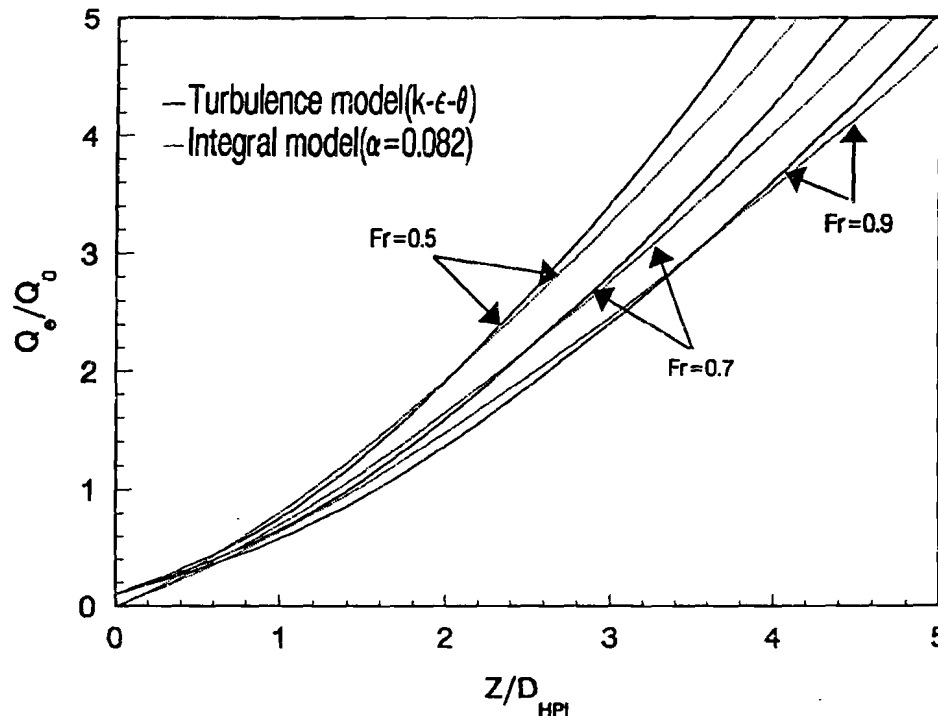


Figure 4.5 Comparison of integral model and $\kappa\text{-}\epsilon\text{-}\overline{T}^{\prime 2}$ turbulence model calculations for the entrainment to axisymmetric vertical buoyant jets discharged to quiescent ambients

4. Physical Models

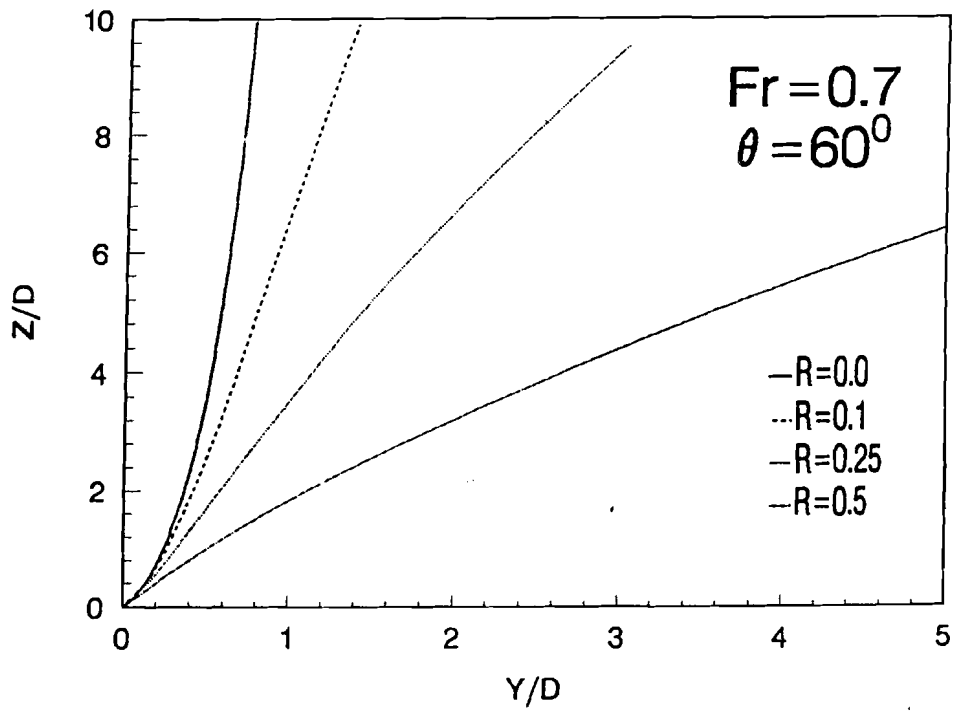


Figure 4.6 Effect of ambient flow on trajectory of buoyant jets

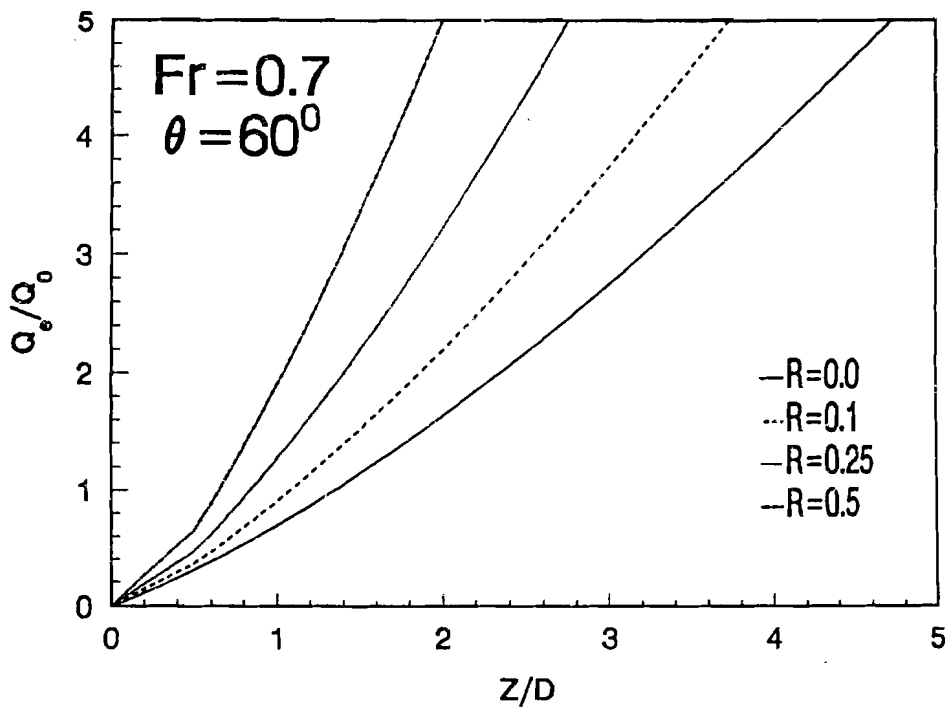


Figure 4.7 Effect of ambient flow on total entrainment to buoyant jets

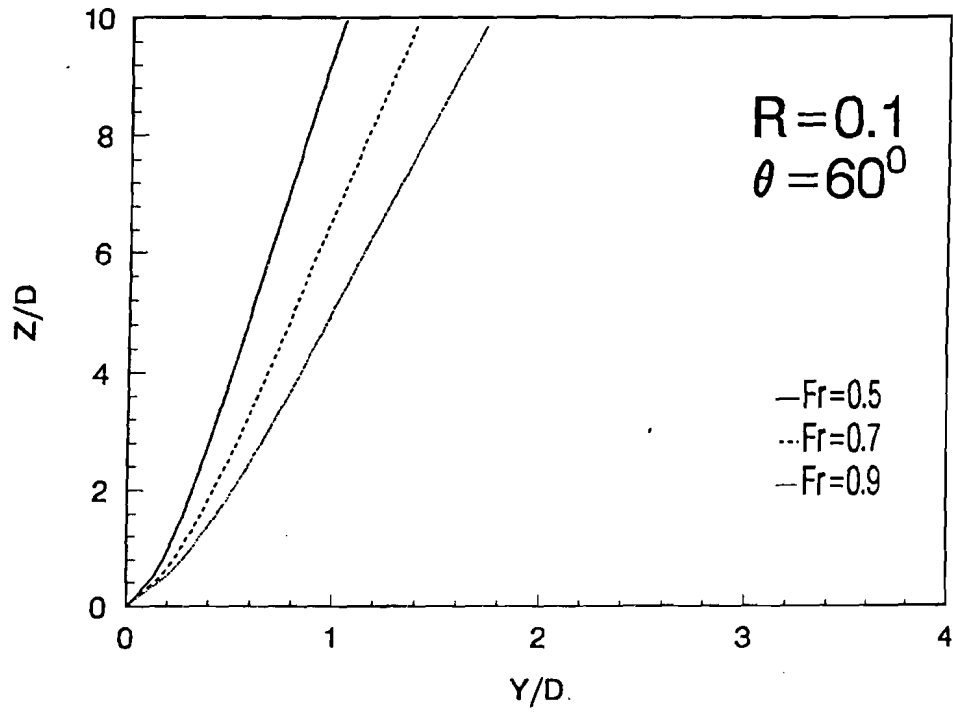


Figure 4.8 Effect of injection Froude number on trajectory of buoyant jets

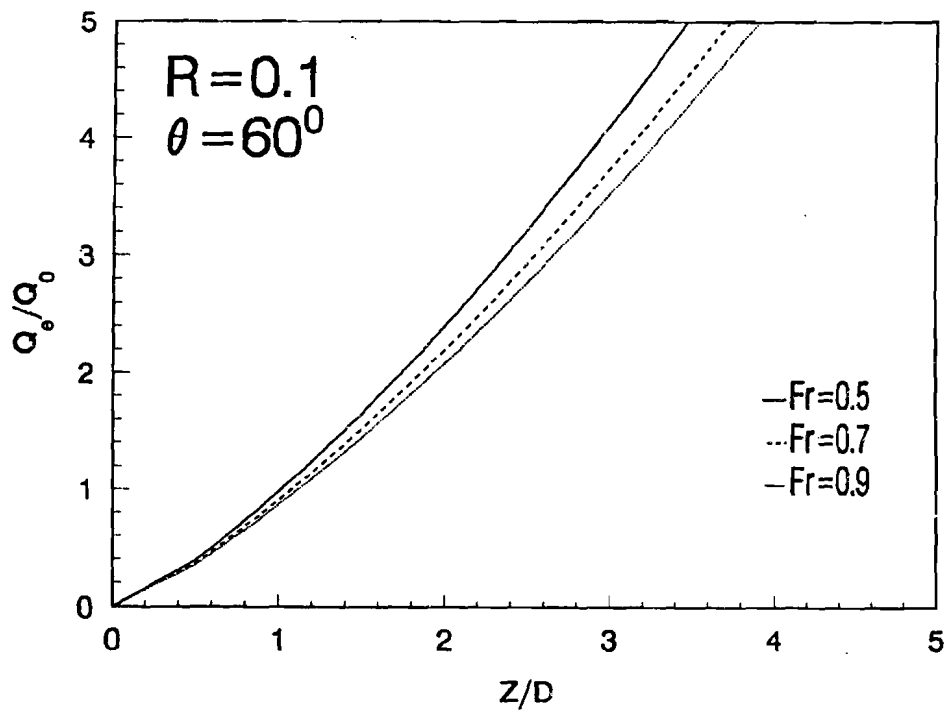


Figure 4.9 Effect of injection Froude number on total entrainment to buoyant jets

4. Physical Models

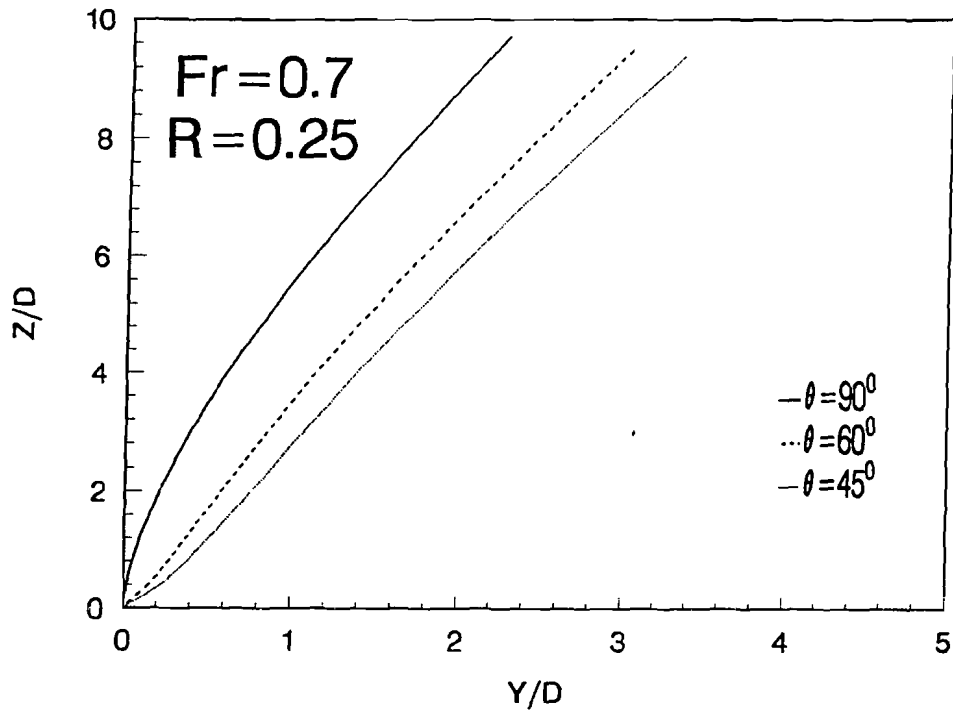


Figure 4.10 Effect of the initial angle of inclination from horizontal on trajectory of buoyant jets

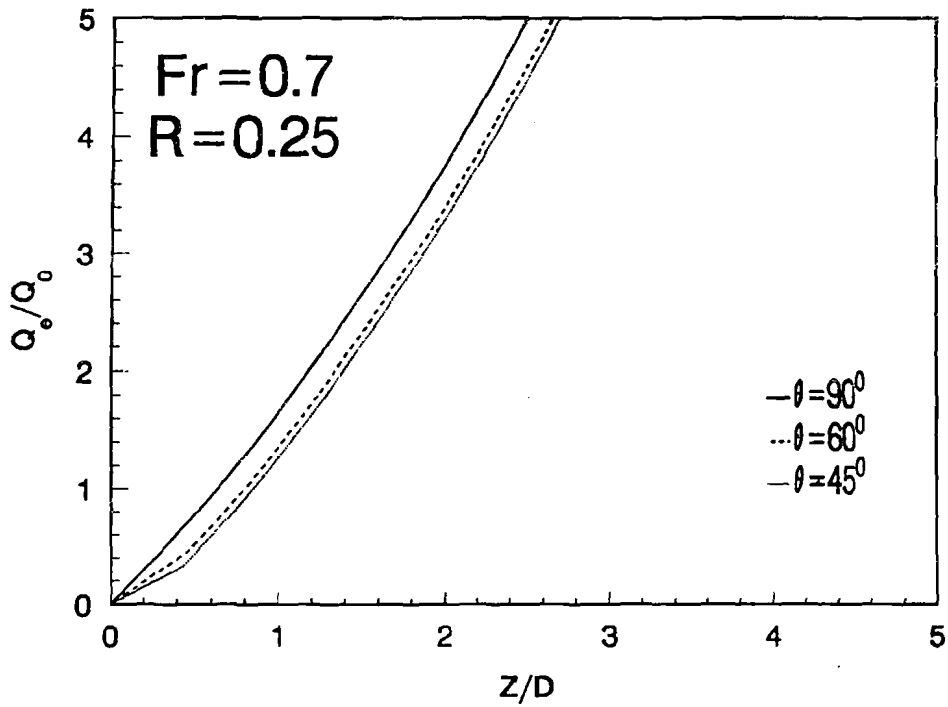


Figure 4.11 Effect of the initial angle of inclination from horizontal on total entrainment to buoyant jets

4.1.2 Mixing Within the HPI Line

For a very low Froude number of injection, the lighter hot fluid in the cold leg is expected to penetrate upward into the HPI line. This buoyant backflow phenomena has been observed in reactor experiments.^{4.4.4.15,4.17}

This backflow contributes somewhat to the entrainment of cold leg fluid into the safety injection jet. In the original REMIX calculations, Purdue's initial 1/2 scale experiments^{4.4.4.18} provided the empirical basis for taking this effect into account. The approach was to consider an effective origin of the HPI injection plume within the injection line (i.e., more plume travel distance available for mixing). This extra length that was consistent with the experimentally observed entrainment rate was found to be approximately equal to one-half that of the observed flow penetration depth into the injection line. The resulting correlation for the effective HPI plume origin that moves into the injection line as the

Fr_{HPI} decreases below the critical value of 0.6, is shown in Figure 4.12.

It should be noted that both the critical Froude number and the backflow penetration depth is also expected to be a function of both the HPI-nozzle inclination and the extent of loop flow. There have been no experimental studies on the backflow of hot stream fluid and mixing within the injection line under low loop flow conditions reported in the literature.

In the present REMIX97 code, the same formulation as the one used in the original REMIX calculations has been adopted for taking into account the additional entrainment into the safety injection jet due to this backflow. The correlation for the effective length increase of the HPI plume to represent mixing within the HPI line has been implemented in a separate module such that it can be easily overridden by a user for any future sensitivity calculations.

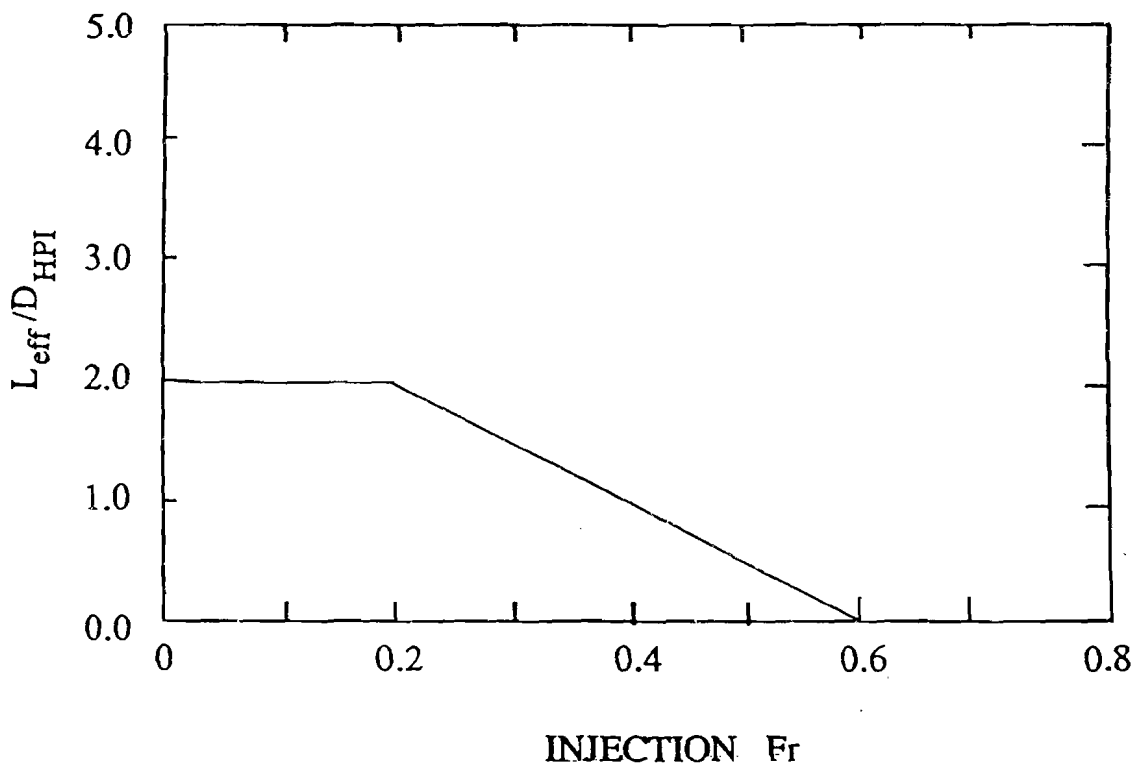


Figure 4.12 Effective increase in plume entrainment length due to back flow in the injection line

4. Physical Models

4.1.3 Counter-current Flow Limited Entrainment in the Presence of Loop Flow

As discussed earlier, for high Froude number injections, the forceful jet impingement on the opposite cold leg boundary result in a significant increase in local mixing at the point of HPI location, reaching to a maximum level of entrainment restricted only by the counter-current flow limitations expressed by Equations (4.15) and (4.16). As a part of the present effort, a systematic analytical study of the counter-current flow limited entrainment in the presence of loop flow was performed to provide the physical basis essential to understanding and analyzing this mixing behavior.

The condition of stationarity of long, neutrally stable waves at the interface between the cold and hot streams in the upstream and downstream regions of the cold leg, Equations (4.15 and 4.16), may be written in terms of flow split ratio, α , as:

$$\frac{[(1 - \alpha)(Q_{HPI} + Q_e)/A_{c,u}]^2}{g \frac{A_{c,u}}{W_u} \frac{\rho_c - \rho_{h,u}}{\rho_c}} + \frac{[(Q_L + (1 - \alpha)(Q_{HPI} + Q_e))/A_{h,u}]^2}{g \frac{A_{h,u}}{W_u} \frac{\rho_c - \rho_{h,u}}{\rho_{h,u}}} = 1 \quad (4.28)$$

$$\frac{[\alpha(Q_{HPI} + Q_e)/A_{c,d}]^2}{g \frac{A_{c,d}}{W_d} \frac{\rho_c - \rho_{h,d}}{\rho_c}} + \frac{[(\alpha(Q_{HPI} + Q_e) - Q_{HPI} - Q_L)/A_{h,d}]^2}{g \frac{A_{h,d}}{W_d} \frac{\rho_c - \rho_{h,d}}{\rho_{h,d}}} = 1 \quad (4.29)$$

Assuming $\rho_{h,u} = \rho_{h,d} = \rho_a$, and eliminating ρ_c with the help of Equation (4.7), Equations (4.28) and (4.29) become:

$$Q_e^{*3} + a_u Q_e^{*2} + b_u Q_e^* + c_u = 0 \quad (4.30)$$

$$Q_e^{*3} + a_d Q_e^{*2} + b_d Q_e^* + c_d = 0 \quad (4.31)$$

where

$$a_u = \left\{ \frac{(1-\alpha)^2(1+2\rho^*)}{A_u^{*3}} + \frac{\rho^*(1-\alpha)(2Q_L^*+3-3\alpha)}{(1-A_u^*)^3} \right\} \bigg/ \rho^*(1-\alpha)^2 \delta_u \quad (4.32)$$

$$b_u = \left\{ \frac{(1-\alpha)^2(2+\rho^*)}{A_u^{*3}} + \frac{\rho^*(Q_L^*+1-\alpha)(Q_L^*+3-3\alpha)}{(1-A_u^*)^3} \right\} \bigg/ \rho^*(1-\alpha)^2 \delta_u \quad (4.33)$$

$$c_u = \left\{ \frac{(1-\alpha)^2}{A_u^{*3}} + \frac{\rho^*(Q_L^*+1-\alpha)^2}{(1-A_u^*)^3} - \frac{1}{Fr_{HPI,cl}^2 W_u^*} \right\} \bigg/ \rho^*(1-\alpha)^2 \delta_u \quad (4.34)$$

$$a_d = \left\{ \frac{(\alpha)^2(1+2\rho^*)}{A_d^{*3}} + \frac{\rho^*(3\alpha^2-2\alpha-2\alpha Q_L^*)}{(1-A_d^*)^3} \right\} \bigg/ \rho^*\alpha^2 \delta_d \quad (4.35)$$

$$b_d = \left\{ \frac{\alpha^2(2+\rho^*)}{A_d^{*3}} + \frac{\rho^*(3\alpha-1-Q_L^*)(\alpha-1-Q_L^*)}{(1-A_d^*)^3} \right\} \bigg/ \rho^*\alpha^2 \delta_d \quad (4.36)$$

$$c_d = \left\{ \frac{\alpha^2}{A_d^{*3}} + \frac{\rho^*(\alpha-1-Q_L^*)^2}{(1-A_d^*)^3} - \frac{1}{Fr_{HPI,cl}^2 W_d^*} \right\} \bigg/ \rho^*\alpha^2 \delta_d \quad (4.37)$$

and

$$\delta_u = \frac{1}{A_u^{*3}} + \frac{1}{(1-A_u^*)^3} \quad (4.38)$$

$$\delta_d = \frac{1}{A_d^{*3}} + \frac{1}{(1-A_d^*)^3} \quad (4.39)$$

4. Physical Models

The dimensionless quantities and $Fr_{HPI,cl}$ are defined as:

$$\begin{aligned}
 Q_e^* &= \frac{Q_e}{Q_{HPI}}, & Q_L^* &= \frac{Q_L}{Q_{HPI}}, \\
 A_u^* &= \frac{A_{c,u}}{A_{cl}}, & A_d^* &= \frac{A_{c,d}}{A_{cl}}, \\
 W_u^* &= \frac{W_u D_{cl}}{A_{cl}}, & W_d^* &= \frac{W_d D_{cl}}{A_{cl}}, \\
 \rho^* &= \frac{\rho_a}{\rho_{HPI}} \\
 Fr_{HPI,cl} &= \frac{Q_{HPI}}{A_{cl}} \left(g D_{cl} \frac{\rho_{HPI} - \rho_a}{\rho_{HPI}} \right)^{-1/2}
 \end{aligned} \tag{4.40}$$

W_u^* and A_u^* may be expressed in terms of dimensionless cold stream depth in the upstream region of the cold leg.

$$d_{c,u}^* = \frac{d_{c,u}}{D_{cl}} \tag{4.41}$$

Likewise W_d^* and A_d^* may be expressed in terms of dimensionless cold depth in the downstream region of the cold leg

$$d_{c,d}^* = \frac{d_{c,d}}{D_{cl}} \tag{4.42}$$

Thus, Equations (4.30) and (4.31) provide two relationships of the forms:

$$Q_e = \mathcal{F}(d_{c,u}^*, Fr_{HPI,cl}, Q_L^*, \alpha, \rho^*) \tag{4.43}$$

$$Q_e = \mathcal{G}(d_{c,d}^*, Fr_{HPI,cl}, Q_L^*, \alpha, \rho^*) \tag{4.44}$$

These two equations express two single parameter family of flows with the depth of cold streams in the upstream and downstream regions of the cold leg being the corresponding parameters. That is, for a given primary fluid temperature, loop flow rate, and HPI temperature and flow rate, each value of the cold stream depth in the upstream region of the cold leg specifies a corresponding value of the rate of entrainment in the HPI jet according to Equation (4.43). Likewise, for each value of the cold stream depth in the downstream region of the cold leg, Equation (4.44) specifies a corresponding value of the rate of entrainment in the HPI jet.

In reactor application ρ^* , is initially at 0.8 and approaches its maximum value of unity if the cooldown transient continues under stagnated loop flow condition. The effect of ρ^* variation on the results of Equations (4.43) and (4.44) is negligible. The flow split ratio depends on many factors including loop flow, injection Froude number and cold leg geometry (e.g., cold leg inclination). The relevant values of α are between 0.5 and 1.00. The Q_L^* is between zero and the value obtained from stratification/mixing boundary (refer to section 3 2). $Fr_{HPI,cl}$ typically begins at the value of ~ 0.02 and increases gradually through cooldown transient. The functional dependence of Equations (4.43) and (4.44) may be visualized, for the appropriate ranges of these parameters, in Figures 4.13 through 4.19.

It should be noted that under certain parameter conditions, the cubic equations of 4.30 and 4.31 have three real roots. However, the only physically acceptable solutions are shown in these figures.

As shown in Figures 4.13 through 4.19, for each value of $Fr_{HPI,cl}$ and Q_L^* , a maximum entrainment restricted by flow limitations in upstream region and a maximum entrainment restricted by flow limitations in downstream region are obtained. These limiting entrainments are strongly dependent on $Fr_{HPI,cl}$ and Q_L^* . For a given $Fr_{HPI,cl}$ and α , as Q_L^* increases the maximum possible entrainment restricted by flow

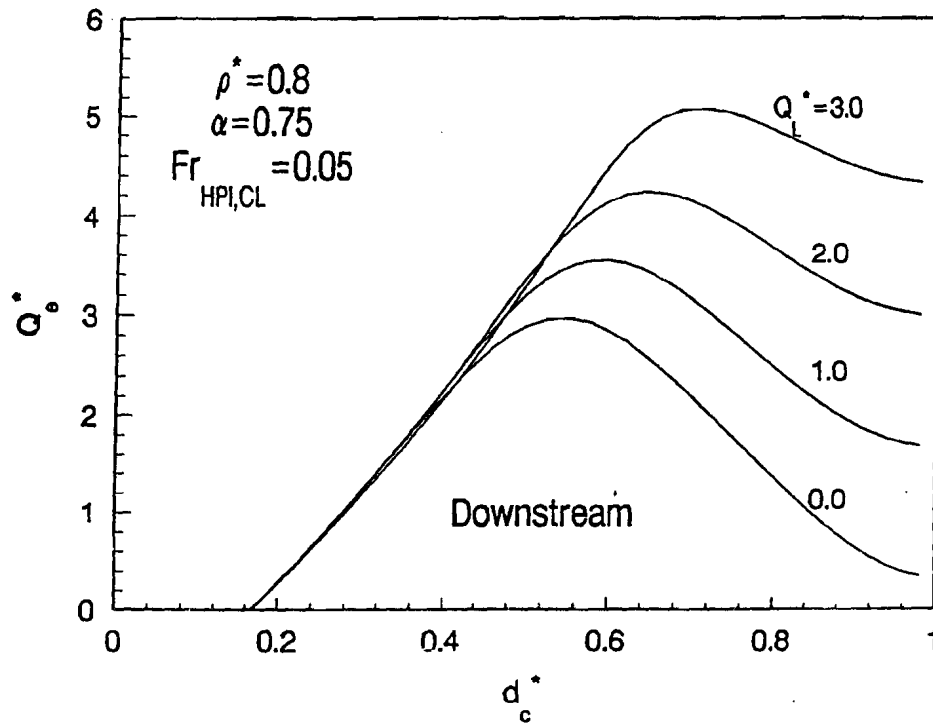


Figure 4.13 Effect of volumetric loop flow ratio, Q_L^* , on the upstream counter-current flow limited entrainment for $\rho^* = 0.8$, $\alpha = 0.75$ and $Fr_{HPI,CL} = 0.05$

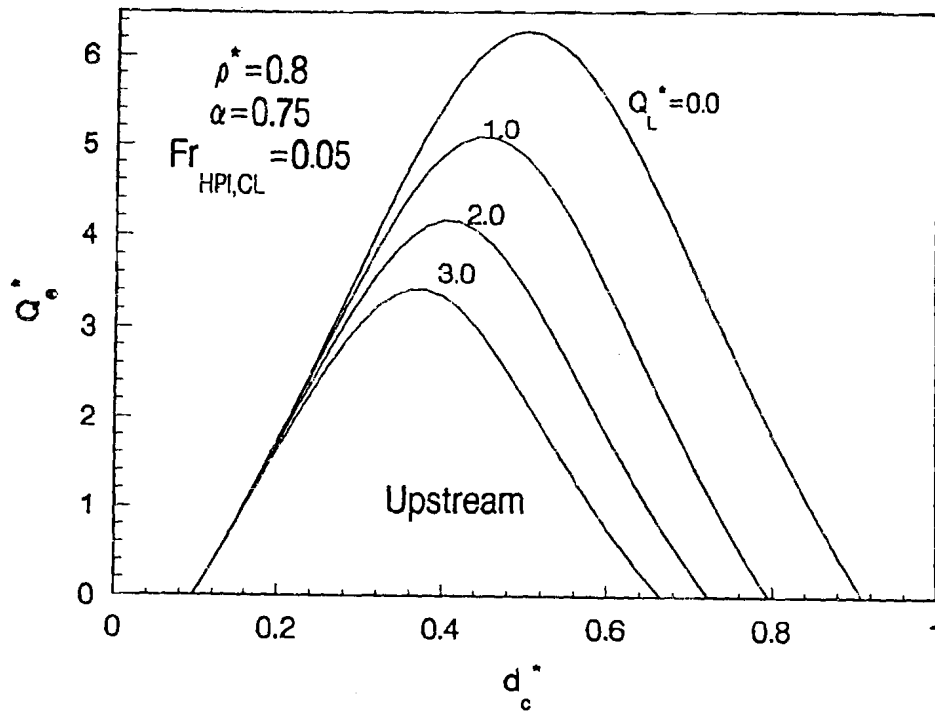


Figure 4.14 Effect of volumetric loop flow ratio, Q_L^* , on the downstream counter-current flow limited entrainment for $\rho^* = 0.8$, $\alpha = 0.75$ and $Fr_{HPI,CL} = 0.05$

4. Physical Models

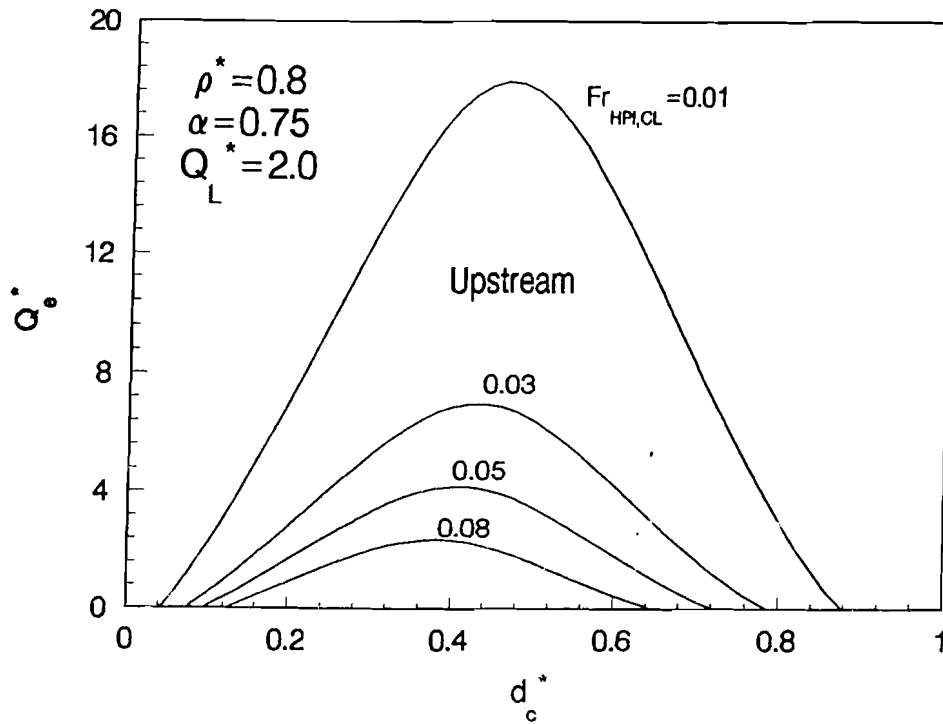


Figure 4.15 Effect of $Fr_{HPI,CL}$ on the upstream counter-current flow limited entrainment for $\rho^* = 0.8$, $\alpha = 0.75$, and $Q_L^* = 2$

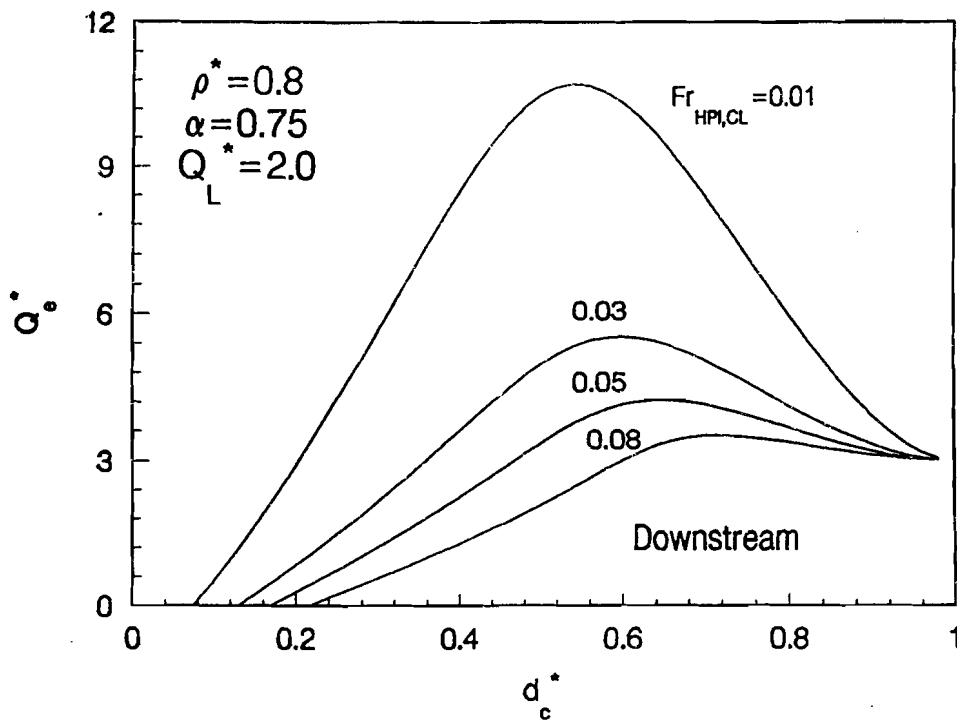


Figure 4.16 Effect of $Fr_{HPI,CL}$ on the downstream counter-current flow limited entrainment for $\rho^* = 0.8$, $\alpha = 0.75$, and $Q_L^* = 2$

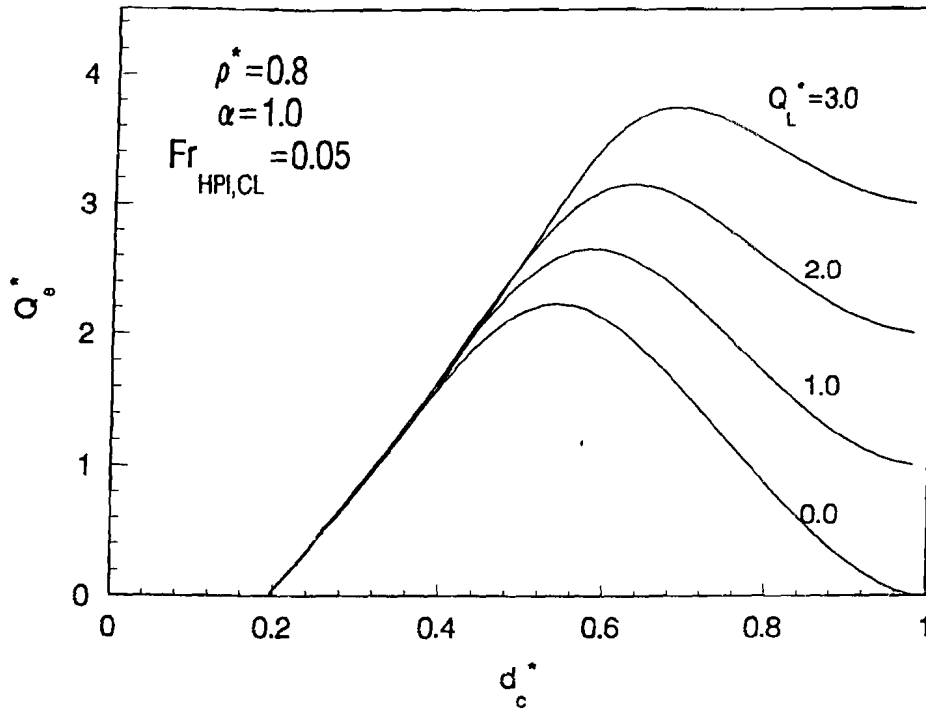


Figure 4.17 Effect of volumetric flow ratio, Q_L^* , on the downstream counter-current flow limited entrainment for $\rho^* = 0.8$, $\alpha = 1$, and $Fr_{HPI,CL} = 0.05$

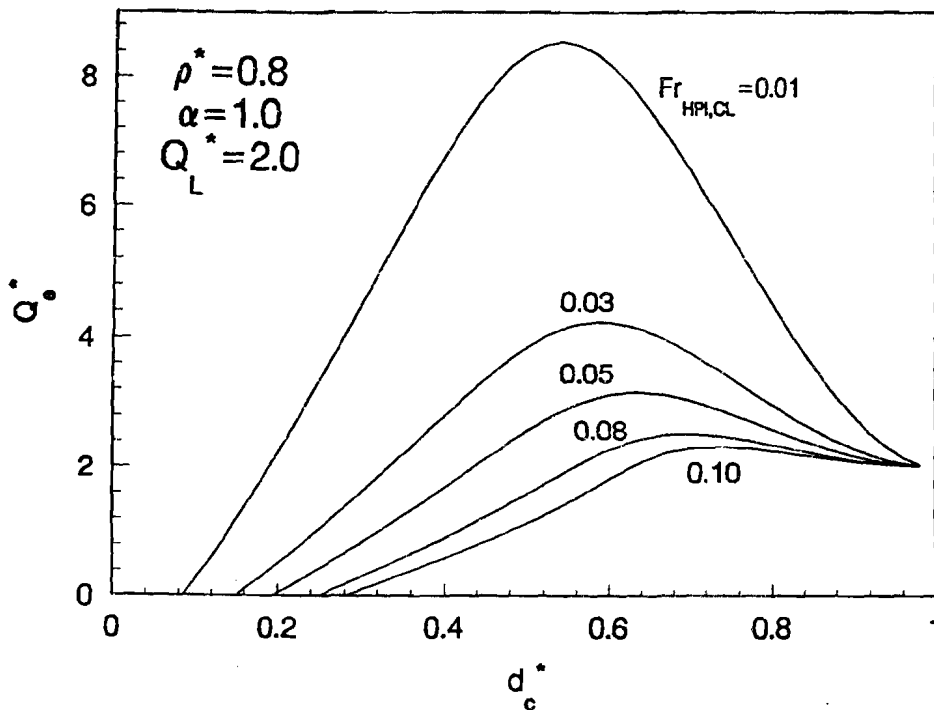


Figure 4.18 Effect of $Fr_{HPI,CL}$ on the downstream counter-current flow limited entrainment for $\rho^* = 0.8$, $\alpha = 1$, and $Q_L^* = 2$

4. Physical Models

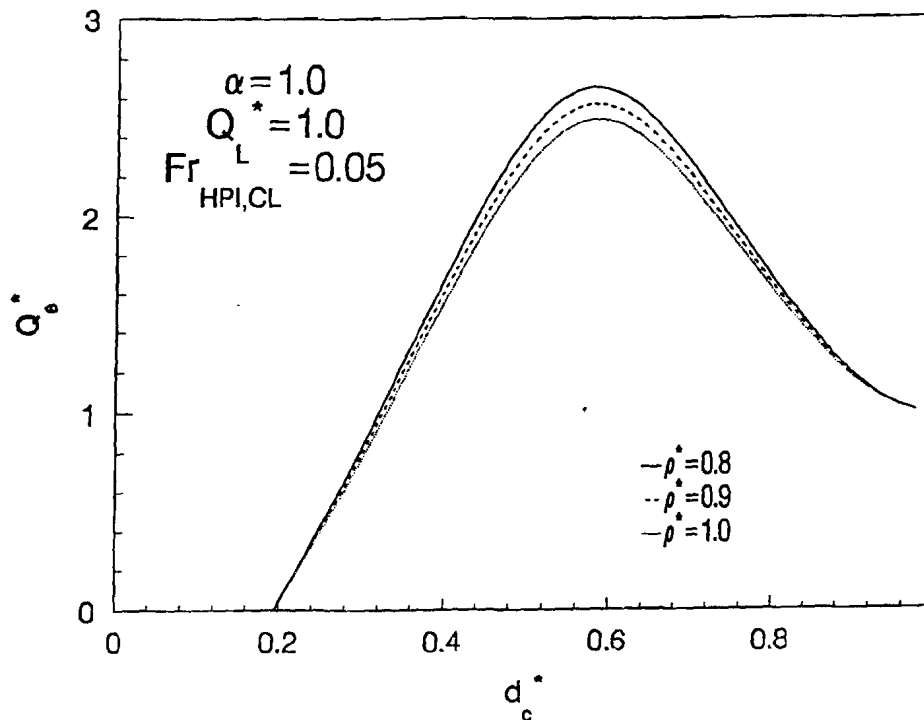


Figure 4.19 Effect of density ratio, ρ^* , on the downstream counter-current flow limited entrainment for $\rho^* = 0.8$, $\alpha = 1$, and $Q_L^* = 1$

limitation in upstream region decreases while the maximum possible entrainment restricted by flow limitation in downstream region increases. It should be noted in the absence of backflow of HPI jet towards the upstream region of cold leg (i.e., $\alpha = 1$), the maximum entrainment is only restricted by flow limitations in the downstream region of the cold leg.

For low Froude number injections, the entrainment rate is also restricted by HPI buoyant jet mixing rate. The HPI jet entrainment depends, among other factors, on the depths of the cold streams (refer to Equations (4.9) and (4.11)). Therefore, the REMIX97 cooldown calculation may be viewed as the solution of the three simultaneous equations for Q_L^* (i.e., Equations (4.43) and (4.44) together with expression for HPI jet entrainment) with continuous variation of $Fr_{HPI,CL}$ and Q_L^* , ρ^* and α with time.

For very high Froude number injections, the forceful jet impingement on the opposite cold leg boundary result in a significant increase in local mixing at the point of HPI location, reaching to a maximum level of entrainment restricted only by the flow limitations expressed by Equations (4.43) and (4.44). With the proper choice of an input parameter, the cooldown transient in REMIX97 is calculated on the basis of this maximum entrainment.

4.1.4 Backflow of HPI Jet Towards the Upstream Region of the Cold Leg

As discussed earlier, at very low loop flow, the HPI jet after some mixing at the point of injection divides into two stably stratified cold streams, one flowing downstream and the other going upstream. However, as the loop flow increases the extent of backflow

towards the upstream region of the cold leg decreases.

In a previous section it was shown that for a given $Fr_{HPI,cl}$, the maximum entrainment (restricted by the condition of stationarity of long, neutrally stable waves at the interface between cold and hot streams in the cold leg) increases as the loop flow rate, Q_L^* , increases. The maximum possible entrainment reaches to a maximum value at certain loop flow rate. For each $Fr_{HPI,cl}$ the corresponding value of Q_L^* that leads to maximum possible entrainment (at $\alpha = 1$ and $\rho^* = 0.8$) were found numerically and could be fit by:

$$Fr_{HPI,cl} = 0.56(1 + Q_L^*)^{-3/2} \quad (4.45)$$

Since for a given $Fr_{HPI,cl}$ as the loop flow increases, the maximum possible entrainment (restricted by downstream flow limitation) increases while the maximum possible entrainment (restricted by

upstream flow limitation) decreases, Equation (4.45) can also be viewed as the criterion for the existence of backflow towards the upstream region of the cold leg. The backflow criterion expressed by Equation (4.45) is compared in Figure 4.20 with the CREARE 1/5-scale data.^{4,19,4.20} Excellent agreement is noted.

It should be noted that the effect of density ratio, ρ^* , on backflow criterion has been neglected. This is a valid assumption for the present application when ρ^* value varies between 0.8 and 1. Further systematic analytical study of flow limited entrainment in the presence of loop flow expressed by Equations (4.30) and (4.31) may be very useful for determining the entire cold leg flow regime map, including the prediction of inverted flow pattern observed in CREARE 1/5-scale thermal mixing tests. However, such study was beyond the scope of the present work.

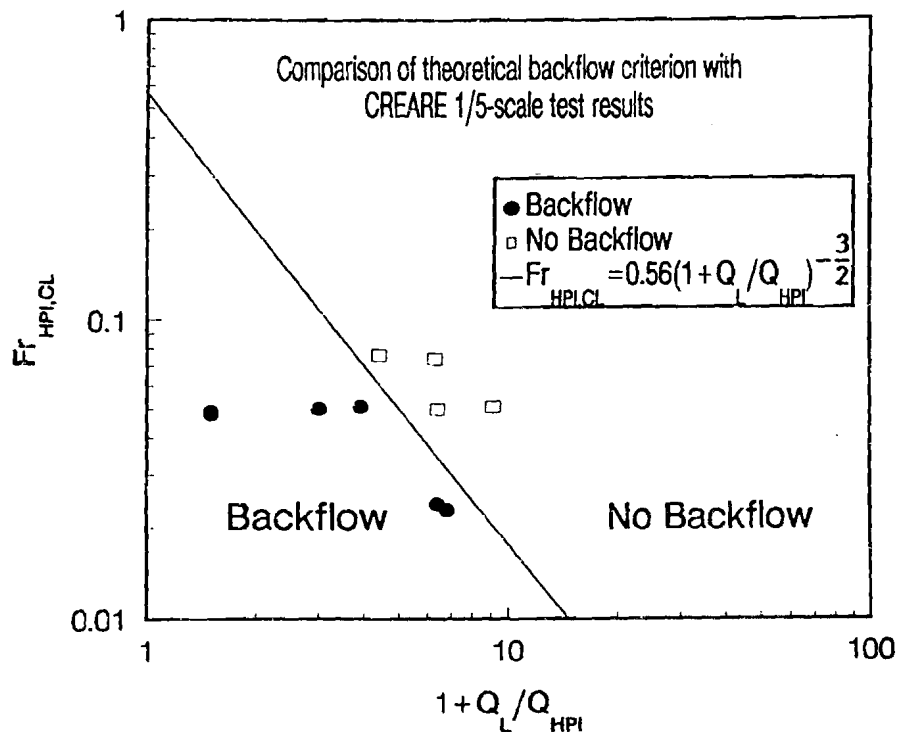


Figure 4.20 Comparison of theoretical backflow criterion, Equation (4.43) with the CREARE 1/5-scale test results

4. Physical Models

4.1.5 Mixing of the Planar Plume in the Downcomer Region Below the Cold Leg

In the regional mixing model a planar plume of initial width equal to D_{cl} , initial temperature of T_j and $Fr = 1$ is assumed to form in the downcomer within a distance of $2D_{cl}$ below the cold leg centerline. Clearly the temperature outside the plume will be $T_{m,d}$.

The turbulent jet model of Chen and Rodi^{4,6} (refer also to section 4.1.1) was adopted to obtain planar plume decay in the downcomer. The calculated results of centerline temperature and velocity variations for a planar buoyant jet with $Fr = 1$ are shown in Figure 4.21. The temperature and velocity profiles (azimuthal variations) at various axial locations are also presented in Figure 4.22 and 4.23.

The dimensionless temperature, T^* , and velocity, U^* , are defined as:

$$T^* = \frac{T - T_{m,d}}{T_j - T_{m,d}} \quad (4.46)$$

$$U^* = \frac{U}{U_i} \quad (4.47)$$

It should be noted that the decay here refers to actual heatup, and the present REMIX97 code calculates only the temperatures at the plume centerline (i.e., the lowest temperature for any given axial distance from the plume origin). However, the temperature and velocity profiles are reported here for any future need for detailed quantification of azimuthal variation of temperature and heat transfer coefficient.

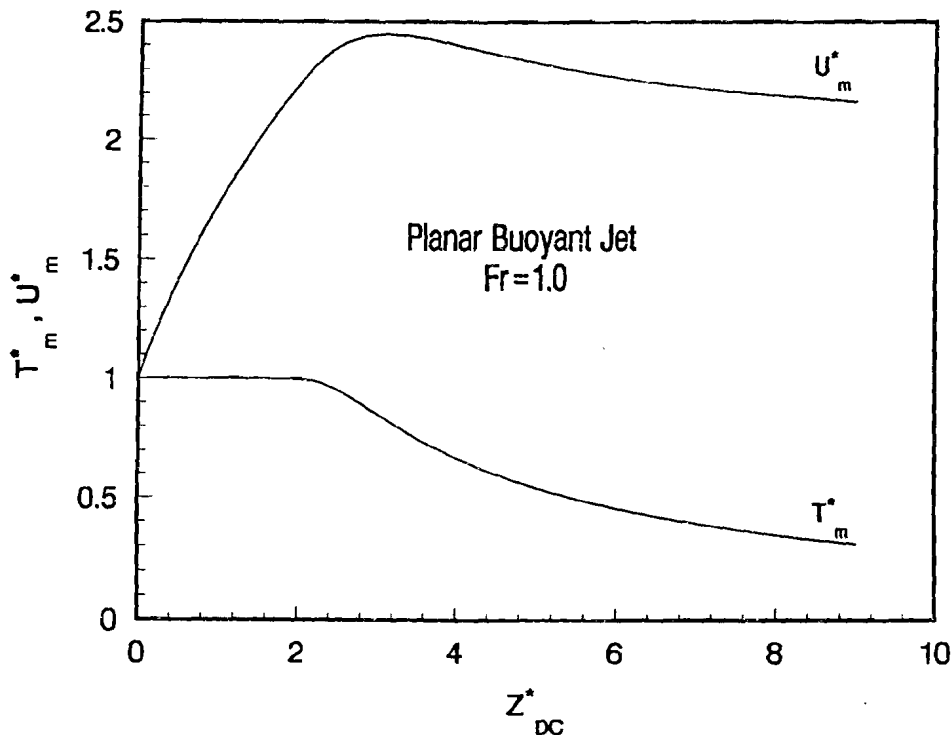


Figure 4.21 Calculated results of centerline temperature and velocity variations for a planar buoyant jet (κ - ϵ - \bar{T} turbulent jet model)

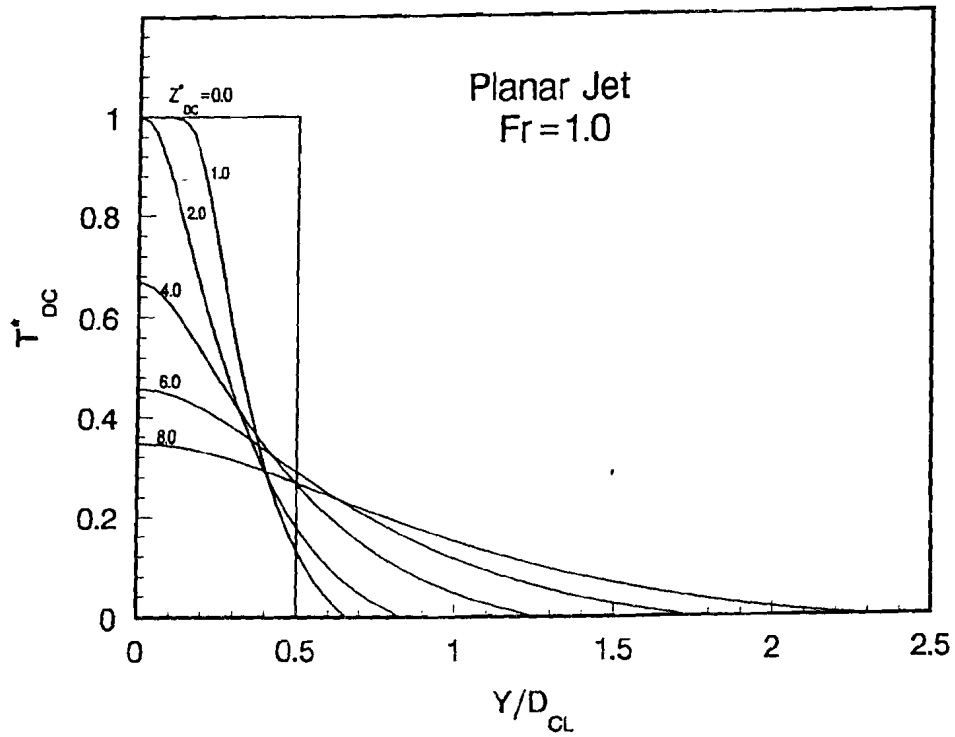


Figure 4.22 Calculated results of temperature profiles for a planar buoyant jet ($\kappa\text{-}\epsilon\text{-}\overline{T'^2}$ turbulent jet model)

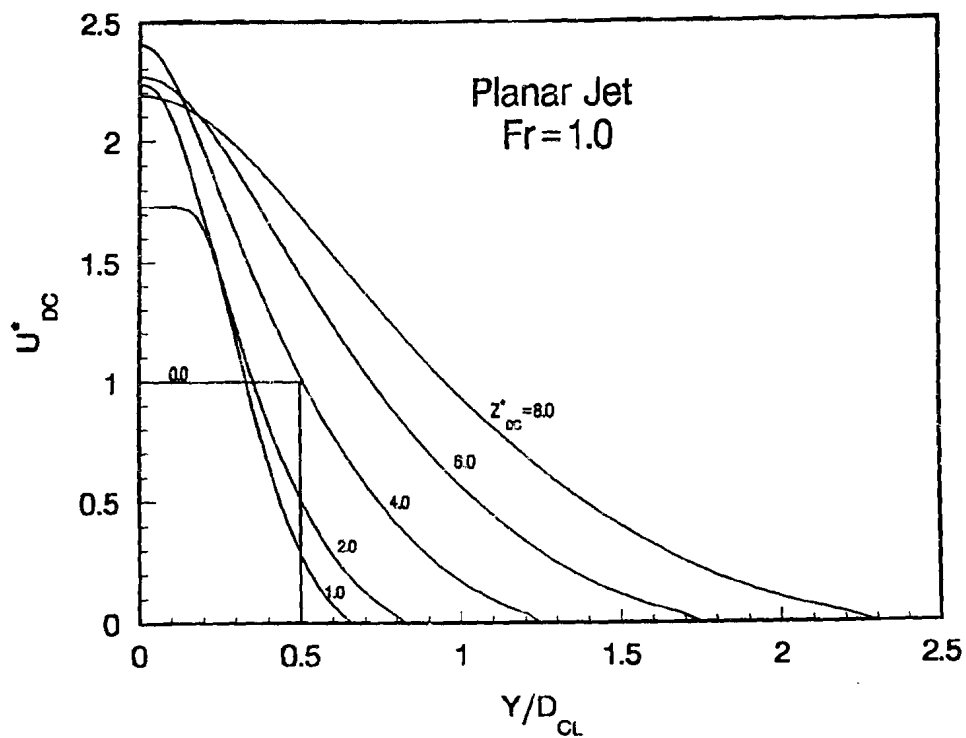


Figure 4.23 Calculated results of velocity profiles for a planar buoyant jet ($\kappa\text{-}\epsilon\text{-}\overline{T'^2}$ turbulent jet model)

4. Physical Models

4.1.6 Heat Transfer in Structures

Heat transfer within the various structures such as the vessel wall, thermal shield, etc. is modeled by heat conduction in one spatial dimension. The one dimensional heat conduction equation for a slab extending over the positive x direction is:

$$(\rho c_p)_s \frac{\partial T_s}{\partial t} = \frac{\partial}{\partial x} \left(k_s \frac{\partial T_s}{\partial x} \right) \quad (4.48)$$

where $(\rho c_p)_s$ is the volumetric heat capacity and k_s is the thermal conductivity of the structure. Initially, the structure temperature T_s is T_{s_0} . The appropriate boundary conditions for $t > 0$ are:

$$-k_s \frac{\partial T_s}{\partial x} \Bigg|_{x=0} = h_i [T_f(t) - T_s(0, t)] \quad (4.49)$$

$$-k_s \frac{\partial T_s}{\partial x} \Bigg|_{x=\delta_s} = h_o [T_s(\delta_s, t) - T_o] \quad (4.50)$$

where T_f and T_o are the fluid temperature and the outside air temperature, respectively. h_i is the convective heat transfer coefficient between the structure and the fluid. h_o is the heat transfer coefficient between the structure and the surrounding air.

Equation (4.46) together with boundary conditions Equations (4.47) and (4.48) are solved numerically to obtain the temperature distribution within various heat structures and heat fluxes to the fluid. The fully implicit subdomain method^{4.21} (control volume formulation) was used to derive the discretization equations. The solution of the resulting discretization equations are obtained by the standard Gaussian elimination method. Because of the particularly simple form of equations, the elimination process turns into the convenient Thomas algorithm or the Tri-Diagonal-Matrix Algorithm (TDMA).

4.1.7 Convective Heat Transfer Coefficient

The values for convective heat transfer coefficients between structures and the primary fluid are provided as a part of the input data to the REMIX97 code. The heat transfer coefficient between the vessel wall and water flow in downcomer can be calculated based on the Fewster-Jackson correlation:^{4.22}

$$\frac{Nu}{Nu_\infty} = \left(1 + 4500 \frac{Gr}{Re^{2.63}} \right)^{0.31} \quad (4.51)$$

$$Nu_\infty = 0.023 Re^{4/5} Pr^{1/3} \quad (4.52)$$

Equation (4.49) indicate an augmentation of heat transfer from its forced convection value (Nu_∞) with increasing wall surface temperature.

4.1.8 Equations of State

The following equations of state for water, which are polynomial fits accurate to ~0.5% in the range of interest (20°C to 300°C), are used in the REMIX97 code:

$$\rho = 62.733 - 4.955 \times 10^{-3} T - 3.745 \times 10^{-5} T^2 - 1.661 \times 10^{-8} T^3 \quad (4.53)$$

$$T = 32.102 + 0.991 h + 1.074 \times 10^{-4} h^2 - 3.562 \times 10^{-7} h^3 \quad (4.54)$$

$$h = -33.419 + 1.041 T - 2.7995 \times 10^{-4} T^2 + 5.724 \times 10^{-7} T^3 \quad (4.55)$$

where ρ is density in lbm/ft^3 , T is temperature in $^\circ\text{F}$ and h is enthalpy in Btu/lbm .

4.2 Solution Procedure

The extended regional mixing model formulated in previous sections are solved numerically to predict the downcomer fluid temperature transients due to safety injection of the cold coolant jet into the hot loop flow.

For low Froude number injections, the entrainment rate at the safety injection point is restricted by buoyant jet mixing rates as well as the flow limitations in downstream and upstream region of the cold leg. The general solution procedure pertinent to low Froude number injections is shown in Figure 4.24. A triple iteration scheme is used in REMIX97. First, initial estimates for the hot stream depth in the downstream region of the cold leg, $d_{h,d}$, the hot stream depth in the upstream region of the cold leg, $d_{h,u}$, and the ambient temperature to the safety injection jet, T_a , are chosen. Based on these quantities, the rate of entrainment to the jet, Q_e , the flow split ration, α , the cold stream volumetric flow rate, Q_c , temperature of the cold streams, T_c , the hot stream volumetric flow rate in the upstream region, $Q_{h,u}$, hot stream temperature in the upstream region, $T_{h,u}$, and the upstream mixed mean temperature, $T_{m,u}$, are determined. The condition of stationarity of long, neutrally stable waves between the cold and hot streams in the upstream region of the cold leg (Equation (4.15)) is then tested. If this equation is not satisfied, within a give tolerance, a new value for $d_{h,u}$ is chosen and the calculation is repeated until convergence is achieved. The interval halving method is used to obtain $d_{h,u}$ iteratively. Calculation is then carried out to determine the hot stream volumetric flow rate in the downstream region, $Q_{h,d}$, hot stream temperature in the downstream region, $T_{h,d}$, and the downstream mixed mean temperature, $T_{m,d}$. The depth of hot stream in the downstream region, $d_{h,d}$ is then obtained iteratively until the condition of stationarity of long, neutrally stable waves between the cold and hot streams in the downstream region of the cold leg (Equation (4.16)) be satisfied. Here again, the interval halving method

is used to find $d_{h,d}$. The energy balance for a control volume around the injection mixing region (Equation (4.6)) together with the energy balance for a control volume enclosing the jet boundaries (Equation 4.8)) are used to recalculate the ambient temperature to the jet, T_a , based on calculated $Q_{h,u}$, $Q_{h,d}$, $h_{h,u}$ and $h_{h,d}$. If the recalculated value of T_a is not acceptable, a new value for T_a is chosen, and the procedure is repeated until convergence is achieved. A successive underrelaxation method is used to obtain new values for T_a . Finally, the temperature distribution within the planar plume in the downcomer is calculated.

The solution procedure for calculating the cooldown transient on the basis of maximum entrainment, pertinent to high Froude number injections, is shown in Figure 4.25. Unlike the original NEWMIX code calculations, the present solution procedure does not require an analytical relationship between the depth of the cold stream and the maximum entrainment rate. The solution procedure for this case is somewhat similar to the one used for low Froude number injection. Except that there Q_e is obtained iteratively until the value of maximum entrainment restricted by flow limitations is obtained.

4.3 Overview of REMIX97 Code

The extended regional mixing model formulations and their solution methods described in previous sections has been implemented in a computer code called REMIX97. The formulation has been augmented with solute mass balances and appropriate equation of state. Thus, with the proper choice of input option parameter, the REMIX97 is also appropriate for applications to experimental simulations involving solute-, or thermal/solute-, induced buoyancy (refer to chapter 5).

In addition to adequacy in modeling of important processes and phenomena, a modular, highly structured and user friendly architecture was required to facilitate both the present modeling improvement to the code and any later modification and/or addition of models. To avoid portability problems, adherence to

4. Physical Models

ANSI standard FORTRAN 77 was desirable for the coding of REMIX97. Finally, an architecture compatible with the short run-times necessary for sensitivity analyses was also required.

The input for REMIX97 is entered via name list. A user's manual for the code is provided in Appendix A.

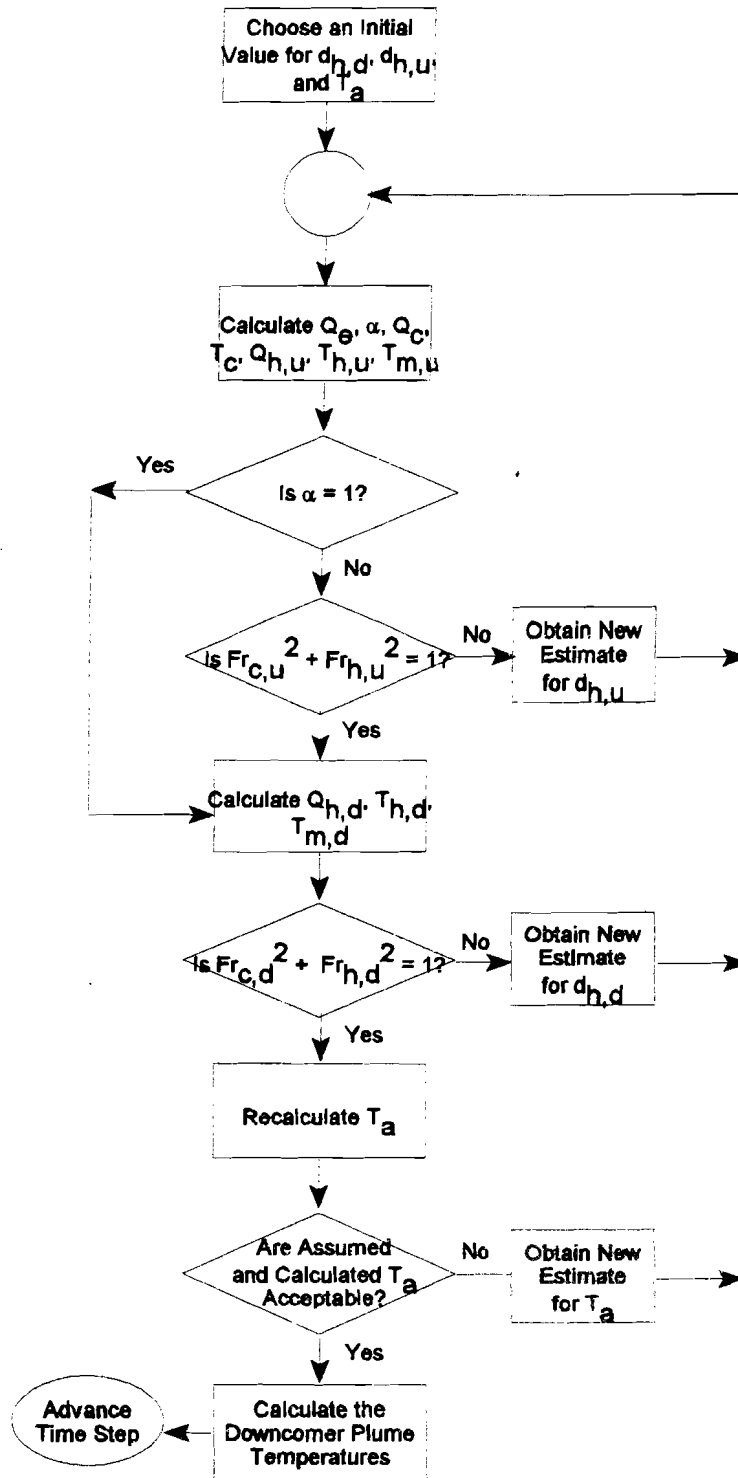


Figure 4.24 General solution procedure for calculating the cooldown transient, pertinent to low Froude number injections

4. Physical Models

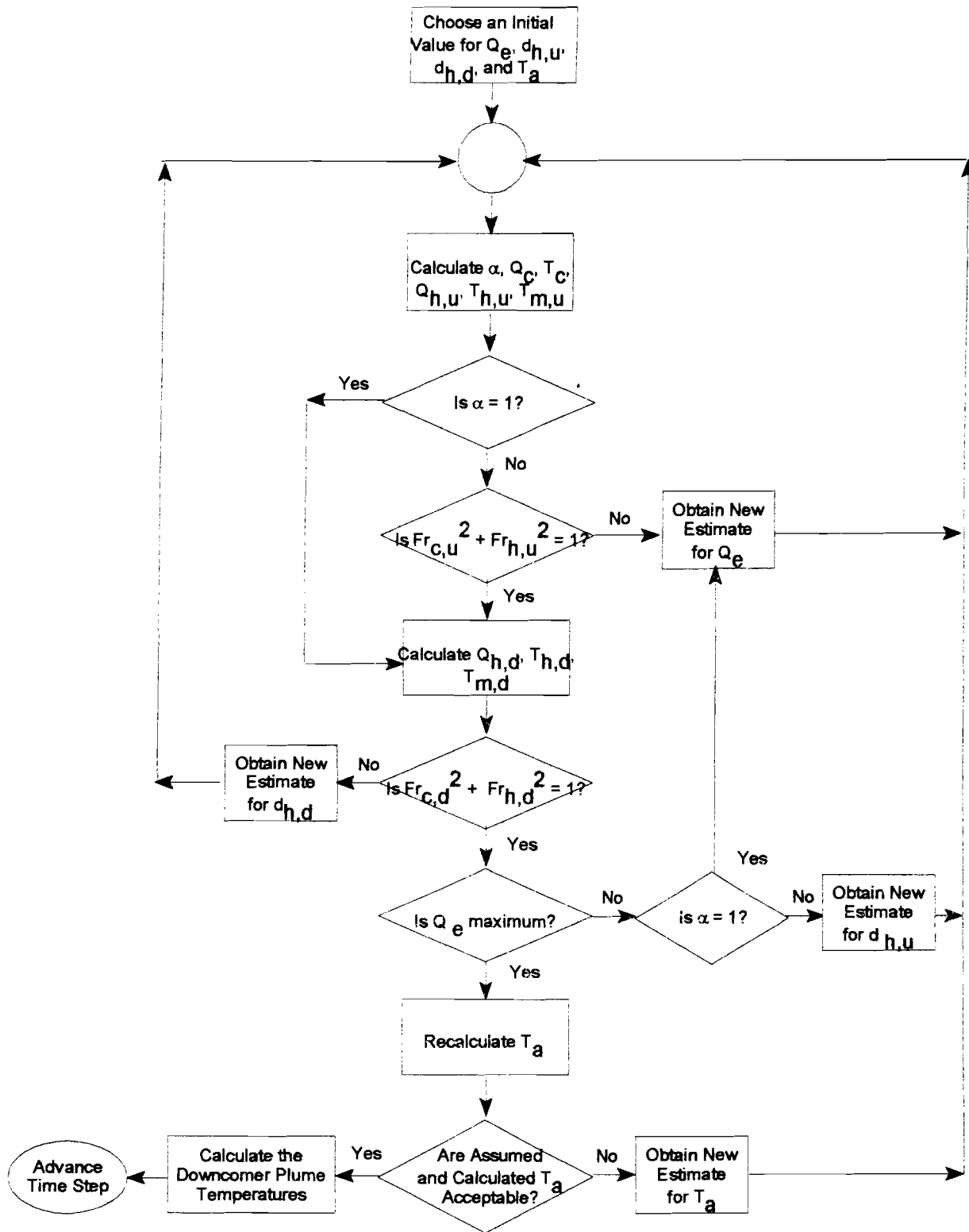


Figure 4.25 General solution procedure for calculating the cooldown transient on the basis of maximum entrainment, pertinent to high Froude number injections

4.4 References

- 4.1 T. G. Theofanous and H. P. Nourbakhsh, "PWR Downcomer Fluid Temperature Transients Due to High Pressure Injection at Stagnated Loop Flow," Proc. Joint NRC/ANS Meeting on Basic Thermal Hydraulic Mechanisms in LWR Analysis, September 14, 15, 1982, Bethesda, Maryland, NUREG/CP-0043, 583-613, 1983.
- 4.2 H. P. Nourbakhsh and T. G. Theofanous, "Decay of Buoyancy-Driven Stratified Layers with Application to Pressurized Thermal Shock, Part I: The Regional Mixing Model," Nucl. Eng. & Design, (in press).
- 4.3 K. Iyer, H. P. Nourbakhsh, and T. G. Theofanous, "REMIX: A Computer Program for Temperature Transients Due to High Pressure Injection After Interruption of Natural Circulation," U.S. Nuclear Regulatory Commission, NUREG/CR-3701, May 1986.
- 4.4 T. G. Theofanous and H. Yan, "A Unified Interpretation of One-Fifth to Full-Scale Thermal Mixing Experiments Related to Pressurized Thermal Shock," NUREG/CR-5677, 1991.
- 4.5 J. S. Turner, *Buoyancy Effects in Fluids*, Cambridge University Press, 1979.
- 4.6 C. J. Chen and W. Rodi, "A Mathematical Model for Stratified Turbulent Flows and Its Application to Buoyant Jets," XVIth Congress, International Association for Hydraulic Research, San Paulo, 1975.
- 4.7 S. V. Patankar and D. B. Spalding, "A Finite Difference Procedure for Solving the Equations of the Two Dimensional Boundary Layer," Intl. J. of Heat and Mass Transfer, Vol. 10, 1389-1411, 1968.
- 4.8 C. J. Chen and Nikitopoulos, "On the Near Field Characteristics of Axisymmetric Turbulent Buoyant Jets in a Uniform Environment," Intl. J. Heat and Mass Transfer, Vol. 22, 245-254, 1979.
- 4.9 C. J. Chen and Chen, "On Prediction and Unified Correlation for Decay of Vertical Buoyant Jets," Journal of Heat Transfer, Vol. 102, 532-537, 1979.
- 4.10 T. G. Theofanous, H. P. Nourbakhsh. P. Gherson, et al., "Decay of Buoyancy Driven Stratified Layers with Application to PTS," Proceedings of the U.S. NRC Eleventh Water Reactor Safety Research Information Meeting, NUREG/CP-0048, Vol. 2, 91-114, October 1983.
- 4.11 E. A. Hirst, "Analysis of Round, Turbulent, Buoyant Jets Discharged to Flowing Stratified Ambients," Oak Ridge National Laboratory, ORNL-4685, 1971.
- 4.12 G. Abraham, "Horizontal Jets in Stagnant Fluid of Other Density," J. Hydraul. Div., Am. Soc. Civil Eng., Vol. 9, 139-154, 1965.
- 4.13 B. Gebhart, D. S. Hilder, and M. Kelleher, "The Diffusion of Turbulent Buoyant Jets,"
- 4.14 E. J. List and J. Imberger, "Turbulent Entrainment in Buoyant Jets and Plumes," J. Hydraul. Div., Am. Soc. Civil Eng., Vol. 99, 1461-1474, 1973.
- 4.15 L. N. Fan, "Turbulent Buoyant Jets into Stratified or Flowing Ambient Fluids," Keck Laboratory of Hydraulics and Water Resources, California Institute of Technology, Report No. KH-R-15, 1967.
- 4.16 J. B. King and J. N. Reyes, "Buoyant Backflow in Vertical Injection Lines,"

4. Physical Models

NURETH

- 4.17 J. A. Valenzuela and P. H. Rothe, "Flow Visualization During Transient Cooldown in a Model PWR Cold Leg and Downcomer," EPRI NP-3871, February 1985.
- 4.18 T. G. Theofanous, K. Iyer, H. P. Nourbakhsh, and P. Gherson, "Buoyancy Effects in Overcooling Transients Calculated for the NRC Pressurized Thermal Shock Study," NUREG/CR-3702, U. S. Nuclear Regulatory Commission, May 1986.
- 4.19 P. H. Rothe and M. W. Fanning, "Thermal Mixing in a Model Cold Leg and Downcomer at Low Flow Rates," EPRI NP-2935, March 1983.
- 4.20 M. W. Fanning and P. H. Rothe, "Transient Cooldown in a Model Cold Leg and Downcomer," EPRI NP-3118, May 1983.
- 4.21 S. V. Pantankar, **Numerical Heat Transfer and Fluid Flow**, New York, Hemisphere Publishing Corp., 1980.
- 4.22 J. D. Jackson and J. FEWSTER, "Enhancement of Turbulent Heat Transfer Due to Buoyancy for Downward Flow of Water in Vertical Tubes," in **Heat Transfer and Turbulent Buoyant Convection** by D. B. Spalding and N. Afgan, New York, Hemisphere Publishing Corp., 1997.

5. CODE VERIFICATION AND VALIDATION

The REMIX97 code has been subjected to a detailed line by line examination to ensure that models have been implemented as intended. Informal tests were also performed to ensure each module and combination of modules are correct.

Thermal mixing in relation to pressurized thermal shock has been examined experimentally throughout the world. The original regional mixing model and associated computer programs REMIX and NEWMIX has been successfully employed to interpret much of the available thermal mixing experimental data obtained from the system simulation tests performed under stagnated loop flow conditions.^{5.1-5.3}

The REMIX97 code were also used to predict various cooldown transients under stagnated loop flow conditions. The results were found to be consistent with the validated results of REMIX/NEWMIX code.

In this chapter a brief description of the world thermal mixing test facilities is presented. Comparison of REMIX97 prediction with all of the available experimental data obtained from these test facilities is beyond the scope of the present study. However, in order to evaluate the technical adequacy of REMIX97 code, the code was used to predict a limited set of data that are relevant to U.S. reactors. These data were obtained under a wide range of experimental conditions including low Froude number injections of interest to Westinghouse and Combustion Engineering designed reactors and very high Froude number HPI injections of interest to

Babcock & Wilcox designed reactors. The experimental conditions also included presence of low loop flow, solute and/or thermally induced buoyancy and concentration or temperature measurement as an indication of mixing. The results of these validation efforts are also discussed in this chapter.

5.1 Overview of the Thermal Mixing Test Facilities

In the 1980's, both U.S. NRC and EPRI sponsored large experimental research programs to establish a data base for thermal mixing phenomena in various integral test facilities. Additional tests were also performed in Belgium,^{5.4} Finland,^{5.5,5.6} Germany,^{5.7,5.8} and Japan.^{5.9} The major characteristics of the world's thermal mixing test facilities are summarized in Table 5.1. In addition to their wide variation in geometric scale and the HPI injector nozzle characteristics (size, location, and orientation), these facilities were operated under a wide range of conditions.

CREARE-1/5,^{5.10-5.14} IVO,^{5.5,5.6} SAI,^{5.15} and Japanese^{5.9} facilities were run at atmospheric conditions with solute induced buoyancy, but mixing was inferred from temperature measurements. Purdue experiments^{5.16} were performed with water and brine at room temperature and mixing was obtained from concentration measurements. The CREARE-1/2,^{5.17,5.18} UCL/TRACT,^{5.4} HDR,^{5.7,5.19} and UPTF^{5.8} tests were all run at high pressure with thermally-induced buoyancy and used temperature as the tracer.

5. Code Verification and Validation

Table 5.1 Comparison of the world PTS thermal mixing facilities

Facility (Country)	Organization/Sponsor	Scale	Downcomer Geometry	No. of Cold Legs	HPI Location (Orientation)	Loop Flow
CREARE (USA)	CREARE, Inc./EPRI	1/5	Planar	1	Top (60° & 90°)	Yes
Japanese	Mitsubishi Heavy Industries, Ltd./ Kansai Electric Co., Inc.	1/3	Planar	1	Top (45° & 90°)	Yes
IVO (Finland)	Imatran Volma Oy/ IVO	2/5	Semiannular	3	Bottom	Yes
IVO (Finland)	Imatran Volma Oy/ U.S. NRC	2/5	Semiannular	3	Top	
PURDUE (USA)	Purdue Univ./ U.S. NRC	1/2	Planar	1	Top and side	No
CREARE (USA)	CREARE, Inc./ U.S. NRC and EPRI	1/2	Planar	1	Top (90°)	No
UCL/TRAC (Belgium)		1/2	Planar	1	Top and downcomer	
SAI (USA)	SAI/EPRI	1/1	Planar	1	Top	Yes
HDR (Germany)	Battelle Institute/BMTF	1/4- 1/1	Annular	1	Top and side	Yes
UPTF (Germany)	KWU/BMTF	1/1	Annular	1	Top	

The IVO facility is unique in applying multi-loop injection to study the plume interactions in a semiannular (circumferentially 1/2) downcomer representation. The original IVO test program was aimed at simulation of Russian-designed Loviisa reactor (a VVER-440 with a small HPI nozzle located at the bottom of the cold leg) in Finland. However, the IVO facility was also modified (with a larger HPI nozzle located at top of cold leg) to simulate U.S. reactor conditions.

The HDR facility, which is the only facility operating at a pressure as high as 11 MPa, does not comply

with the principle of strict geometrical similarity as compared to real plants. The HDR experiments with a reduced scale of downcomer gap (1/2) and cold leg (1/4) involved single loop operation on a fully three-dimensional downcomer representation.

In performing thermal mixing experiments, emphasis was placed on those experiments where cold HPI-coolant was injected into a stagnant system. However, experiments with injection into the cold leg with finite loop flows were also performed in some of the test facilities.

5.2 Comparison of Code Predictions with CREARE 1/5-Scale Test Data

The present extended regional mixing model and associated computer code REMIX97 was applied to some of the CREARE 1/5-scale tests. Comparisons of the code prediction with the experimental measurements are presented here.

Transient cooldown tests were performed in CREARE 1/5-scale, transparent model typical of Combustion Engineering and Westinghouse reactors

A number of different geometric configurations were tested, but they all had the horizontal cold leg and planar downcomer in Common. The different configurations were variations of the two basic geometries, MIX3 and MIX4, schematic of which together with thermocouple locations are shown in Figures 5.1 and 5.2. The relevant geometric features of MIX4 test facility is presented in Table 5.2

Some of the tests were carried out with thermally induced buoyancy and some with solute induced buoyancy while the temperature was used as a "tracer."

Table 5.2 Geometric data of CREARE 1/5-scale test facility (MIX4)

	Cold Leg	Vessel/ Downcomer	Lower Plenum	Pump	Loop Seal	Core Barre I	Thermal Shield
Inner diameter (cm)	14.29	—	—	—	14.29	—	—
Length (cm)	157.97	121.16	—	—	121.90	121.16	84.46
Acrylic wall thickness (cm)	1.27	1.90	1.27	—	1.27	1.90	1.27
Wall heat transfer area to water ($\text{cm}^2 \times 10^{-3}$)	7.9	8.16	7.90	4.76	5.47	8.16	11.37 ^(a)
Fluid volume ($\text{cm}^3 \times 10^{-3}$)	25.34 ^(b)	30.48	42.30	32.54	19.55	—	—

(a) both sides included

The MIX3 test program^{5,14} focused on situations with low flow ratio ($Q_L^* < 5$). The MIX3 test facility was later modified to MIX4 by adding a lower plenum, a

pump simulator and a loop seal. All the MIX4 tests were performed with zero loop flow.^{5,11}

5. Code Verification and Validation

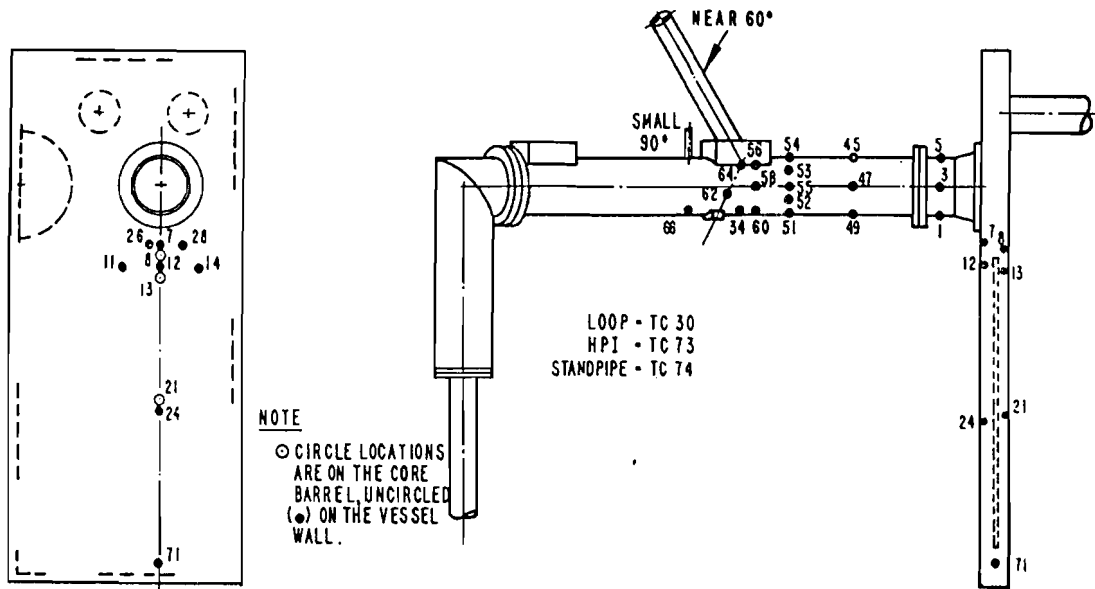


Figure 5.1 Schematic of CREARE 1/5-scale (MIX3) test facility

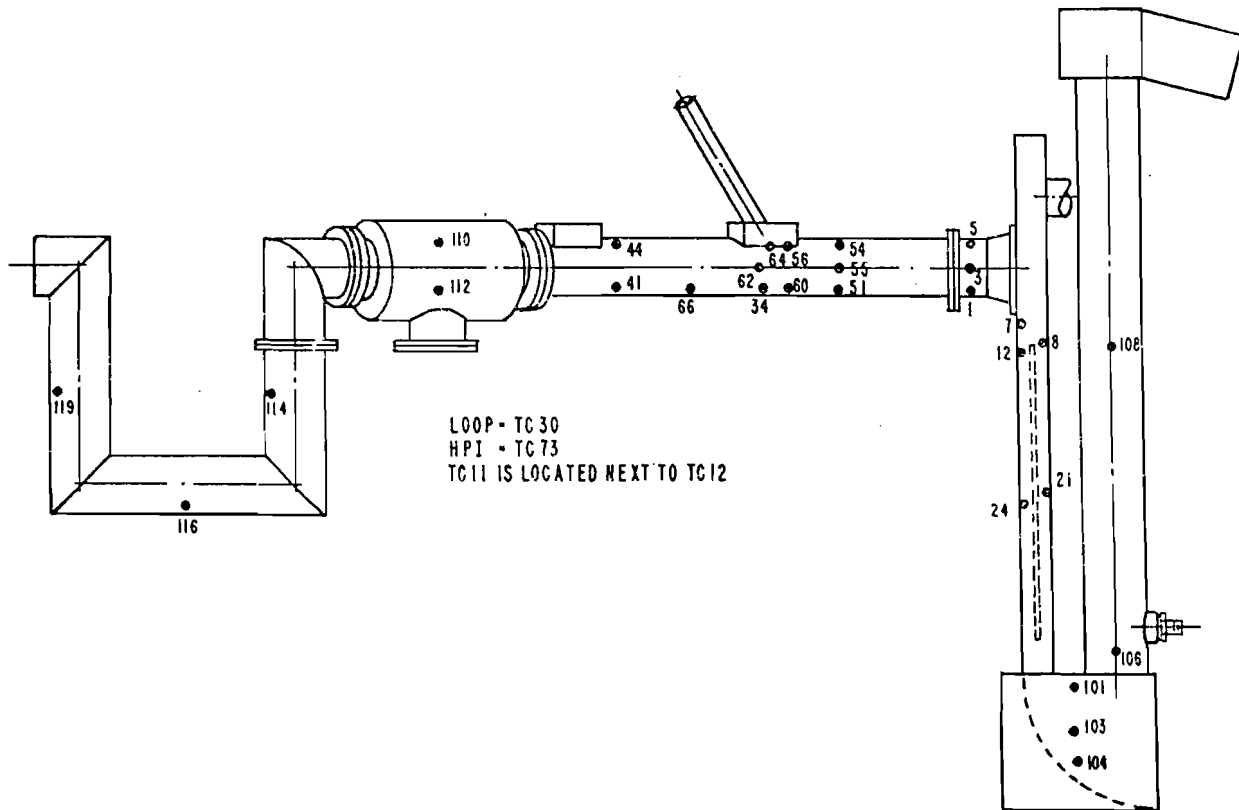


Figure 5.2 Schematic of CREARE 1/5-scale (MIX4) test facility

In addition to quantitative temperature data obtained from the MIX3 and MIX4 test programs, a series of flow visualization tests were also conducted in MIX4 geometry. Localized dye injection within the model and controlled cooling of the HPI water were used to mock the flow patterns. The same test conditions were run repeatedly to film different views and to obtain data throughout the transient without dye accumulation in the facility. In addition to qualitative descriptions of the flow patterns in various regions of the facility, many quantitative data including HPI buoyant jet entrainment rate and flow split ratio were obtained based on velocity and density measurements.^{5,20}

In an attempt to reasonably represent the variations in both geometric configurations and experimental conditions a total of four experimental runs were

chosen for the present code validation efforts. Test numbers and respective experimental conditions are summarized in Table 5.3. In addition to the temperature data, REMIX97 code predictions were also compared to the HPI buoyant jet entrainment rate and flow split ratio data obtained from the velocity and density measurements of flow visualization study.

Figure 5.3 shows the REMIX97 predictions for time variation of the HPI entrainment rate as compared to the results obtained from the CREARE 1/5-scale tests. The entrainment rates were computed from both velocity and density profile measurements. Also shown in Figure 5.3 are the entrainment rates predicted by the original REMIX code. The REMIX97 predictions are consistent with the results of original REMIX code and compares well with the experimental results.

Table 5.3 Test conditions of CREARE 1/5-scale tests used for REMIX97 code comparisons

Test No.	Geometry	T/S	ρ_L (kg/m ³)	ρ_{HPI} (kg/m ³)	\dot{m}_{HPI} (kg/s)	Q_L^*	Fr_{HPI}
71	MIX3 (CE)	T ^(a)	979.7	997.6	0.064	2.223	0.32
74	MIX3 (CE)	T	978.7	998	0.135	0.533	0.64
100	MIX4 (CE)	S ^(b)	980.0	1164	0.441	0	0.68
106	MIX3/MIX4	T	978.3	998	0.126	0	0.57
Flow visualization tests	MIX4 (CE)	S	980.0	1164	0.33	0	0.51

(a) T = thermally induced buoyancy

(b) S = solute induced buoyancy

(c) This geometry was a hybrid of MIX3 and MIX4 facilities. It includes the cold leg and downcomer common to MIX3, MIX4, and the lower plenum and standpipe, but not the pump simulator or loop seal of MIX4.

5. Code Verification and Validation

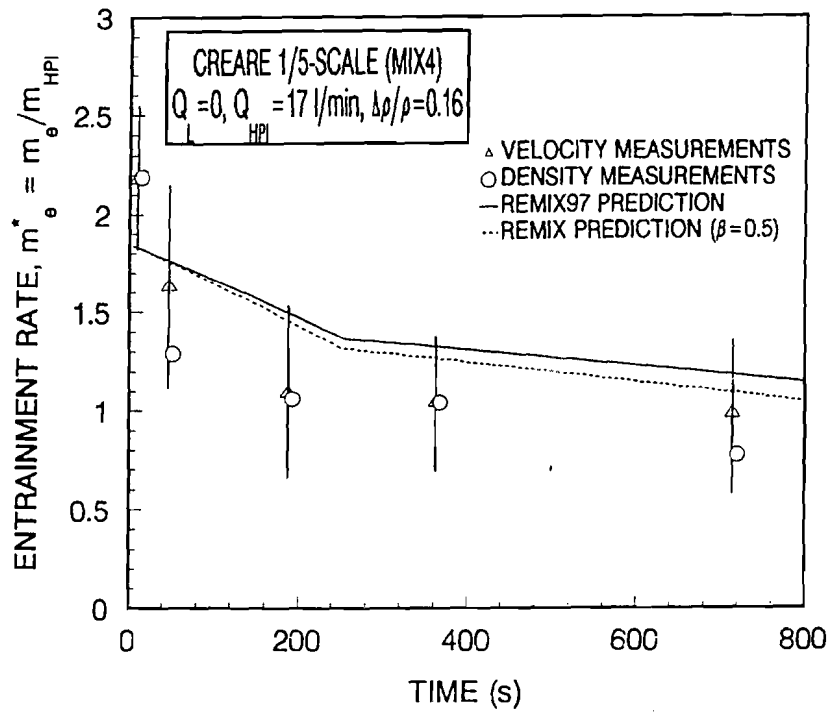


Figure 5.3 Comparison of HPI entrainment rate between code predictions and CREARE 1/5-scale data

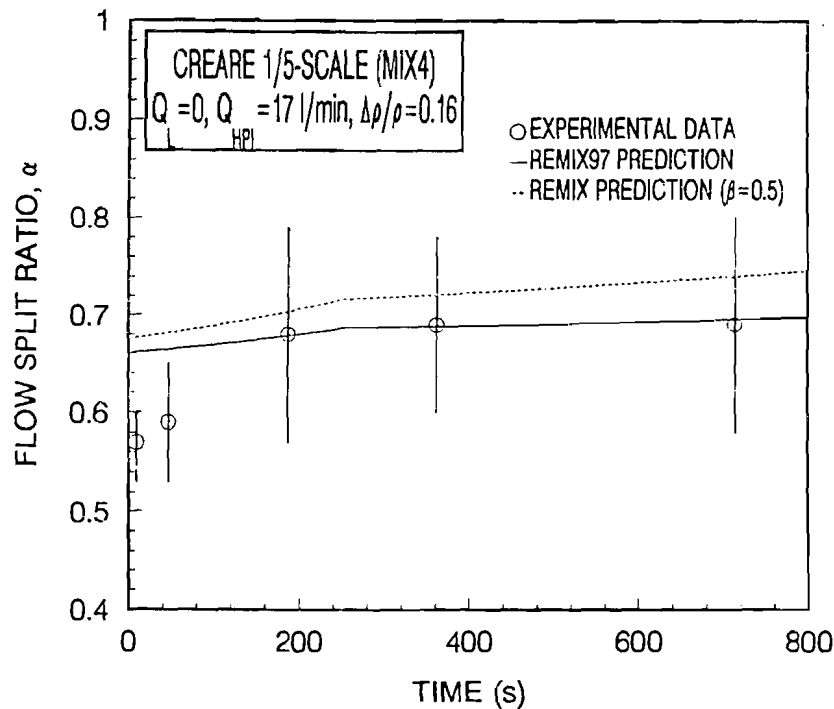


Figure 5.4 Comparison of HPI buoyant jet flow split ratio between code predictions and CREARE 1/5-scale data

Comparison of HPI buoyant jet flow split ratio, α , between REMIX97 code predictions and data obtained from CREARE 1/5-scale tests are shown in Figure 5.4. Except for the initial part of the transient, the predicted flow split ratio shows excellent agreement with the test data. Also shown in Figure 5.4 are the flow split ratios predicted by the original REMIX code using an input value of 0.5 for a fraction of plume entrainment supplied from downcomer side, ($\beta = 0.5$). As shown in Figure 5.4, REMIX predicts higher flow split ratios than the REMIX97 predictions.

The REMIX code predictions of cooldown transients under low loop flow conditions are compared to the experimental data of tests 71 and 74 in Figures 5.5 through 5.16. The agreement is excellent. In the comparison of downcomer fluid temperatures, the predicted results for both the downcomer planar plume temperature and the mixed mean (well mixed)

temperature of the downstream region, $T_{m,d}$, are presented. With the presence of thermal shield in these tests, the plume is contained between the core barrel and the thermal shield. Therefore, the downcomer fluid temperatures along the vessel wall is nearly uniform and equal to the predicted $T_{m,d}(t)$, while the downcomer fluid temperatures in the core side are in agreement with the predicted plume temperature. It should be noted that the REMIX97 code capability to address the cooldown behavior under low loop flow conditions has been tested in an absolute prediction mode without benefit of any adjustable empirical input parameter.

Figures 5.16 through 5.31 show the REMIX97 predictions for cooldown transients under stagnated loop flow condition as compared to the results obtained from the tests 100 and 106 excellent agreement is noted.

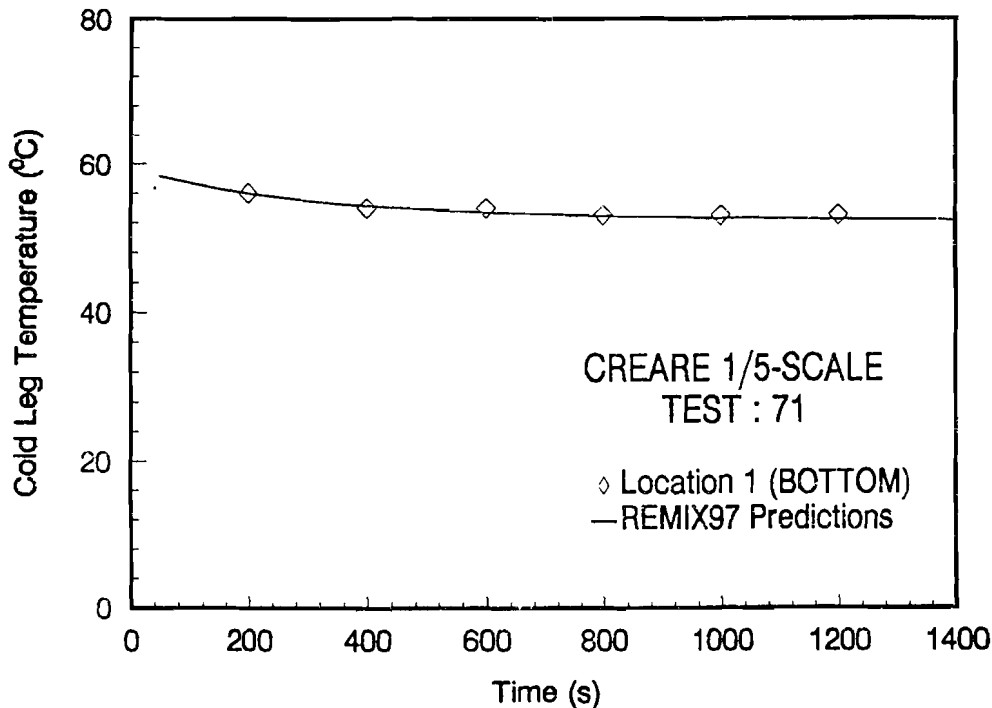


Figure 5.5 Comparison of the fluid temperature transients at the bottom of the cold leg for CREARE 1/5-scale test No. 71 with the REMIX97 prediction

5. Code Verification and Validation

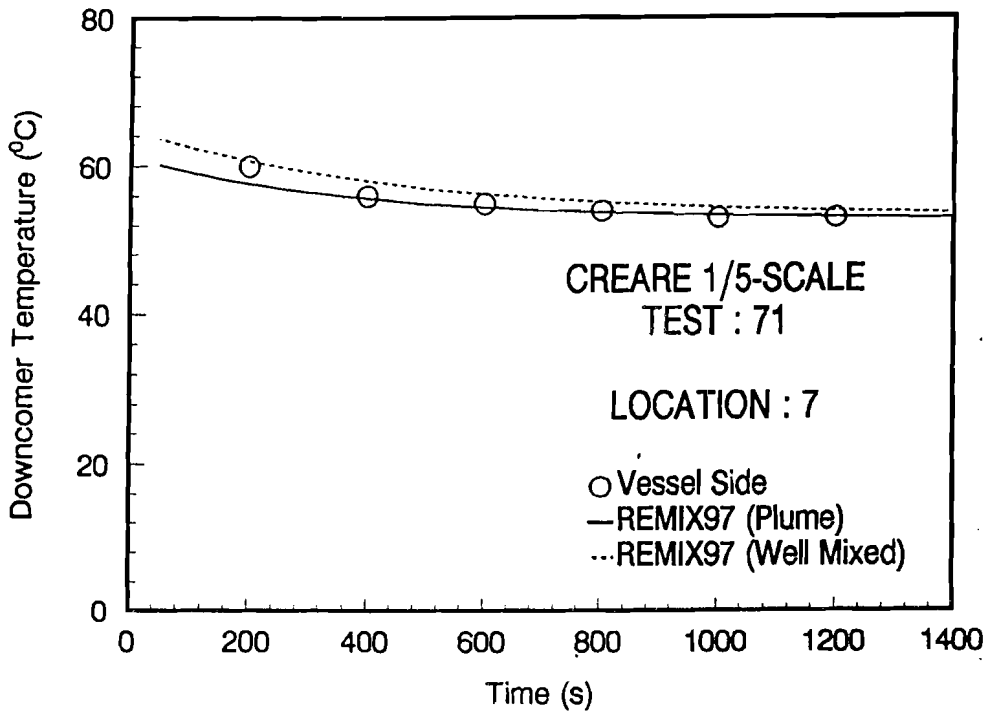


Figure 5.6 Comparison of the downcomer fluid temperature transients for CREARE 1/5-scale test No. 71 with the REMIX97 prediction (for thermocouple location 7; refer to Figure 5.1)

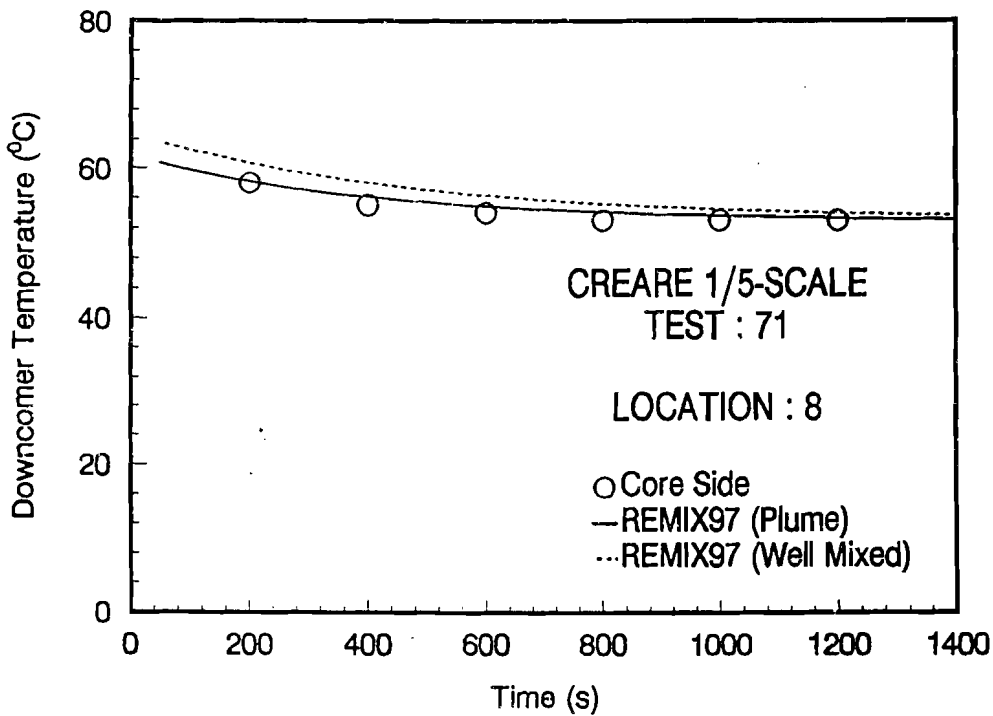


Figure 5.7 Comparison of the downcomer fluid temperature transients for CREARE 1/5-scale test No. 71 with the REMIX97 prediction (for thermocouple location 8; refer to Figure 5.1)

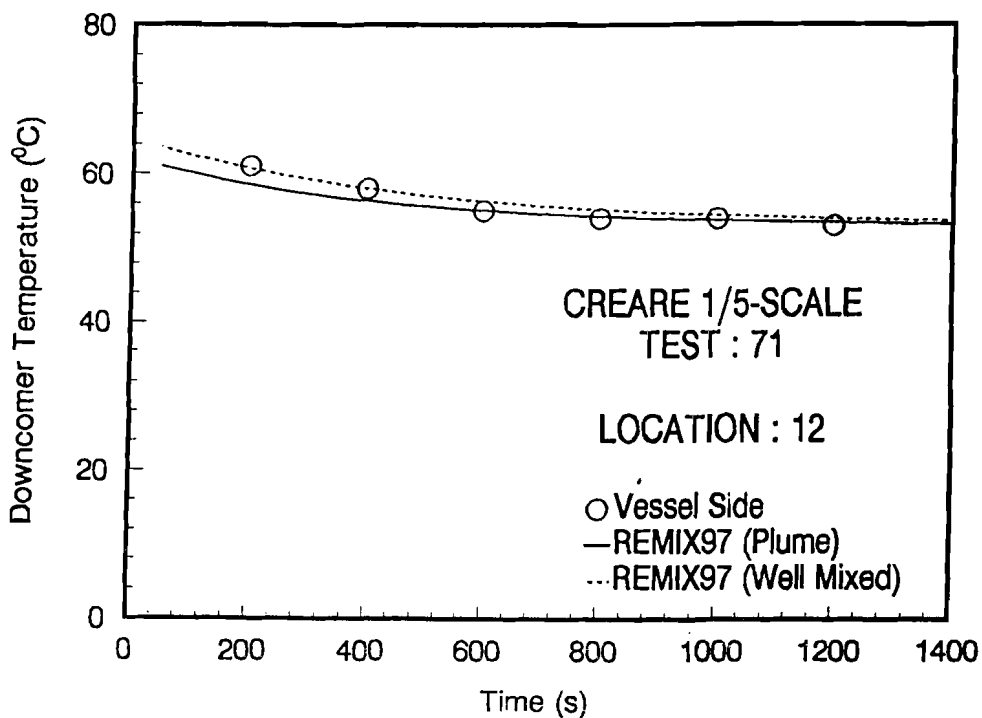


Figure 5.8 Comparison of the downcomer fluid temperature transients for CREARE 1/5-scale test No. 71 with the REMIX97 prediction (for thermocouple location 12; refer to Figure 5.1)

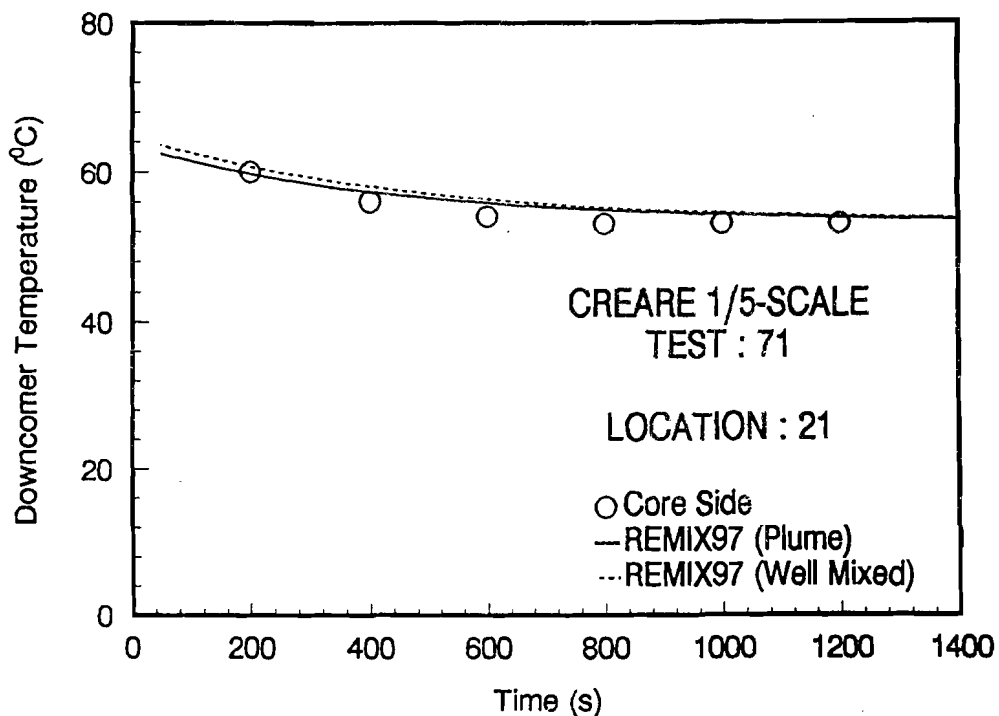


Figure 5.9 Comparison of the downcomer fluid temperature transients for CREARE 1/5-scale test No. 71 with the REMIX97 prediction (for thermocouple location 21; refer to Figure 5.1)

5. Code Verification and Validation

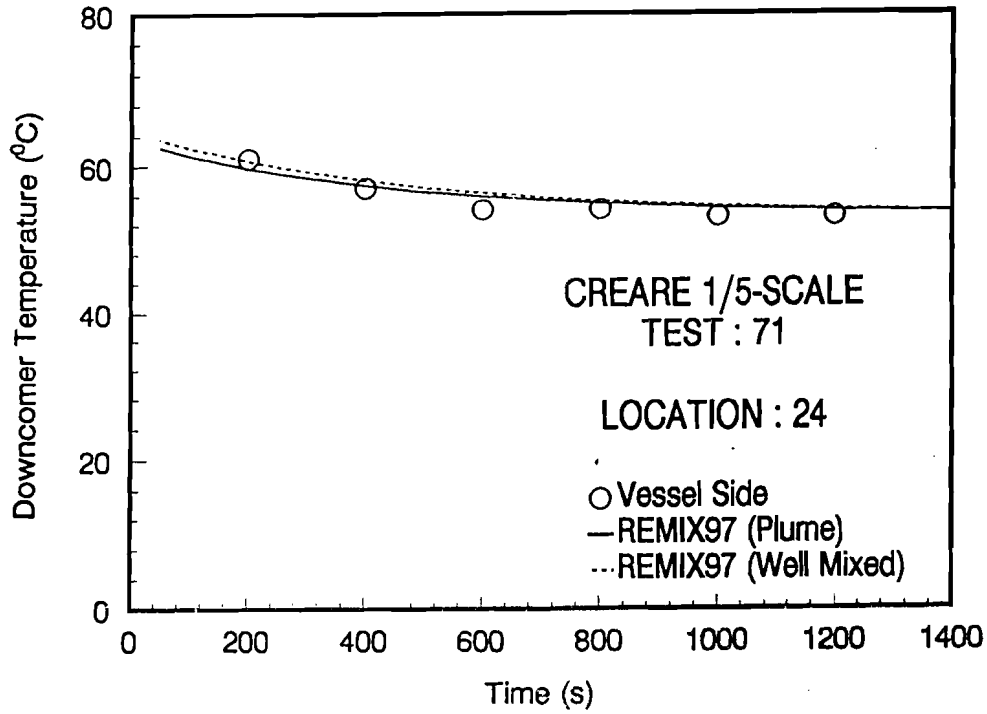


Figure 5.10 Comparison of the downcomer fluid temperature transients for CREARE 1/5-scale test No. 71 with the REMIX97 prediction (for thermocouple location 24; refer to Figure 5.1)

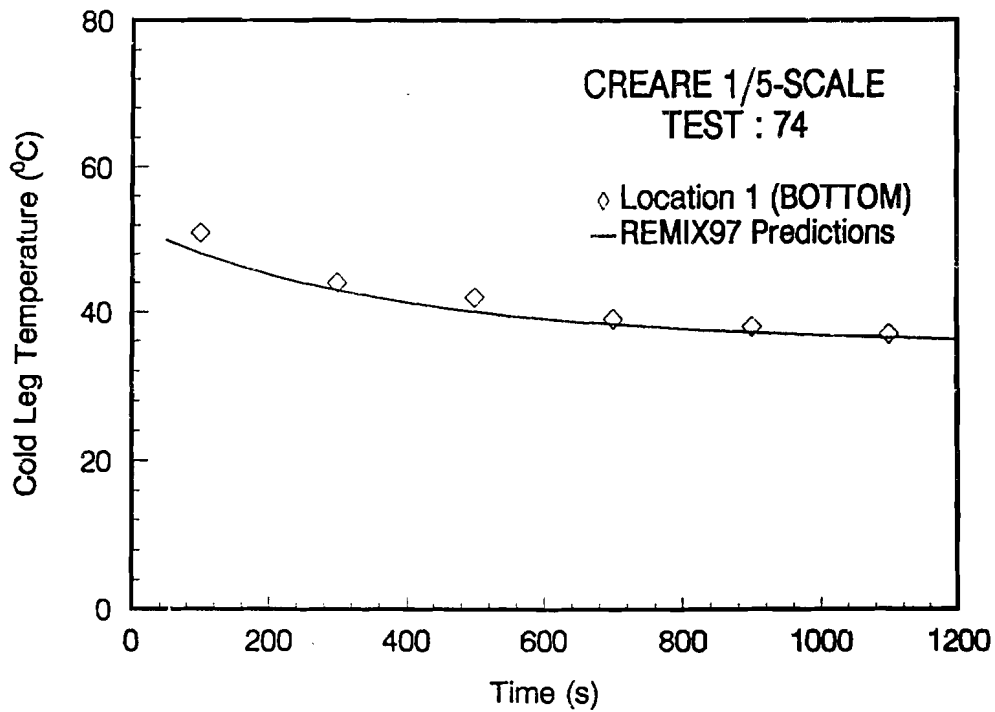


Figure 5.11 Comparison of the fluid temperature transients at the bottom of the cold leg for CREARE 1/5-scale test No. 74 with the REMIX97 prediction

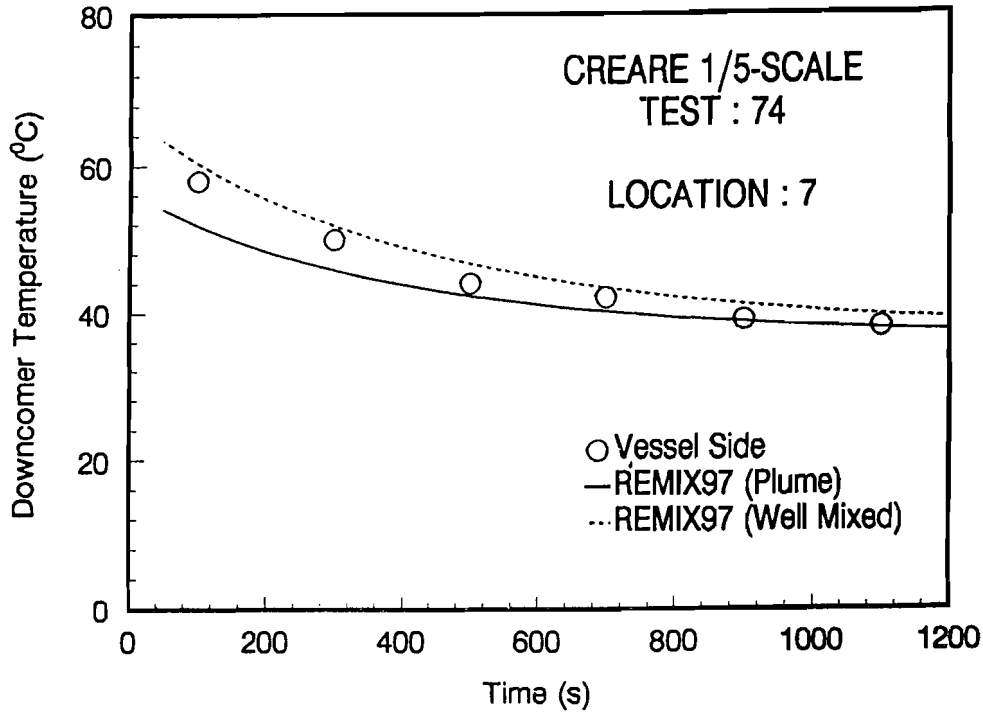


Figure 5.12 Comparison of the downcomer fluid temperature transients for CREARE 1/5-scale test No. 74 with the REMIX97 prediction (for thermocouple location 7; refer to Figure 5.1)

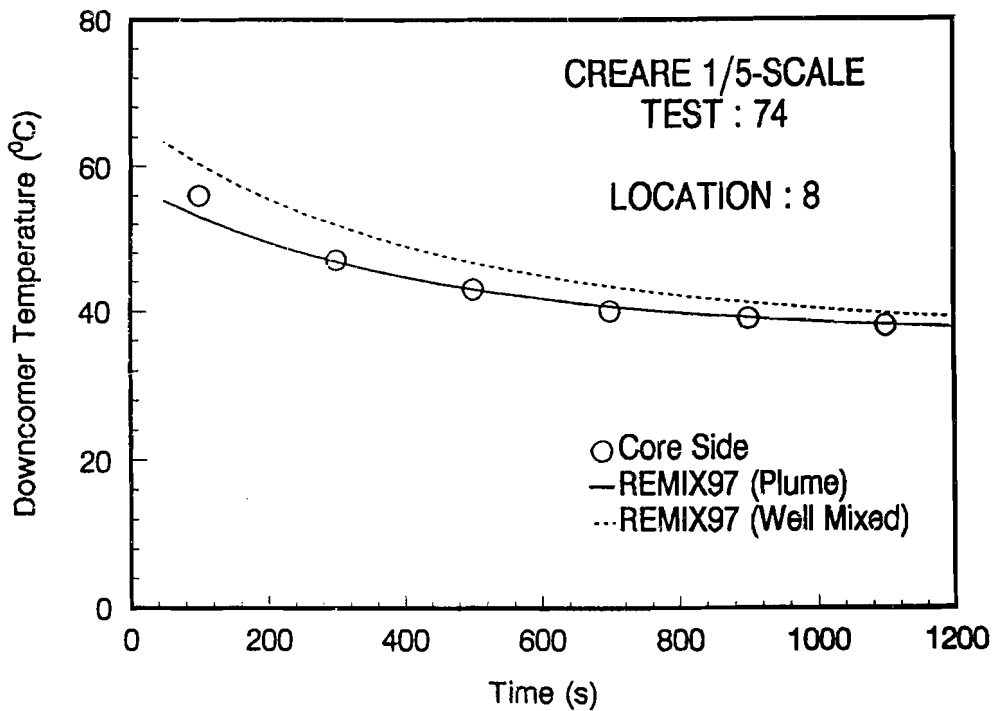


Figure 5.13 Comparison of the downcomer fluid temperature transients for CREARE 1/5-scale test No. 74 with the REMIX97 prediction (for thermocouple location 8; refer to Figure 5.1)

5. Code Verification and Validation

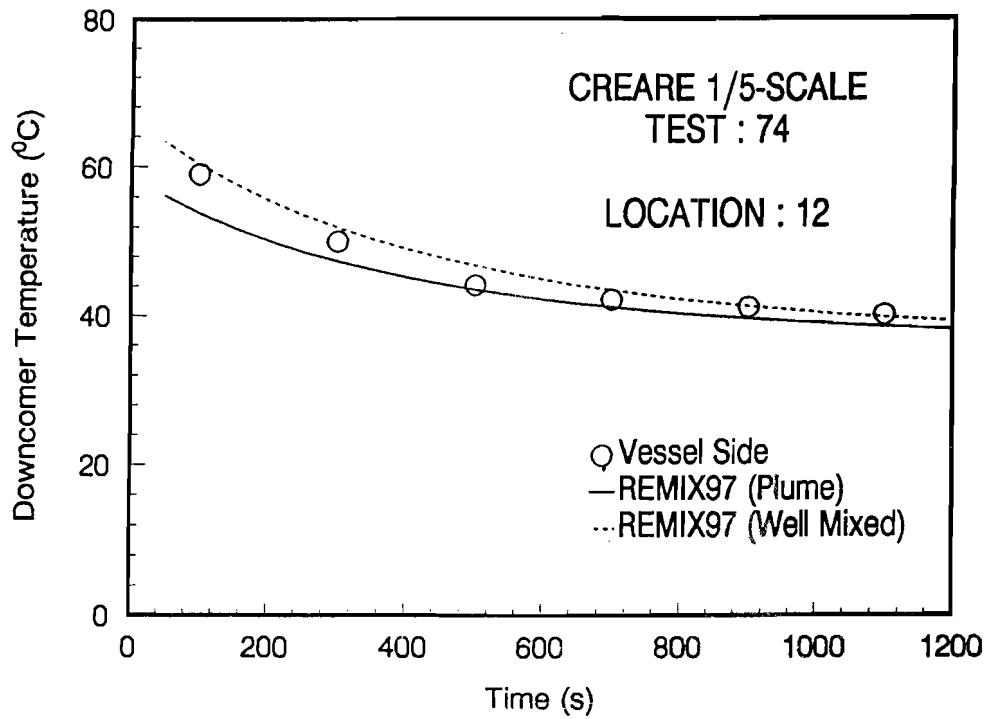


Figure 5.14 Comparison of the downcomer fluid temperature transients for CREARE 1/5-scale test No. 74 with the REMIX97 prediction (for thermocouple location 12; refer to Figure 5.1)

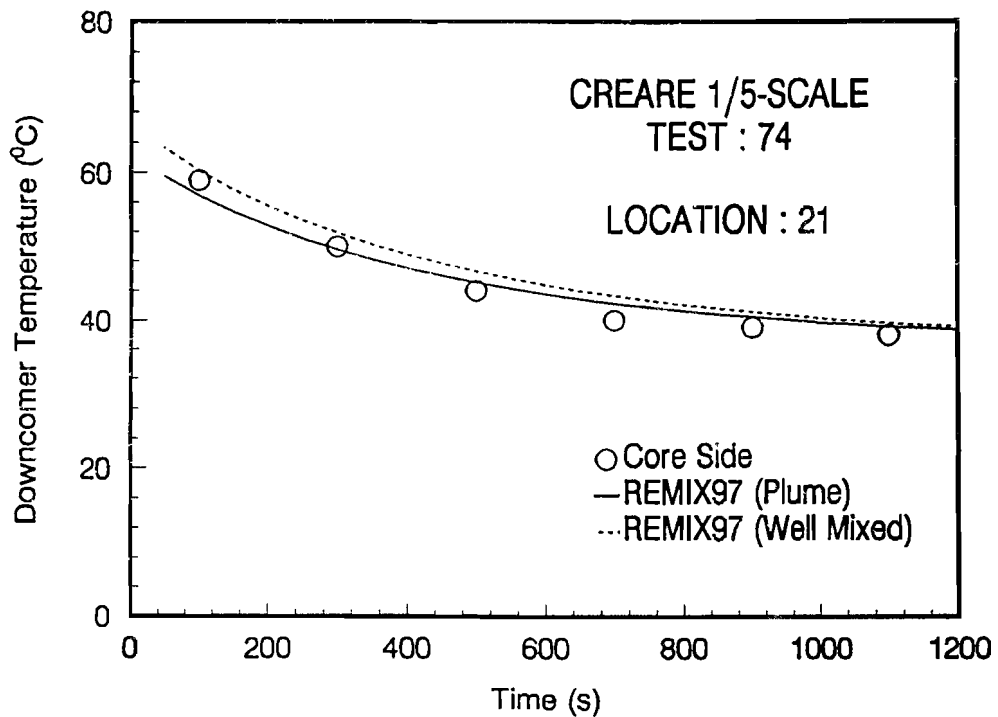


Figure 5.15 Comparison of the downcomer fluid temperature transients for CREARE 1/5-scale test No. 74 with the REMIX97 prediction (for thermocouple location 21; refer to Figure 5.1)

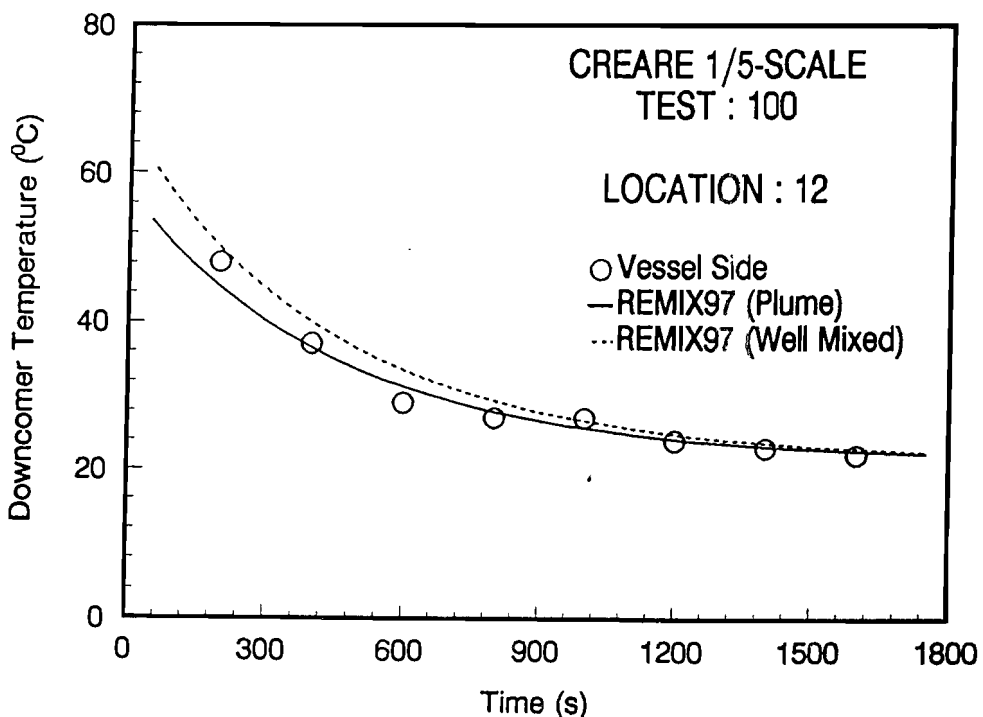


Figure 5.20 Comparison of the downcomer fluid temperature transients for CREARE 1/5-scale test No. 100 with the REMIX97 prediction (for thermocouple location 12; refer to Figure 5.1)

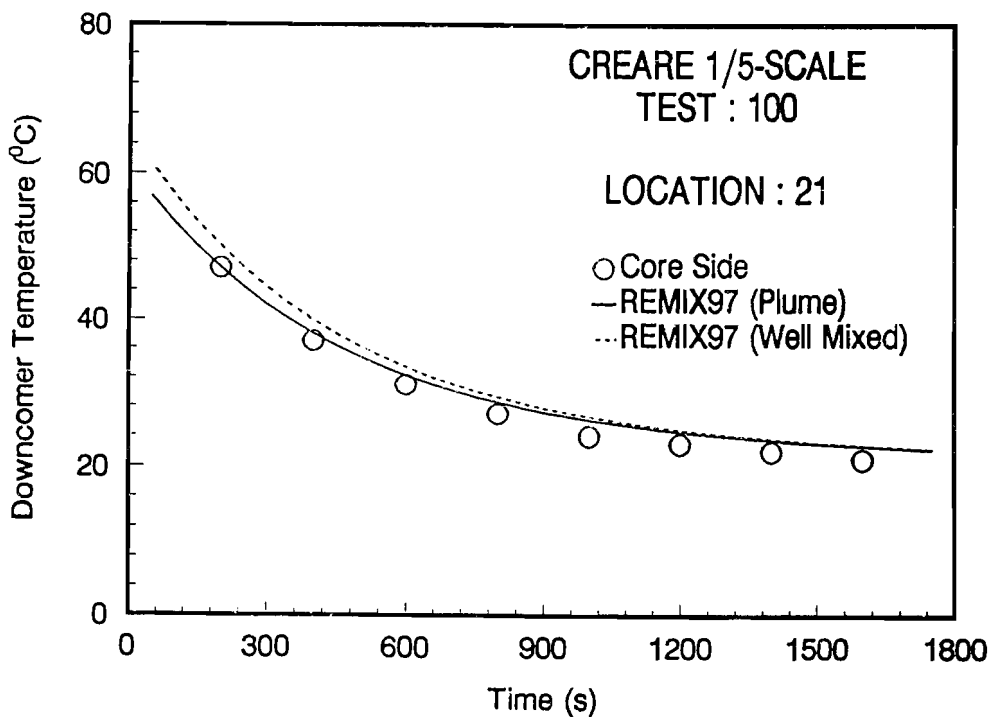


Figure 5.21 Comparison of the downcomer fluid temperature transients for CREARE 1/5-scale test No. 100 with the REMIX97 prediction (for thermocouple location 21; refer to Figure 5.1)

5. Code Verification and Validation

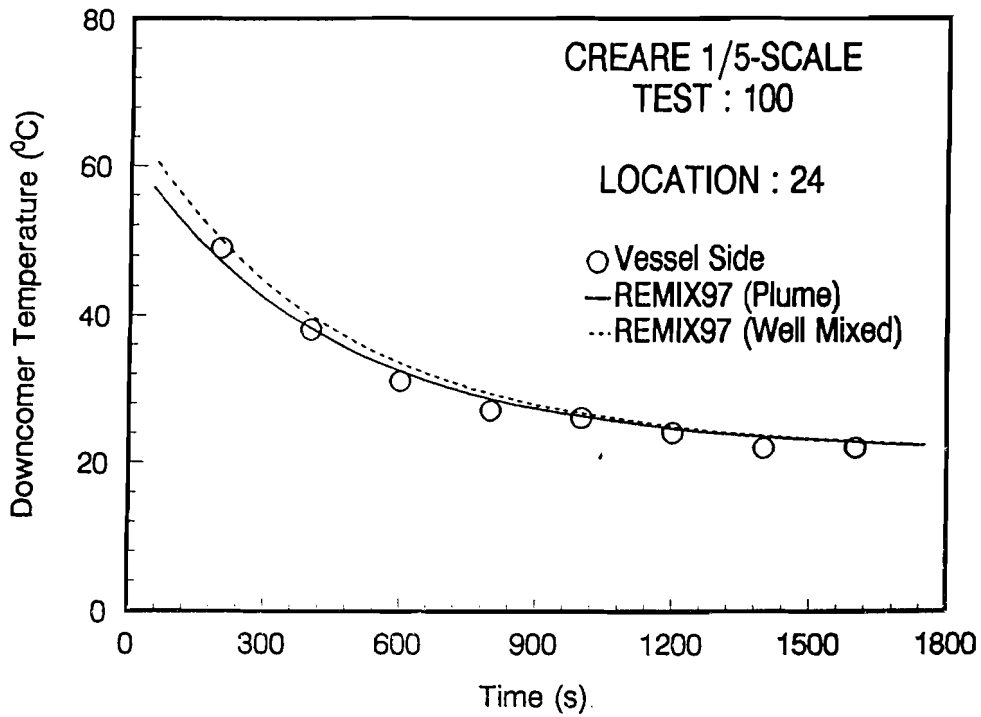


Figure 5.22 Comparison of the downcomer fluid temperature transients for CREARE 1/5-scale test No. 100 with the REMIX97 prediction (for thermocouple location 24; refer to Figure 5.1)

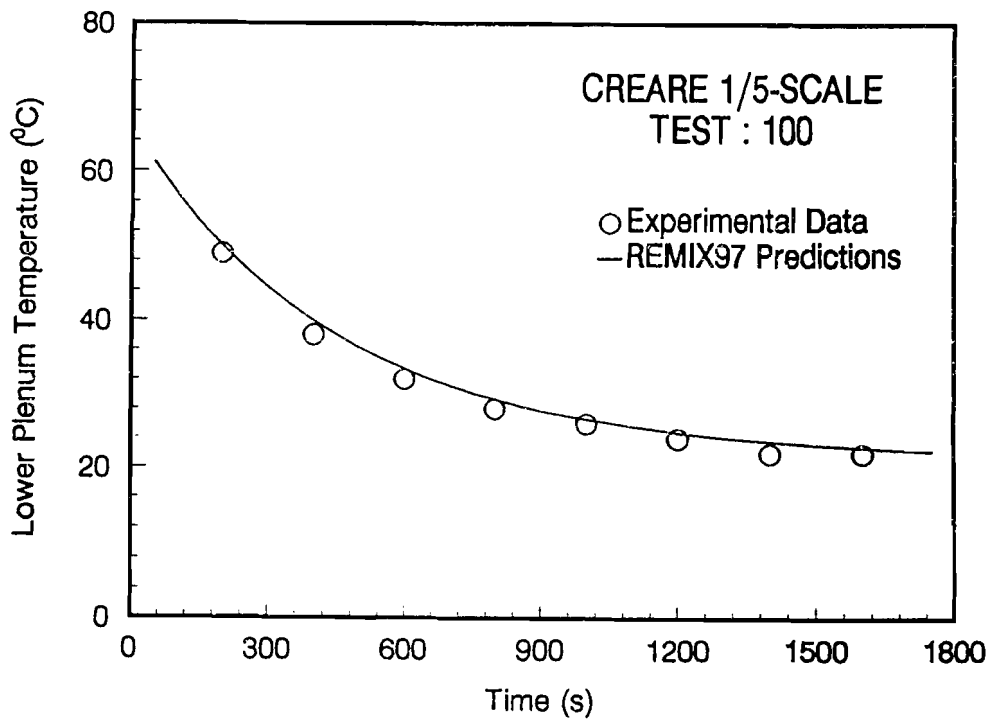


Figure 5.23 Comparison of the lower plenum fluid temperature transients for CREARE 1/5-scale test No. 100 with the REMIX97 prediction

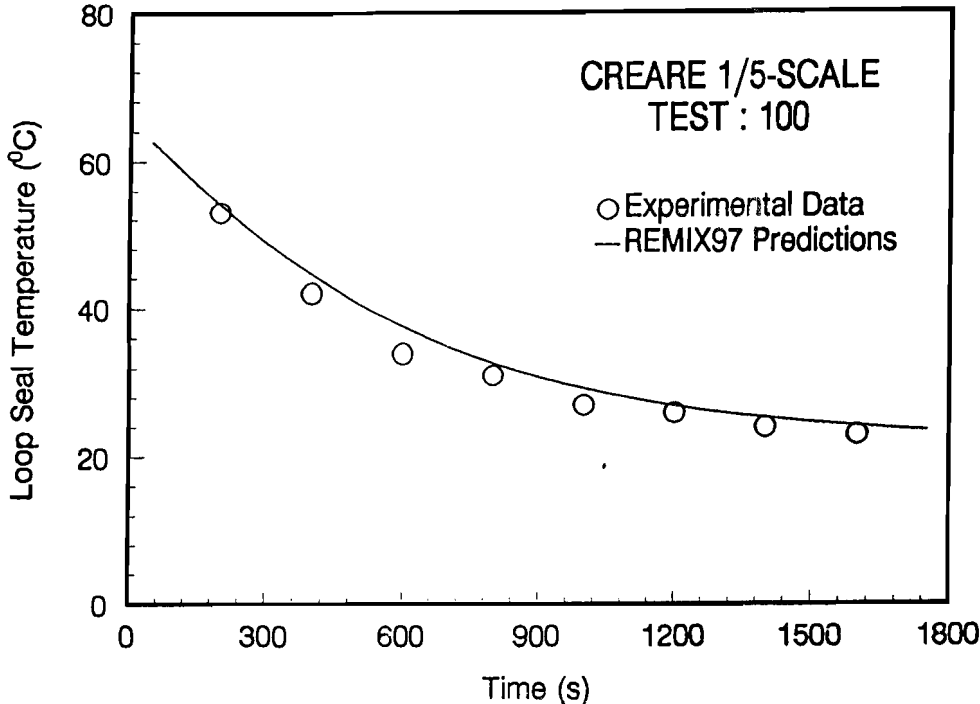


Figure 5.24 Comparison of the loop seal fluid temperature transients for CREARE 1/5-scale test No. 100 with the REMIX97 prediction

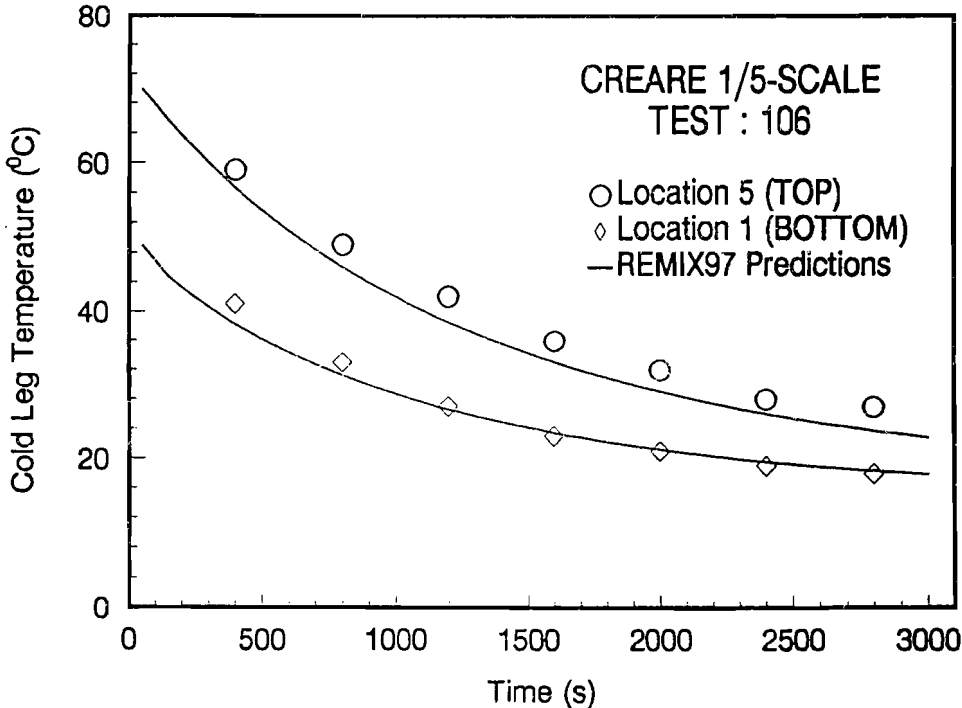


Figure 5.25 Comparison of the fluid temperature transients at the bottom of the cold leg for CREARE 1/5-scale test No. 106 with the REMIX97 prediction

5. Code Verification and Validation

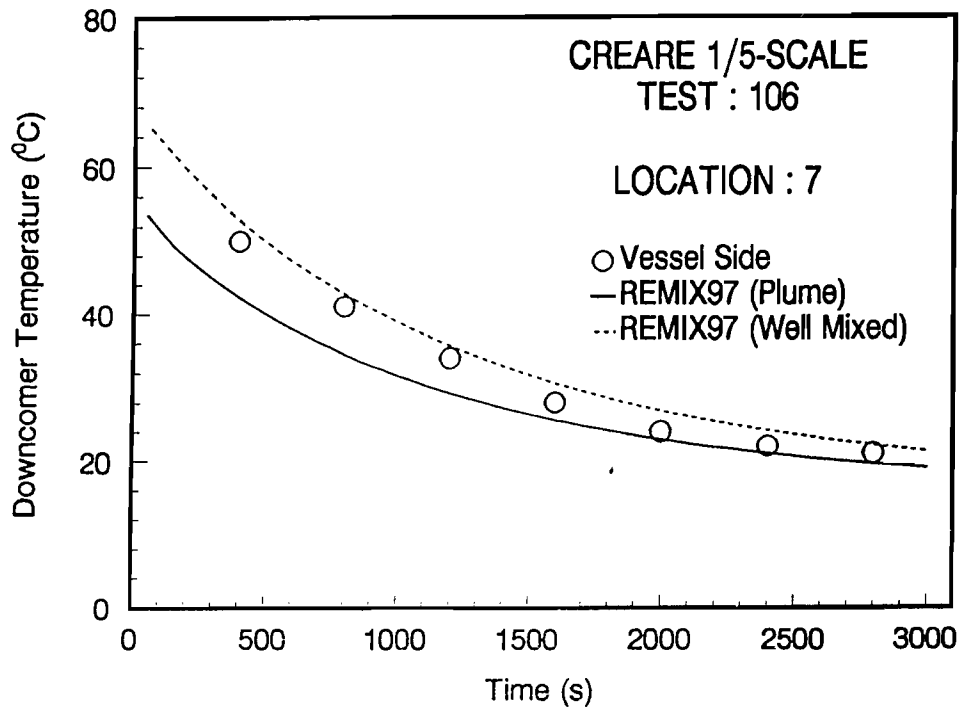


Figure 5.26 Comparison of the downcomer fluid temperature transients for CREARE 1/5-scale test No. 106 with the REMIX97 prediction (for thermocouple location 7; refer to Figure 5.1)

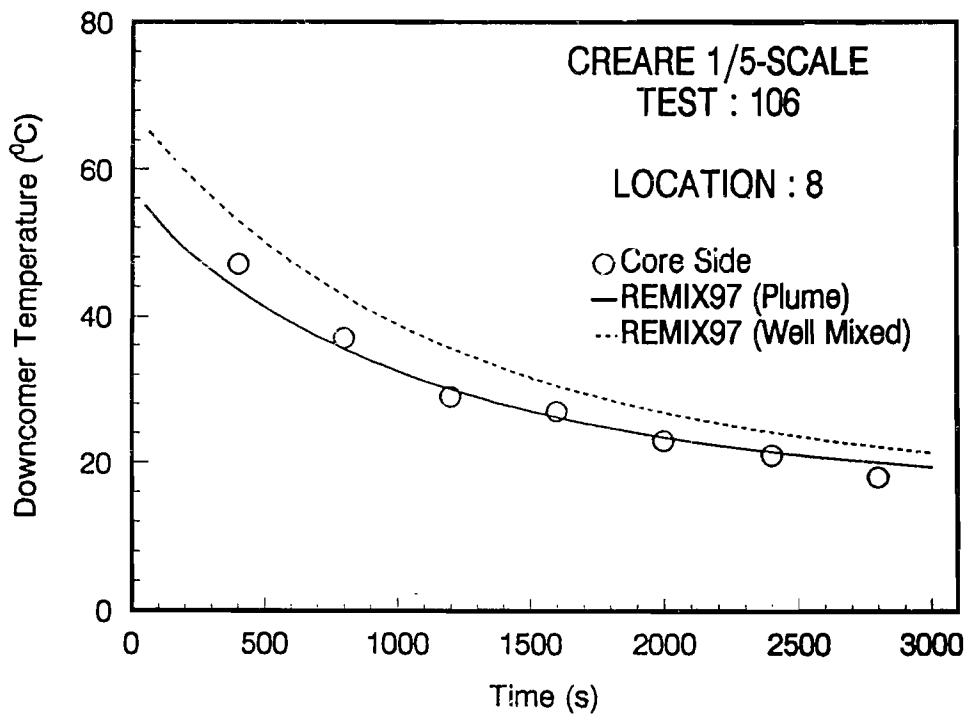


Figure 5.27 Comparison of the downcomer fluid temperature transients for CREARE 1/5-scale test No. 106 with the REMIX97 prediction (for thermocouple location 8; refer to Figure 5.1)

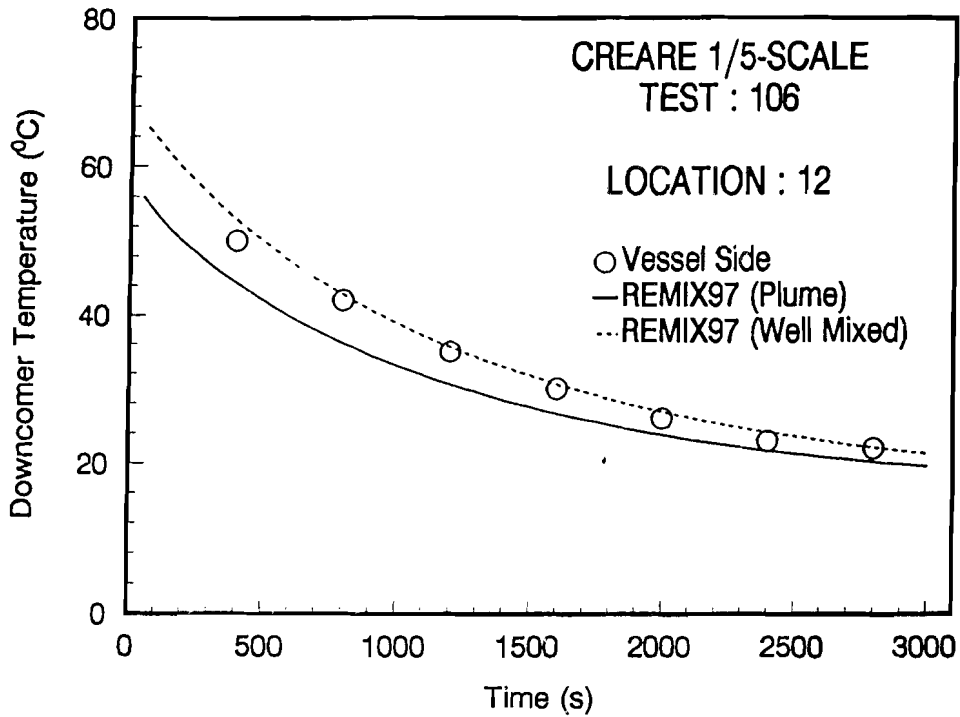


Figure 5.28 Comparison of the downcomer fluid temperature transients for CREARE 1/5-scale test No. 106 with the REMIX97 prediction (for thermocouple location 12; refer to Figure 5.1)

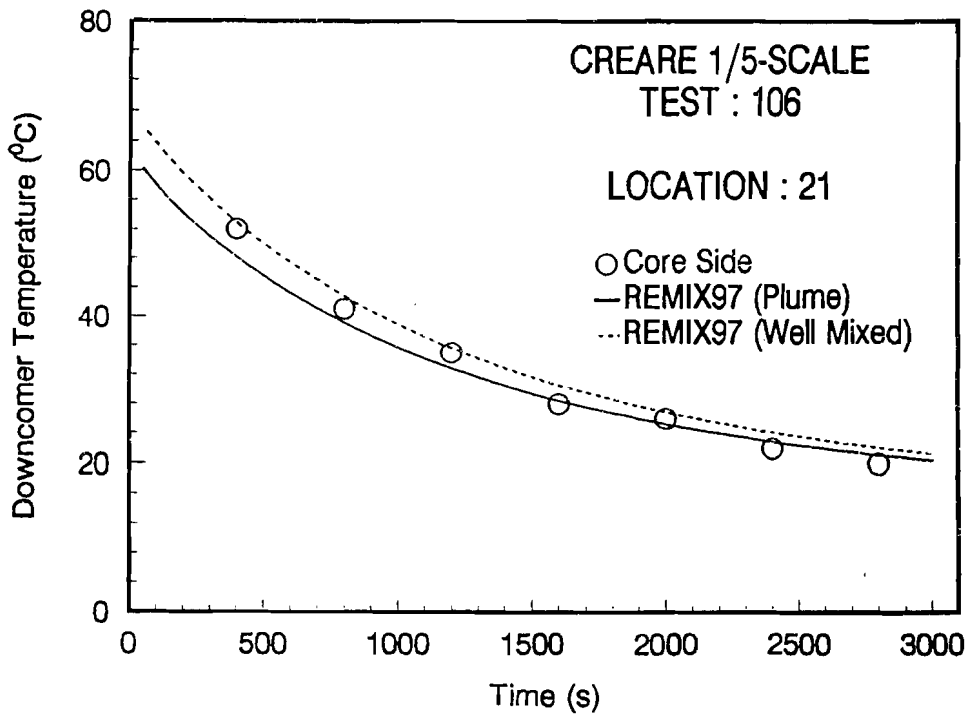


Figure 5.29 Comparison of the downcomer fluid temperature transients for CREARE 1/5-scale test No. 106 with the REMIX97 prediction (for thermocouple location 21; refer to Figure 5.1)

5. Code Verification and Validation

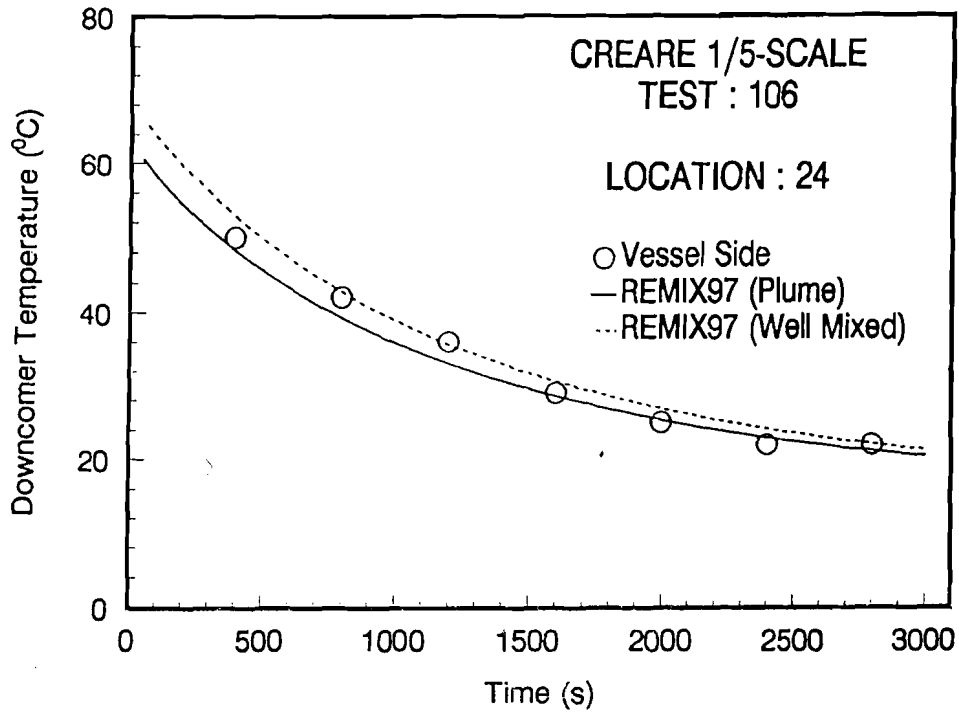


Figure 5.30 Comparison of the downcomer fluid temperature transients for CREARE 1/5-scale test No. 106 with the REMIX97 prediction (for thermocouple location 24; refer to Figure 5.1)

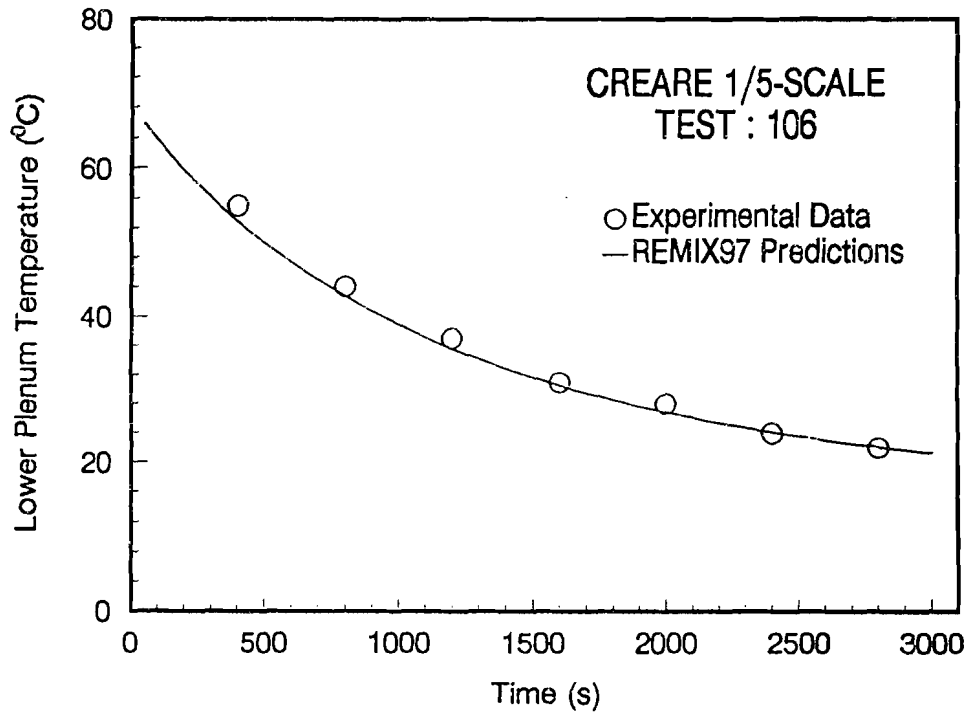


Figure 5.31 Comparison of the lower plenum fluid temperature transients for CREARE 1/5-scale test No. 106 with the REMIX97 prediction

5.3 Comparison of Code Predictions with CREARE 1/2-Scale Tests Data

The present extended regional mixing model and associated computer code REMIX97 was also applied to one of the CREARE-1/2 scale test. Comparisons of the code predictions with the test data are discussed in this section.

Figure 5.32 shows the schematic of the experimental

facility. Two tests were performed in a Westinghouse configuration, that is, the geometries of the cold leg, loop seal, pump simulator, HPI injector and cold leg nozzle were characteristics of the Westinghouse design. Major linear dimensions were scaled to approximately one-half of the dimensions of prototype PWR plants. The principal dimensions and thermocouple locations are shown in Figures 5.33 and 5.34. The relevant geometric features of the test facility is summarized in Table 5.4.

Table 5.4 Geometric data of CREARE 1/2-scale test facility

	Cold Leg	Vessel/ Downcomer	Lower Plenum	Pump	Loop Seal	Core Barrel	Thermal Shield
Inner diameter (cm)	36.32	—	—	—	38.10	—	—
Length (cm)	377.60	353.15	—	—	272.41	353.15	243.54
Base metal wall thickness (cm)	2.10	7.00	0.6	—	2.10	7.0	3.81
Insulation thickness	5.10	5.10	5.10	5.10	5.10	5.10	—
Wall heat transfer area to water (cm ² × 10 ⁻³)	4.30	5.71	3.70	—	3.26	5.71	7.88 ^(a)
Fluid volume (cm ³ × 10 ⁻⁵)	4.07	5.38	6.05	2.72	3.11	—	—

(a) Both sides included

5. Code Verification and Validation

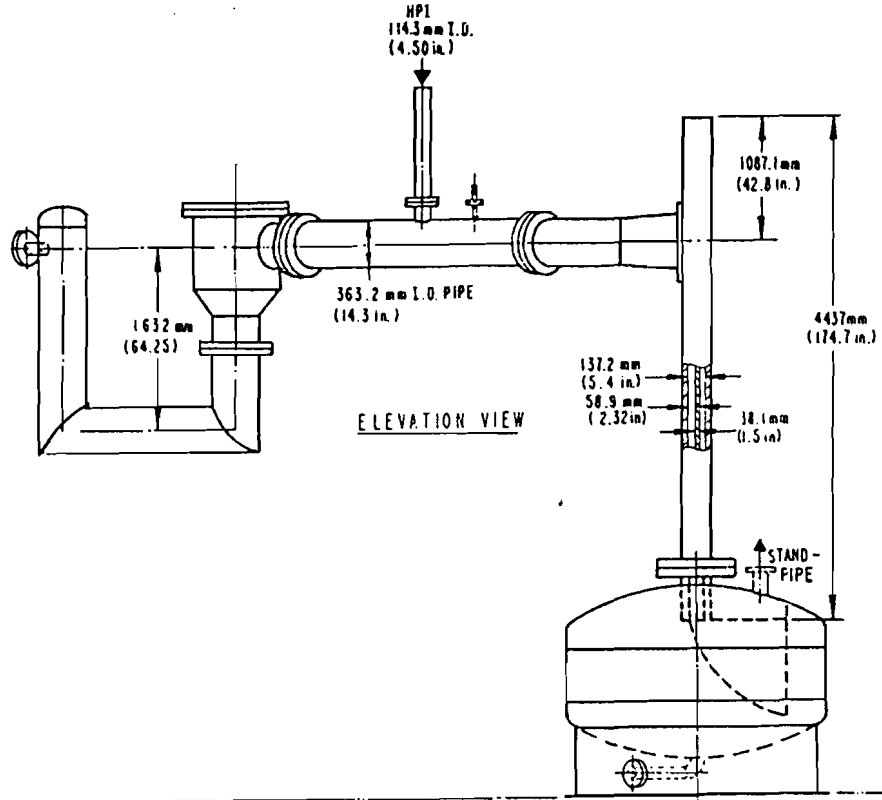


Figure 5.32 Schematic of CREARE 1/2-scale test facility

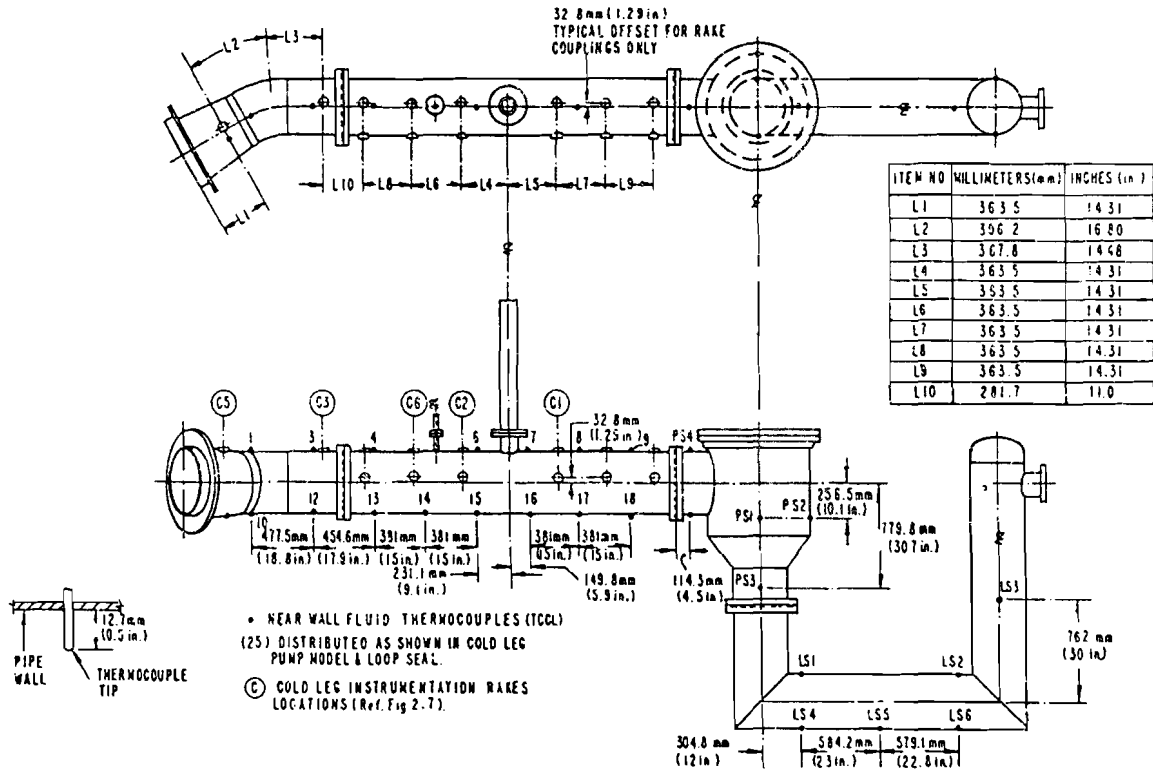


Figure 5.33 Cold leg instrument locations for CREARE 1/2-scale test facility

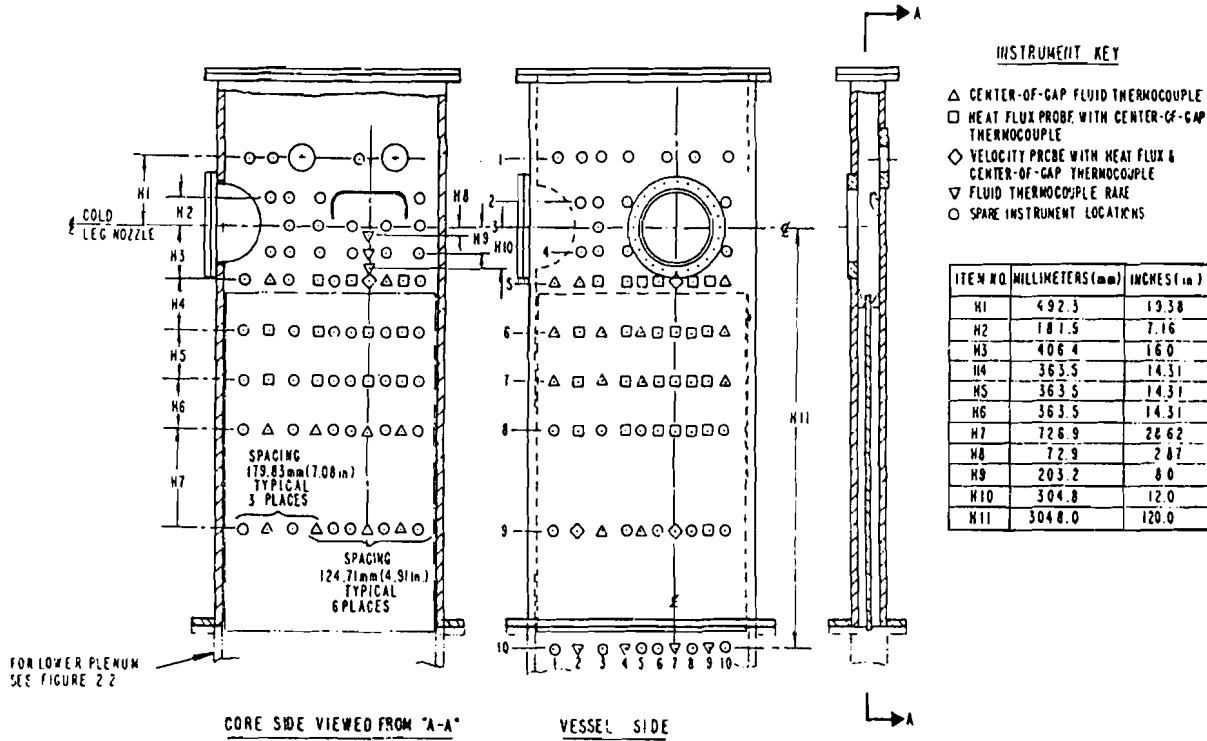


Figure 5.34 Downcomer instrument locations for CREARE 1/2-scale test facility

Two transient cooldown tests were performed (May 105 and May 106). Both tests were performed under stagnated loop conditions. Prior to initiation of the test, loop flow was circulated through the facility until the whole system reached thermal equilibrium at the loop flow temperature of about 190°C (375°F). The loop flow then turned off and HPI injection at temperature of 142°C (57.6°F) initiated.

Only one test (May 105) was chosen for the present code validation efforts. This test was run with the following experimental conditions:

$$\rho_{HPI} = 1000 \text{ kg/m}^3$$

$$\rho_L = 878 \text{ kg/m}^3$$

$$\dot{m}_{HPI} = 5.17 \text{ kg/sec}$$

$$Fr_{HPI} = 1.42$$

Figure 5.35 shows the transient fluid temperature measurements at the top and at the bottom of the cold leg (downstream from the injector) as compared with the REMIX97 predictions. Excellent agreement is noted.

Cold leg temperature profiles at two distinct times (192 s and 462 s) are compared with the REMIX97 predictions in Figure 5.36. REMIX97 predicts well the thermal stratification in the cold leg with the colder region occupying less than one-half of the pipe diameter.

5. Code Verification and Validation

Figures 5.37 through 5.39 show comparisons of transient fluid temperature measurements in the downcomer below the cold leg nozzle (instrument column 7 in Figure 5.34) at three different heights (instrument rows 5, 6 and 7 in Figure 5.34) with REMIX97 predictions. The downcomer vessel side temperatures are practically uniform and are in agreement with the downstream mixed mean (well mixed) temperature, $T_{m,d}$ predicted by REMIX97

code. The core barrel side temperatures are significantly lower than the vessel side and are in agreement with the code predictions for centerline plume temperatures.

Finally, as shown in Figures 5.40 and 5.41, the transient fluid temperature measurements in lower plenum and loop seal region are in excellent agreement with the code predictions.

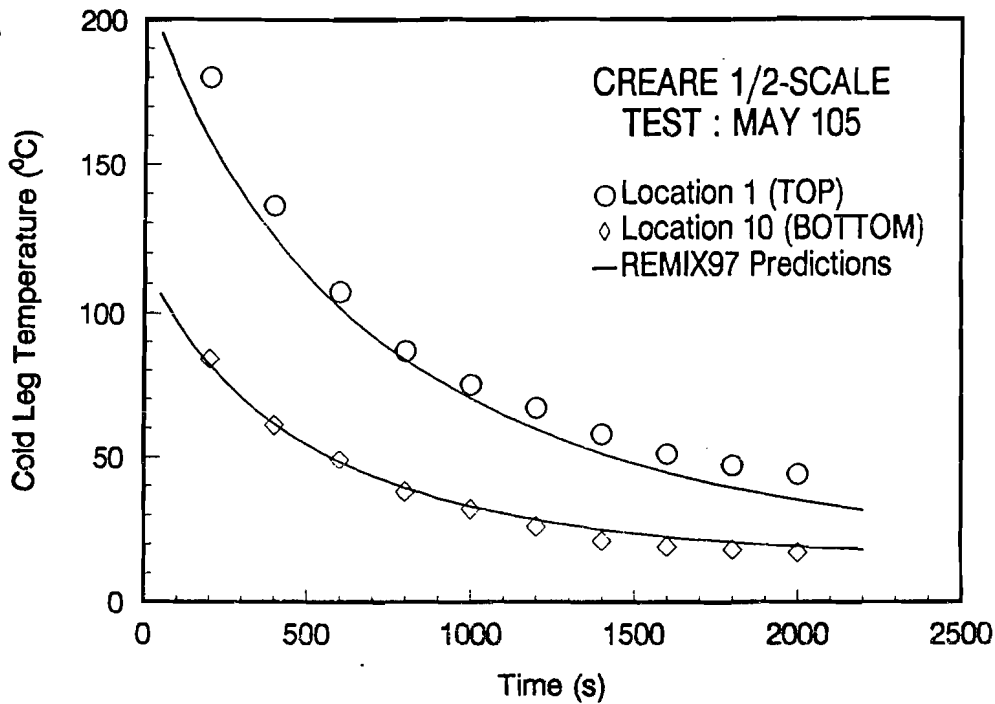


Figure 5.35 Comparison of the fluid temperature transients at the top and the bottom of the cold leg for CREARE 1/2 scale test (May 105) with the REMIX97 prediction

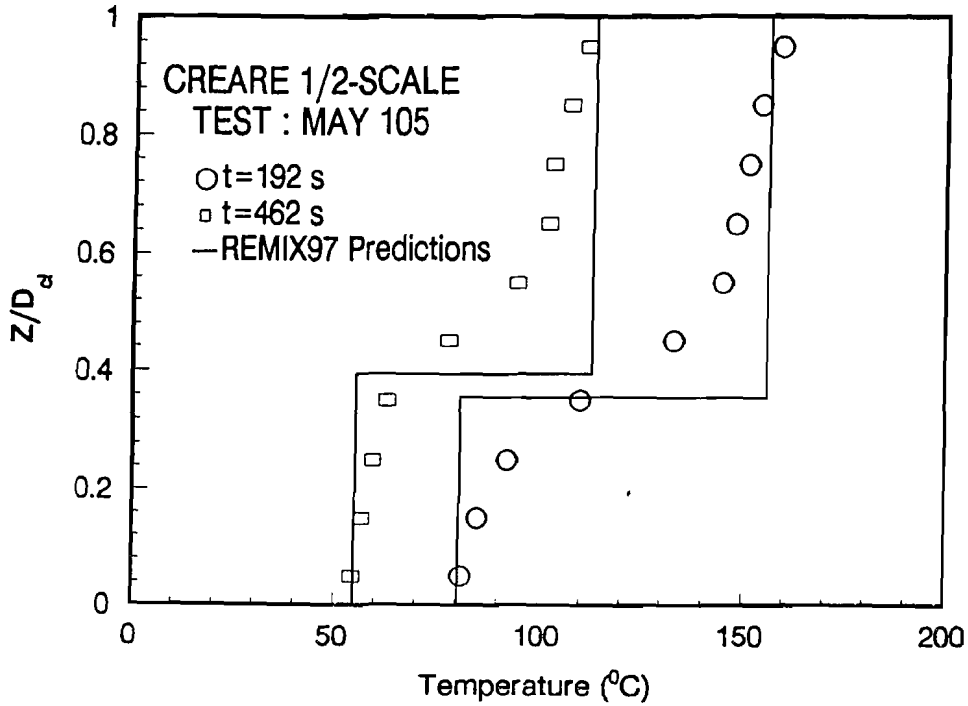


Figure 5.36 Comparison of the spatial variation of the fluid temperature in the cold leg (downstream from the injector) for the CREARE $\frac{1}{2}$ -scale test (May 105) with the REMIX97 prediction

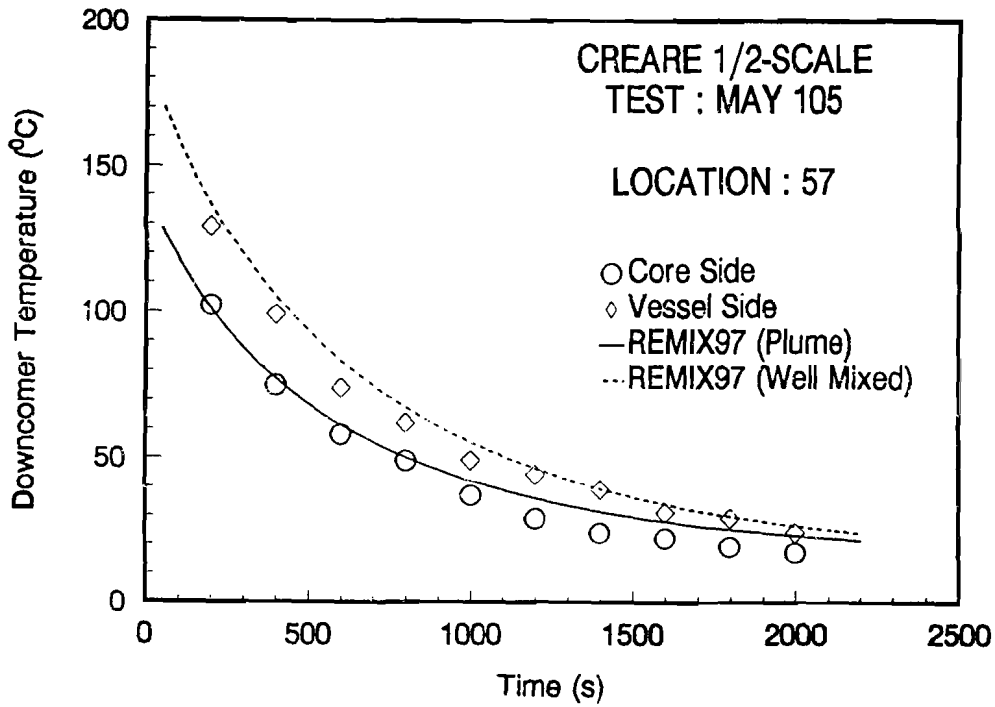


Figure 5.37 Comparison of the downcomer fluid temperature transients for CREARE $\frac{1}{2}$ -scale test (May 105) with the REMIX97 prediction (thermocouple location 57: 0.41 m below cold leg centerline)

5. Code Verification and Validation

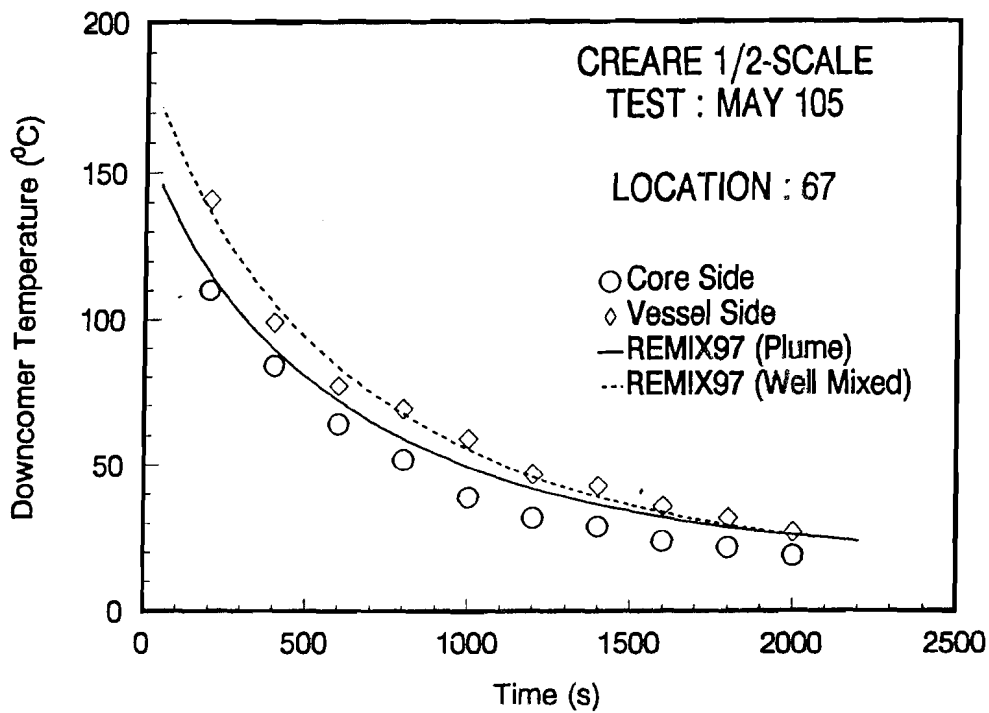


Figure 5.38 Comparison of the downcomer fluid temperature transients for CREARE 1/2-scale test (May 105) with the REMIX97 prediction (thermocouple location 67: 0.77 m below cold leg centerline)

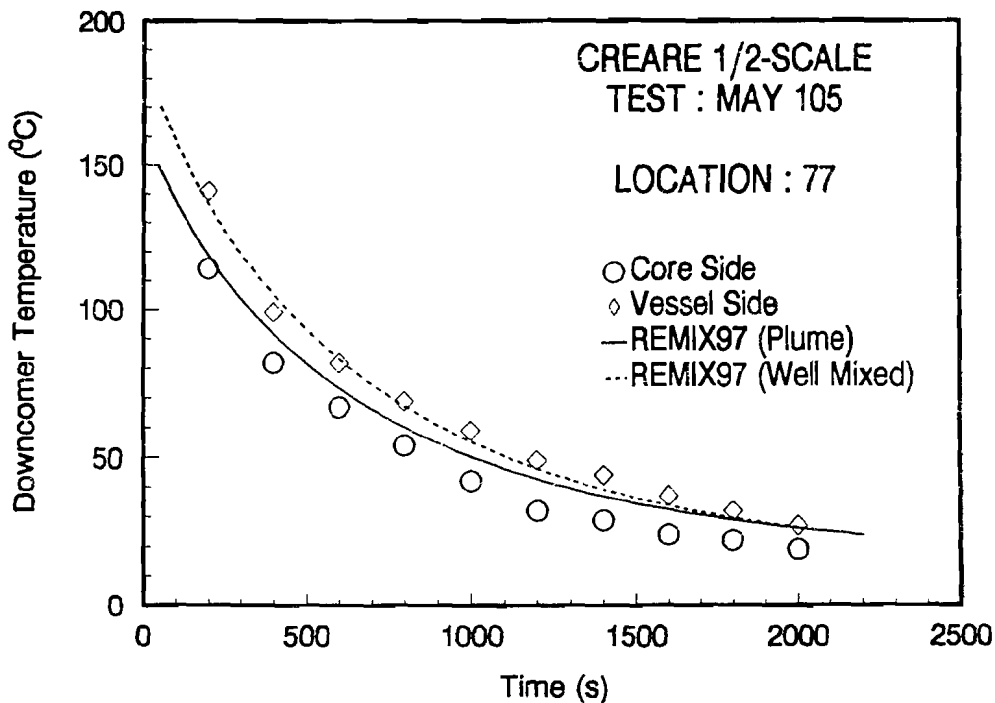


Figure 5.39 Comparison of the downcomer fluid temperature transients for CREARE 1/2-scale test (May 105) with the REMIX97 prediction (thermocouple location 77: 1.13 m below cold leg centerline)

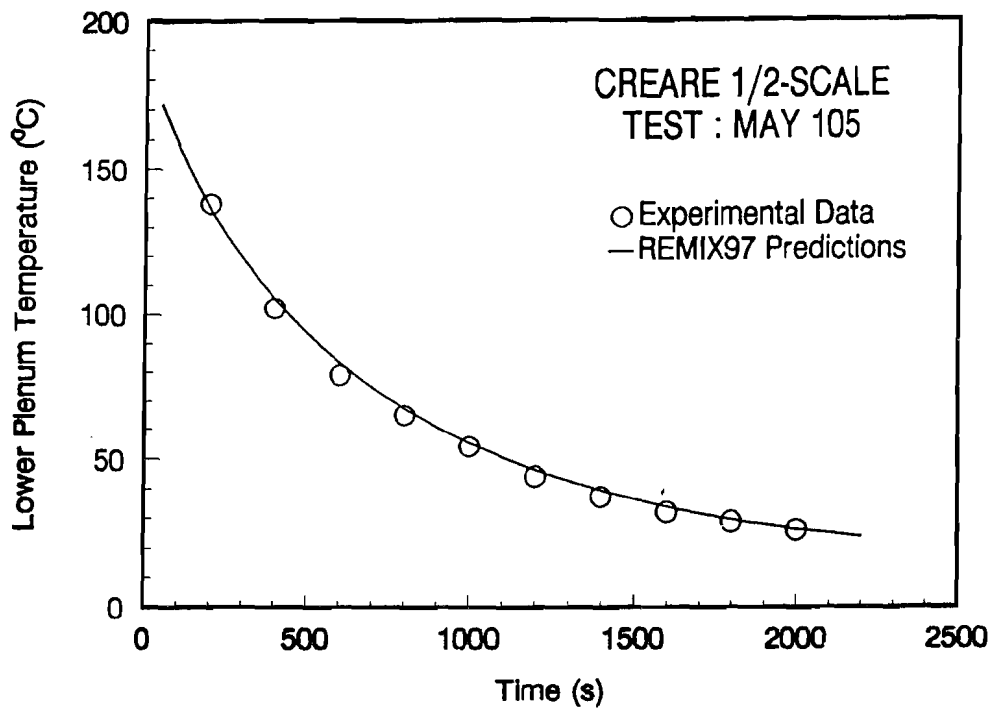


Figure 5.40 Comparison of the lower plenum fluid temperature transients for CREARE 1/2-scale test (May 105) with the REMIX97 prediction

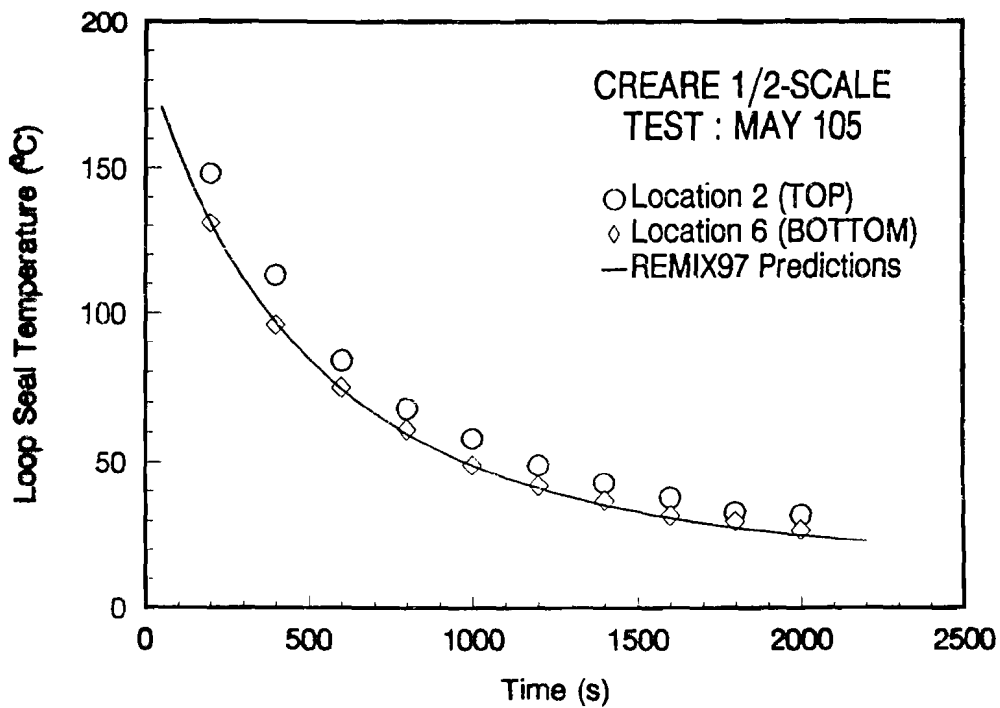


Figure 5.41 Comparison of the loop seal fluid temperature transients for CREARE 1/2-scale test (May 105) with the REMIX97 prediction

5. Code Verification and Validation

5.4 Comparison of Code Predictions with PURDUE 1/2-Scale Test Data

To evaluate the technical adequacy of REMIX97 for predicting the cooldown behavior at very high injection Froude numbers, the code was applied to B&W-IC test that was run at PURDUE'S 1/2 scale test facility.

The basic experimental facility consists of a transparent (acrylic) 1/2-scale model of a typical PWR cold-leg/ downcomer/lower-plenum

configuration. The lower portion of the downcomer and the lower plenum were geometrically distorted to keep the overall height of the facility manageable. The essential features of different geometric configurations could be assembled by making appropriate attachments to the cold leg. Schematic view of the experimental facility (configuration B&W) is shown in Figure 5.42.

The B&W-IC test was intended to specifically simulate the Oconee plant geometry. All the geometric features relevant to the simulation are summarized in Table 5.5.

Table 5.5 Geometric data of PURDUE 1/2-scale test facility (Configuration B&W)

	Cold Leg	Vessel/Downcomer	Lower Plenum
Inner diameter (cm)	34.3	12.5 ^(a)	—
Length (cm)	282.0	192.0	—
Fluid volume (cm ³ × 10 ⁻⁵)	2.6	2.9	9.9

(a) Gap between vessel wall and core barrel

The essential features of configuration B&W are the inclined portion of the cold leg and the small diameter (2.68 cm) HPI line.

Test B&W-IC was performed under stagnated loop conditions. A salt solution (brine) was injected into the system filled with fresh water. This test was run with the following experimental conditions:

$$\begin{aligned} \rho_{HPI} &= 1180 \text{ kg/m}^3 \\ \rho_L &= 998.2 \text{ kg/m}^3 \\ \dot{m}_{HPI} &= 2.21 \text{ kg/sec} \\ Fr_{HPI} &= 18.00 \end{aligned}$$

Salt concentration measurements were made by means of conductivity probe traverses at positions TR1 and TR2 shown in Figure 5.42. Spatial profiles

and temporal variations in concentration were then constructed from these data. The concentration of the exiting stream was also measured continuously.

Figure 5.43 shows the transient concentration measurements at the exit stream, at the bottom of the cold-leg and at the top of the cold-leg as compared to the REMIX97 predictions. The agreements appears satisfactory.

Samples of cold leg concentration profiles are compared with the REMIX97 code predictions in Figure 5.44. The REMIX97 predictions of degree of stratification in the cold-leg are in good agreement with the data.

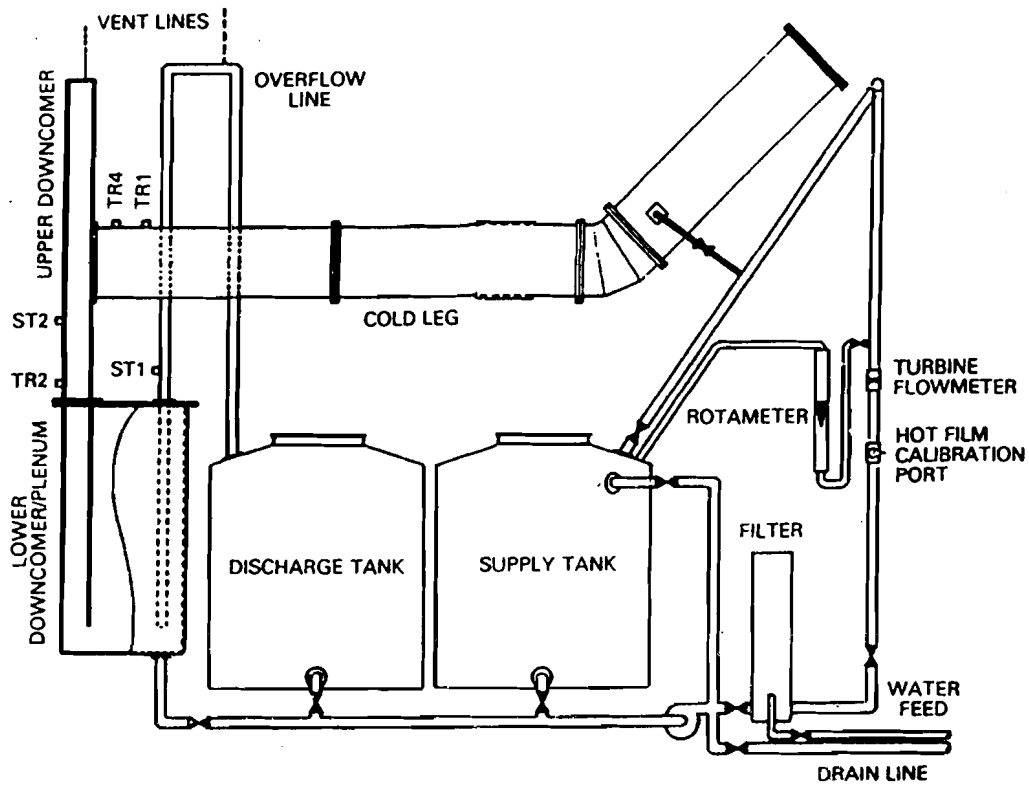


Figure 5.42 Schematic view of PURDUE's 1/2-scale facility (configuration B&W)

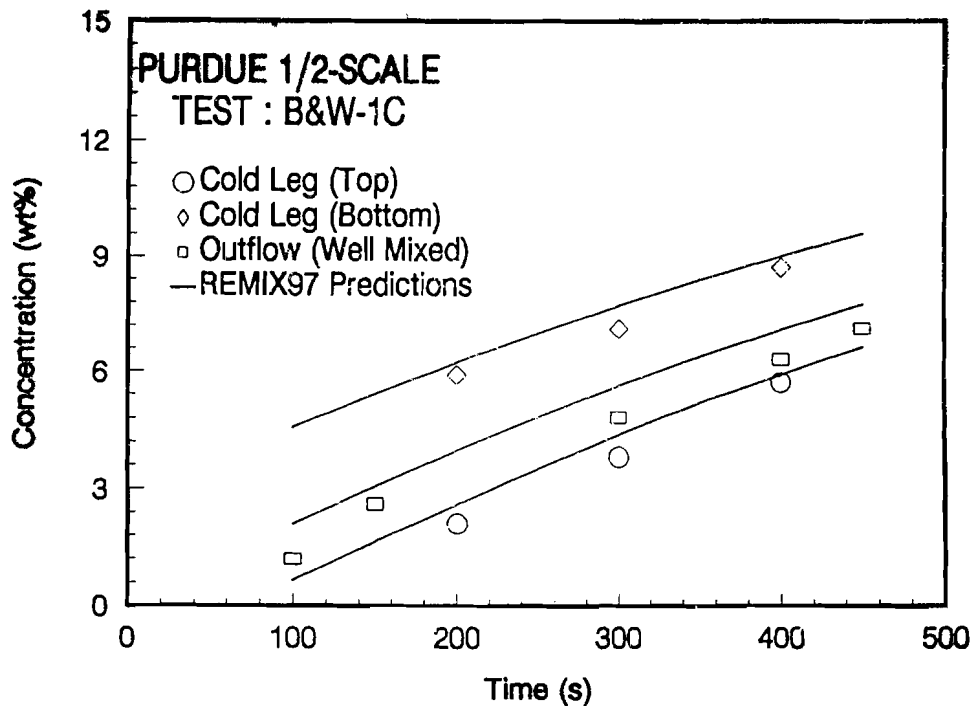


Figure 5.43 Comparison of the concentration transients in the cold leg and at the exit stream for the PURDUE 1/2-scale test B&W-1C with the REMIX97 prediction

5. Code Verification and Validation

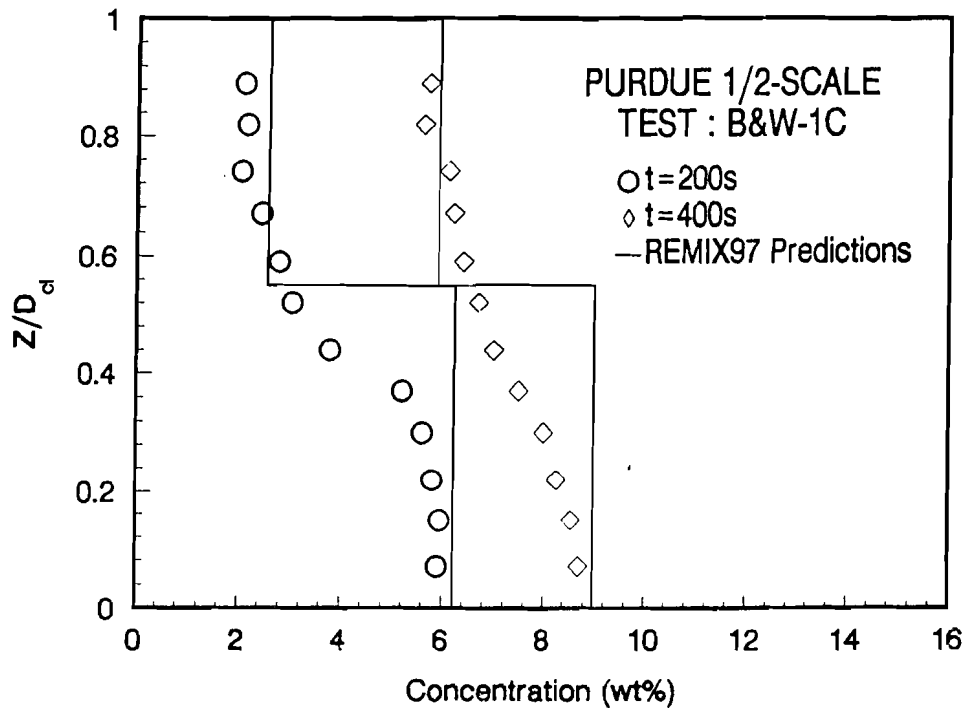


Figure 5.44 Comparison of the spatial variation of the concentration in the cold leg for the PURDUE 1/2-scale test B&W-1C with the REMIX97 prediction

5.3 References

- 5.1 H. P. Nourbakhsh and T. G. Theofanous, "Decay of Buoyancy Driven Stratified Layers with Applications to Pressurized Thermal Shock, Part I: The Regional Mixing Model," NUREG/CR-3700, 1984; also Nuclear Eng. Design (in press).
- 5.2 T. G. Theofanous, K. Iyer, H. P. Nourbakhsh, and P. Gherson, "Buoyancy Effects in Overcooling Transients Calculated for the NRC Pressurized Thermal Shock Study," NUREG/CR-3702, U.S. Nuclear Regulatory Commission, May 1986.
- 5.3 T. G. Theofanous and H. Yan, "A Unified Interpretation of One-Fifth to Full-Scale Thermal Mixing Experiments Related to Pressurized Thermal Shock," U. S. Nuclear Regulatory Commission, NUREG/CR-5677, 1991.
- 5.4 M. Giot, P. Hernalsteen and E. Stubbe, "Pressurized Thermal Shock-Mixing of a Direct Safety Injection Flow in a PWR Reactor Vessel Downcomer-Experimental and Analytical Results," Trans. Eighth Intl. Conf. SMIRT, Brussels, Belgium, Aug. 19-23, 1985, Vol. F1, F2, pp. 367-374.
- 5.5 H. Tuomisto, "Experiments and Analysis of Thermal Mixing and Stratification During Overcooling Accidents in a Pressurized Water Reactor," ANS Proceedings 1987 National Heat Transfer Conference, Pittsburgh, PA, August 9-12, 1987, American Nuclear Society.
- 5.6 H. Tuomisto, Y. Hytönen, and P. Mustonen, "Two-Fifths Scale Thermal Mixing Tests in a Semiannular Downcomer and Cold Legs," Proc. Intl. ANS/ENS Topical Meeting on Thermal Reactor Safety, San Diego, CA, Feb. 2-6, 1986.

5. Code Verification and Validation

- 5.7 L. Wolf, et al., "Results of Thermal Mixing Tests at the HDR Facility and Comparisons with Best Estimates and Simple Codes," Proc. of the Third Topical Meeting on Reactor Thermal Hydraulics, Newport, RI, October 15-18, 1985, Vol. 1, paper 8.E.
- 5.8 P. A. Weiss, et al., "Fluid-Fluid Mixing Test: Experimental Data Report," KWU R515/87/09, Erlangen, FRG, April 1987.
- 5.9 S. Yoshimura, et al., "Mixing Behavior of Safety Injection Water Within the Cold Leg and the Downcomer Under Postulated Accidents," Proc. of the Third Topical Meeting on Reactor Thermal Hydraulics, Newport, RI, October 15-18, 1985.
- 5.10 P. H. Rothe and M. F. Ackerson, "Fluid and Thermal Mixing in a Model Cold Leg and Downcomer with Loop Flow," EPRI NP-2312, April 1982.
- 5.11 M. W. Fanning and P. H. Rothe, "Transient Cooldown in a Model Cold Leg and Downcomer," EPRI NP-3118, May 1983.
- 5.12 P. H. Rothe and W. D. Marscher, "Fluid and Thermal Mixing in a Model Cold Leg and Downcomer with Vent Valve Flow," EPRI NP-2227, March 1982.
- 5.13 P. H. Rothe and M. W. Fanning, "Evaluation of Thermal Mixing Data from a Model Cold Leg and Downcomer," EPRI NP-2773, December 1982.
- 5.14 P. H. Rothe and M. W. Fanning, "Thermal Mixing in a Model Cold Leg and Downcomer at Low Flow Rates," EPRI NP-2935, March 1983.
- 5.15 A. Hashemi and J. Goodman, "Thermal Mixing a Rectangular Geometry Model of a Cold Leg with High-Pressure Injection and a Downcomer," EPRI NP-2924, March 1983.
- 5.16 T. G. Theofanous, P. Gherson, H. P. Nourbakhsh, and K. Iyer, "Decay of Buoyancy-Driven Stratified Layers with Application to Pressurized Thermal Shock, Part II: PURDUE's 1/2-Scale Experiments," NUREG/CR-3700, 1984; also Nucl. Eng. Design (in press).
- 5.17 F. X. Dolan and J. A. Valenzuela, "Thermal and Fluid Mixing in a 1/2-Scale Test Facility," Vol. 1: Facility and Test Design Report, EPRI NP-3802, NUREG/CR-3426, September 1985.
- 5.18 F. X. Dolan and J. A. Valenzuela, "Thermal and Fluid Mixing in a 1/2-Scale Test Facility," Vol. 2: Data Report, EPRI NP-3802, NUREG/CR-3426, September 1985.
- 5.19 L. Wolf, et al., "Application of Engineering and Multi-Dimensional Finite Difference Codes to HDR Thermal Mixing Experiments TEMB," Proceedings of the Fourteenth Water Reactor Safety Information Meeting, Gaithersburg, MD, October 27-31, 1986, Vol. 4, pp. 395-444.
- 5.20 J. A. Valenzuela and P. H. Rothe, "Flow Visualization During Transient Cooldown in a Model PWR Cold Leg and Downcomer," EPRI NP-3871.

6. SUMMARY AND CONCLUSIONS

Many thermal hydraulic aspects of overcooling events, except the thermal stratification effects, can be analyzed by using system codes, such as TRAC and REAP. Such thermal stratification is obtained at low loop flow, and it is not represented in system codes currently used to simulate overcooling events with PTS potential.

The regional mixing model and the associated computer codes REMIX and NEWMIX, which has been previously documented, is based on a fundamentally-oriented zonal approach which integrates local stratification and mixing behavior into an overall system response. These codes are only applicable when there is no loop flow (complete loop stagnation condition). Specific versions of these codes, REMIX-S and NEWMIX-S have also been previously developed for applications to experimental simulations involving solute induced buoyancy.

A study was conducted to provide a number of modeling improvements to the REMIX code that include extending the regional mixing model to include low loop flow conditions. This improved version of the code combines REMIX, NEWMIX, REMIX-S and NEWMIX-S into a single code REMIX97.

To provide a framework for assessment of modeling requirements (improvements to the REMIX code) for predicting the downcomer fluid temperature transients due to safety injection at low loop flow conditions, an integrated methodology somewhat similar to the one developed for severe accident technical issue resolution was adopted. The integration is achieved by specifying the technical issue and prioritizing the physical processes which need to be considered to resolve an issue and by expressing them in terms of specification for code development/modeling improvement, and experimentation.

In the original formulation of regional mixing model the thermal response (i.e., mixed mean temperature, hot stream temperature, etc.) of the upstream and the downstream of safety injection point were assumed to be identical. Although this is a good approximation under stagnated loop flow condition, its validity in the presence of loop flow may be questionable. Therefore, in the present extension of regional mixing model, both at the global and at the local level of computation, the upstream and the downstream of the safety injection point were treated separately.

At very low loop flow, the HPI jet after some mixing at the point of injection divides into two stably stratified cold streams, one flowing downstream toward the downcomer and the other going upstream toward the pump and loop seal. However, as the loop flow increases the extent of backflow toward the upstream region of the cold leg decreases. As a part of present study a criterion for the existence of backflow toward the upstream region of the cold leg was obtained analytically. The backflow criterion was compared with the CREARE 1/5-scale data. Excellent agreement was noted.

Thermal mixing in relation to pressurized thermal shock has been examined experimentally throughout the world. The original regional mixing model and associated computer programs REMIX and NEWMIX has been successfully employed to interpret much of the available thermal mixing experimental data obtained from the system simulation tests performed under stagnated loop flow conditions.

The REMIX97 code was also used to predict various cooldown transients under stagnated loop flow conditions. The results were found to be consistent with the validated results of REMIX/NEWMIX code.

5. Code Verification and Validation

Comparison of REMIX97 prediction with all available experimental data obtained from the world thermal mixing test facilities was beyond the scope of the present study. However, in order to evaluate the technical adequacy of the REMIX97 code, the code was used to predict a limited set of data that are relevant to U.S. reactors. These data were obtained under a wide range of experimental conditions including low Froude number injections of interest to Westinghouse and Combustion Engineering designed

reactors and very high Froude number injections of interest to Babcock & Wilcox designed reactors. The experimental conditions also included the presence of low loop flow, solute and/or thermally induced buoyancy and concentration or temperature measurement as an indication of mixing. Excellent agreement between the REMIX97 code calculated results and experimental data was noted.

APPENDIX A

A USER'S MANUAL FOR THE REMIX97 COMPUTER CODE

A.1 Introduction

The Computer Code REMIX97 has been developed to evaluate the thermal stratification and mixing phenomena in relation to pressurized thermal shock (PTS) risk analysis. This program is based on an extension to the regional mixing model to include low loop flow conditions. The formulation has been augmented with solute mass balances and appropriate equation of state. Thus, with the proper choice of input option parameter, the REMIX97 is also appropriate for applications to experimental simulations involving solute-, or thermal/solute-, induced buoyancy.

This Appendix describes the code requirements, installation, input and output.

A.2 Requirements

The REMIX97 Code runs on IBM-Compatible computers. Basic requirements are:

- DOS 3.0 or higher
- A Fortran compiler
- A monitor
- 640K of standard memory. Expanded or Extended memory is not required.
- A hard disk
- A math co-processor is recommended
- A printer (required only if you want to print output files)

A.3 Installation

The REMIX97 software is distributed on a single 1.44M 3.5-inch diskette. The files contained on the diskette are the Fortran source code REMIX97.FOR, COM..FOR and the input data file INPUT97.DAT. These files should be put together in a directory before generating the executable file REMIX97.EXE.

A.4 Input

The input for REMIX97 is somewhat similar to a name list. The following are the names of variables, their definition and units together with some guidance for their specifications:

ACBH :	Heat transfer area of core barrel (ft ²)
ACLHD	Heat transfer area of cold leg wall, downstream of injection point (ft ²)
ACLHU	Heat transfer area of cold leg wall, upstream of injection point (ft ²)
ADCH	Heat transfer area of downcomer wall (ft ²)
AKCB	Thermal conductivity of core barrel (Btu/ft-sec-°F)
AKCL	Thermal conductivity of cold leg wall (Btu/ft-sec-°F)
AKDC	Thermal conductivity of downcomer wall (Btu/ft-sec-°F)
AKDCC	Thermal conductivity of downcomer cladding (Btu/ft-sec-°F)
AKINS	Thermal conductivity of insulation (Btu/ft-sec-°F)
AKLP	Thermal conductivity of lower plenum wall (Btu/ft-sec-°F)
AKLS	Thermal conductivity of loop seal wall (Btu/ft-sec-°F)
AKP	Thermal conductivity of pump structures (Btu/ft-sec-°F)
AKTS	Thermal conductivity of thermal shield (Btu/ft-sec-°F)
ALCB	Thermal diffusivity of core barrel (ft ² /sec)

Appendix A

ALCL	Thermal diffusivity of cold leg wall (ft ² /sec)	BQHPI	A constant to compute HPI flow (ft ³ /sec)
ALDC	Thermal diffusivity of downcomer wall (ft ² /sec)	DCL :	Diameter of cold leg (ft)
ALDCC	Thermal diffusivity of downcomer cladding (ft ² /sec)	DDCC :	Thickness of clad (ft)
ALFINS :	Thermal diffusivity of insulation (ft ² /sec)	DELCB :	Thickness of core barrel (ft)
ALLP :	Thermal diffusivity of lower plenum wall (ft ² /sec)	DELCL :	Thickness of cold leg wall (ft)
ALLS	Thermal diffusivity of loop seal wall (ft ² /sec)	DELDC :	Thickness of downcomer (vessel) wall (ft)
ALP :	Thermal diffusivity of pump structures (ft ² /sec)	DELLP :	Thickness of lower plenum wall (ft)
ALPH	Heat transfer area of lower plenum wall (ft ²)	DELLS :	Thickness of loop seal wall (ft)
ALSH	Heat transfer area of loop seal wall (ft ²)	DELP :	Thickness of pump structures (ft)
ALTS	Thermal diffusivity of thermal shield (ft ² /sec)	DELT :	Time step for computation (sec)
APH	Heat transfer area of pump structures (ft ²)	DELTS :	Half the thickness of thermal shield (ft)
AQHPI	A constant to compute HPI flow (ft ³ /sec ²)	DI :	Diameter of injector (ft)
ATSH :	Heat transfer area of thermal shield (ft ²)	DPOS(I) :	Number of diameters below cold leg centerline at which downcomer temperatures are to be evaluated
BCLD	Length of cold leg, downstream of injection point (ft)	DTIMPR :	Incremental print time step (sec)
BCLU	Length of cold leg, upstream of injection point (ft)	HCB :	Heat transfer coefficient of core barrel (Btu/ft ² -sec-°F)
BETA :	Under relaxation coefficient	HCL	Cold leg heat transfer coefficient (Btu/ft ² -sec-°F)
		HDC :	Downcomer heat transfer coefficient (Btu/ft ² -sec-°F)
		HLP	Lower plenum heat transfer coefficient (Btu/ft ² -sec-°F)
		HLS :	Loop seal heat transfer coefficient (Btu/ft ² -sec-°F)

HO :	Heat transfer coefficient to surrounding air (Btu/ft ² -sec-°F)	INOP :	Option for providing input data on high pressure injection flow (QHPI) and loop flow (QL).
HP :	Pump heat transfer coefficient (Btu/ft ² -sec-°F)	INOP = 0:	REMIX97 Code uses a constant loop flow, QL, and the following linear equation for calculating QHPI: QHPI = A HPI * TIME + B HPI Where the values for constants AHPI, BHPI, and QL are specified in the Input Data file. For this input option the code also uses constant values for HPI flow temperature (THPI) and loop flow temperature (TL)
ICASE:	Case option for various calculations performed by the code:	INOP = 1:	REMIX97 Code uses time dependent input data for loop flow rate (QL), loop flow temperature (TL), HPI flow (QHPI), and HPI flow temperature (THPI). These data should be provided by two separate input data files QL.DAT , and QHPI.DAT . QL.DAT should contain data on time, QL and TL. QHPI.DAT should contain data on time, QHPI, and THPI.
ICASE = 1:	REMIX97 Code predicts the thermally induced stratification and mixing associated with High Pressure safety Injection (HPI) into the cold legs of a Pressurized Water Reactor (PWR).		
ICASE = 2:	This case is intended for predicting solute-induced stratification and mixing without thermal effects as found in Purdue 1/2 scale experiments.		
ICASE = 3:	This case is intended for predicting solute-induced stratification and mixing with thermal effects as found in several experimental simulations such as CREARE 1/5 Scale.		
IDCCB:	Number of material layers in core barrel.	INOPH :	Option for providing input data on heat transfer coefficients, HCL, HDC, HLP, HP, HLS, HCB and HO.
IDCCL:	Number of material layers in the cold leg wall.	INOPH = 0:	REMIX97 Code uses a constant values for the heat transfer coefficients, specified in the Input Data file.
IDCDC:	Number of material layers in the downcomer wall.	INOPH = 1:	REMIX97 Code uses time dependent input data for the heat transfer coefficients. These data should be provided by a separate input data files HT.DAT , containing data on time and heat transfer coefficients, HCL, HDC, HLP, HP, HLS, HCB and HO.
IDCLP:	Number of material layers in the lower plenum wall.		
IDCLS:	Number of material layers in the loop seal wall.		
IDCP :	Number of material layers in the pump wall.		
IDCTS:	Number of material layers in the thermal shield.		

Appendix A

IQE	Option for internal code calculation of entrainment at the point of HPI injection.	THPI :	Temperature of injected stream ($^{\circ}\text{F}$)
IQE = 0	The code uses an entrainment correlation internally	THSO :	Initial temperature of structures ($^{\circ}\text{F}$)
IQE = 1	The code uses maximum entrainment (flooding criteria) internally	TIMPR:	First time to print downcomer temperatures (sec)
M :	Total number of nodes including cladding and insulation	TIN :	Initial starting time for analysis (sec)
MKS :	Option of unit systems for output printout	TINS :	Insulation thickness
MKS = 0	The output is printed in British units	TL :	Temperature of loop flow ($^{\circ}\text{F}$)
MKS = 1	The output is printed in SI units	TMAX:	Total time for the analysis (sec)
MP2 :	Number of nodes in slab2 (base material)	TMDO :	Initial fluid temperature of the downstream region ($^{\circ}\text{F}$)
MP3 :	Number of nodes in slab3 (insulation)	TMUO :	Initial fluid temperature of the upstream region ($^{\circ}\text{F}$)
NPOS :	Number of positions at which downcomer temperatures are to be evaluated	TO :	Outer wall air temperature ($^{\circ}\text{F}$)
QL :	Flow rate of the loop flow (ft^3 / sec)	VOLD :	Total fluid volume of the downstream system participating in mixing
RATIO:	Fraction of entrained flow coming from the downcomer side (If RATIO is less than one, then the code calculates its value internally)	VOLMD:	The fluid volume of the downstream system which is assumed to be well mixed
RHOI :	Density of injected stream ($\text{lb}/\text{ft}^{**3}$)	VOLMU:	The fluid volume of the upstream system which is assumed to be well mixed
RHOL :	Density of loop flow ($\text{lb}/\text{ft}^{**3}$)	VOLU :	Total fluid volume of the upstream system participating in mixing
RHOMDO :	Initial fluid density of the downstream region ($\text{lb}/\text{ft}^{**3}$)	WDC :	Width of downcomer (ft)
RHOMUO :	Initial fluid density of the upstream region ($\text{lb}/\text{ft}^{**3}$)		
SIANG:	Injection angle (degree)		

A sample input listing is shown in Table A.1. This particular case corresponds to a REMIX97 calculation for the CREARE 1/5 scale test No. 100 discussed in the result section of the present report (refer to section 5) It should be noted that the first line of input is reserved for the title of the calculation.

A.5 Output

The code generates three output files: F01.DAT, F02.DAT and F03.DAT.

The short-format F01.DAT output file provides data on times and corresponding code calculated results for the following variables:

TC	:	Temperature of cold stream entering the downcomer
TMU		Mixed mean temperature of the upstream region
TMD		Mixed mean temperature of the downstream region
THU		Temperature of the hot stream in the cold leg, upstream of safety injection point
THD		Temperature of the hot stream in the cold leg, downstream of safety injection point
TM		Ambient temperature of the safety injection jet
DCU		Depth of the cold stream in the cold leg, upstream of the safety injection point
DCD		Depth of the cold stream in the cold leg, downstream of the safety injection point
FR HPI		Froud number of the safety injection jet

A sample short format output listing of F01.DAT file is presented in Table A.2. These results correspond to the input of Table A.1.

F02.DAT output file provides more details of the code calculated results including the temperature distribution in the downcomer and in the vessel wall. For a better quality assurance the input data used by the code is echoed in the F02.DAT output file. Table A.3 provides a sample listing of the F02.DAT output file.

F03.DAT output file provides data on times and corresponding downcomer temperatures to be used for plotting purposes. A sample listing of the F03.DAT output file is presented in Table A.4.

Appendix A

Table A.1 Sample input listing with CREARE 1/5 scale test No. 100 as reference

```
THIS IS A SAMPLE PROBLEM (TEST 100) WITH CREARE 1/5 SCALE FACILITY AS REFERENCE
UNITS OPTION
MKS= 0
CASE OPTION
ICASE= 3
INPUT DATA OPTION
INOP= 0
HEAT TRANSFER INPUT OPTION
INOPH= 0
ENTRAINMENT CALCULATION OPTION
IQE= 0
INJECTION ANGLE DEGREE
SIANG= 60.0
INITIAL TEMPERATURE (DEG. F)
THSO= 150.20
THPI= 69.50
TL= 150.20
TMDO= 150.20
TMUO= 150.20
RHOI= 72.630
RHOL= 60.960
RHOMDO= 60.960
RHOMUO= 60.960
TO= 80.0
INITIAL FLOW RATE (FT**3/SEC)
QL= 0.0
AQHPI= 0.0
BQHPI= 0.0135
MIXING VOLUME (FT**3)
VOLU= 2.18
VOLD= 2.76
VOLMU= 1.29
VOLMD= 2.09
DIAMETER, LENGTH & WIDTH (FT)
DI= 0.167
DCL= 0.47
BCLU= 2.22
BCLD= 2.96
WDC= 0.15
THICKNESS OF CORRESPONDING WALLS (FT)
DELCL= 0.04
DELDC= 0.06
DELTS= 0.02
DELLP= 0.04
DELP= 0.04
DELLS= 0.04
DELCB= 0.04
DDCC= 0.02
TINS= 0.330
```

Table A.1 Sample input listing with CREARE 1/5 scale test No. 100 as reference (Cont'd)

```

HEAT TRANSFER AREA OF CORRESPONDING WALLS (FT**2)
ACLHU= 5.53
ACLHD= 4.37
ADCH= 16.5
ATSH= 12.238
ALPH= 8.47
APH= 0.
ALSH= 5.9
ACBH= 0.
THERMAL DIFFUSIVITY OF CORRESPONDING WALLS (FT**2/SEC)
ALCL= 0.13E-05
ALDC= 0.13E-05
ALTS= 0.13E-05
ALLP= 0.13E-05
ALP= 0.13E-05
ALLS= 0.13E-05
ALCB= 0.13E-05
ALDCC= 0.13E-05
ALFINS= 0.311E-05
THERMAL CONDUCTIVITY OF CORRESPONDING WALLS (BTU/FT/SEC/F)
AKCL= 0.34E-04
AKDC= 0.34E-04
AKTS= 0.34E-04
AKLP= 0.34E-04
AKP= 0.34E-04
AKLS= 0.34E-04
AKCB= 0.34E-04
AKDCC= 0.34E-04
AKINS= 0.747E-05
HEAT TRANSFER COEFFICIENT OF CORRESPONDING WALLS (BTU/FT**2/SEC/F)
HCL= 0.14
HDC= 0.14
HLP= 0.14
HP= 0.14
HLS= 0.14
HCB= 0.14
HO= 0.55E-03
NUMBER OF NODES
M= 51
MP2= 5
MP3= 5
IDCCL= 1
IDCDC= 1
IDCTS= 1
IDCLP= 1
IDCP= 1
IDCLS= 1
IDCCB= 1

```

Appendix A

Table A.1 Sample input listing with CREARE 1/5 scale test No. 100. as reference (Cont'd)

COMPUTATIONAL PARAMETERS

TIN=	0.0
TMAX=	1800.0
DELT=	50.
TIMPR=	500.
DTIMPR=	500.
RATIO=	0.5
BETA=	0.5
NPOS=	7
I	DPOS (I)
1	0.
2	2.0
3	3.0
4	4.0
5	5.0
6	6.0
7	6.866

Table A.2 Sample short format output listing of F01.DAT file

THIS IS A SAMPLE PROBLEM (TEST 100) WITH CREARE 1/5 SCALE FACILITY AS REFERENCE

TIME	TC	TMU	TMD	THU	THD	TM	DCU	DCD	FR HPI
50.000	119.299	144.743	142.015	146.362	147.141	146.727	.100	.147	.684
100.000	114.040	139.378	134.628	141.005	139.695	140.415	.100	.152	.725
150.000	109.376	134.195	127.971	135.821	132.894	134.512	.101	.157	.767
200.000	105.189	129.230	122.001	130.841	126.780	129.050	.101	.161	.811
250.000	101.449	124.524	116.656	126.109	121.266	123.995	.102	.166	.857
300.000	98.108	120.099	111.876	121.645	116.307	119.335	.103	.171	.905
350.000	95.131	115.966	107.611	117.464	111.859	115.058	.104	.175	.955
400.000	92.479	112.128	103.800	113.572	107.869	111.143	.105	.180	1.007
450.000	90.117	108.587	100.396	109.972	104.284	107.574	.106	.184	1.062
500.000	88.011	105.325	97.354	106.656	101.063	104.317	.107	.189	1.119
550.000	86.132	102.331	94.634	103.602	98.172	101.348	.108	.193	1.178
600.000	84.456	99.588	92.200	100.798	95.574	98.648	.109	.198	1.240
650.000	82.959	97.079	90.021	98.230	93.239	96.194	.110	.202	1.304
700.000	81.623	94.788	88.067	95.881	91.135	93.962	.111	.207	1.371
750.000	80.430	92.698	86.316	93.734	89.241	91.934	.112	.211	1.441
800.000	79.361	90.791	84.744	91.773	87.536	90.092	.113	.216	1.513
850.000	78.405	89.053	83.331	89.984	85.998	88.418	.115	.220	1.588
900.000	77.549	87.468	82.061	88.350	84.608	86.895	.116	.225	1.666
950.000	76.816	86.027	80.927	86.861	83.355	85.515	.117	.230	1.742
1000.000	76.126	84.713	79.904	85.502	82.229	84.260	.118	.234	1.825
1050.000	75.506	83.514	78.980	84.261	81.208	83.116	.119	.239	1.911
1100.000	74.949	82.419	78.145	83.127	80.281	82.072	.120	.244	2.000
1150.000	74.448	81.419	77.391	82.089	79.441	81.121	.121	.249	2.092
1200.000	73.997	80.505	76.708	81.140	78.677	80.252	.123	.253	2.187
1250.000	73.590	79.669	76.091	80.271	77.982	79.457	.124	.258	2.285
1300.000	73.224	78.905	75.532	79.475	77.340	78.723	.125	.263	2.386
1350.000	72.890	78.204	75.024	78.745	76.769	78.060	.126	.268	2.489
1400.000	72.591	77.562	74.564	78.075	76.247	77.452	.127	.273	2.596
1450.000	72.318	76.975	74.145	77.451	75.773	76.890	.128	.279	2.705
1500.000	72.074	76.436	73.765	76.888	75.340	76.380	.130	.284	2.818
1550.000	71.853	75.941	73.420	76.371	74.944	75.912	.131	.289	2.934
1600.000	71.652	75.486	73.106	75.895	74.582	75.481	.132	.295	3.053
1650.000	71.470	75.067	72.820	75.456	74.254	75.086	.133	.300	3.176
1700.000	71.305	74.682	72.560	75.052	73.954	74.722	.134	.306	3.301
1750.000	71.155	74.327	72.322	74.679	73.680	74.387	.135	.312	3.430
1800.000	71.018	74.000	72.106	74.336	73.432	74.078	.137	.318	3.561

Appendix A

Table A.3 Sample listing of the F02.DAT output file

RUN CONDITIONS

THIS IS A SAMPLE PROBLEM (TEST 100) WITH CREARE 1/5 SCALE FACILITY AS REFERENCE

MKS = 0 PRINT RESULTS IN BRITISH UNITS
ICASE = 3 SALT-THERMAL CASE
INOP = 0 USE CONSTANT INPUT
INOPH = 0 USE CONSTANT INPUT FOR HEAT TRANSFER COEFFICIENTS
IQE = 0 USE ENTRAINMENT CORRELATION ALWAYS
INJECTION ANGLE = 60.00
THSO = 150.20 THPI = 69.50
RHOL = 60.96 RHOT = 72.63
TMDO = 150.20 TMUO = 150.20
RHOMDO = 60.96 RHOMUO = 60.96
AQHPI = .00E+00 BQHPI = .14E-01

DIMENSIONS FOR MIXING COMPUTATIONS

VOL = 4.94 VOLM = 3.38
DI = .167 DCL = .470 BCL = 5.180 WDC = .150

COMPUTATIONAL PARAMETERS

TIN = .00 TMAX = 1800.00 DELT = 50.00
TIMPR = 500.00 DTIMPR = 500.00
RATIO = .50 BETA = .50

DIMENSIONS AND PROPERTIES FOR HEAT TRANSFER

DELCL = .40E-01 DELDC = .60E-01 DELTS = .20E-01 DELLP = .40E-01
DELP = .40E-01 DELLS = .40E-01 DELCB = .40E-01 DDCC = .20E-01
ACLH = 9.900 ADCH = 16.500 ATSH = 12.238 ALPH = 8.470
APH = .000 ALSH = 5.900 ACBH = .000
ALCL = .13E-05 ALDC = .13E-05 ALTS = .13E-05 ALLP = .13E-05
ALP = .13E-05 ALLS = .13E-05 ALCB = .13E-05 ALDCC = .13E-05
AKCL = .34E-04 AKDC = .34E-04 AKTS = .34E-04 AKLP = .34E-04
AKP = .34E-04 AKLS = .34E-04 AKCB = .34E-04 AKDCC = .34E-04
HCL = .14E+00 HDC = .14E+00 HLP = .14E+00 HP = .14E+00
HLS = .14E+00 HCB = .14E+00 HO = .55E-03 TO = 80.00

Table A.3 Sample listing of the F02.DAT output file (Cont'd)

NODES AND CLAD PARAMETERS

M = 51 MP2 = 5 MP3 = 5

IDCCL = 1 IDCDC = 1 IDCTS = 1 IDCLP = 1
IDCP = 1 IDCLS = 1 IDCCB = 1

TINS = .3300 AKINS =.747E-05 ALFINS =.311E-05

NPOS = 7

DPOS = .00

DPOS = 2.00

DPOS = 3.00

DPOS = 4.00

DPOS = 5.00

DPOS = 6.00

DPOS = 6.87

Appendix A

Table A.3 Sample listing of the F02.DAT output file (Cont'd)

TIME	TC	TMU	TMD	THU	THD	T JUMP	DCU	DCD	FR HPI
50.000	119.299	144.743	142.015	146.362	147.142	131.550	.100	.147	.684
100.000	114.040	139.378	134.628	141.005	139.695	125.328	.100	.152	.725
150.000	109.376	134.195	127.971	135.821	132.894	119.724	.101	.157	.767
200.000	105.189	129.230	122.001	130.841	126.780	114.689	.101	.161	.811
250.000	101.449	124.524	116.656	126.109	121.266	110.168	.102	.166	.857
300.000	98.108	120.099	111.876	121.645	116.307	106.116	.103	.171	.905
350.000	95.131	115.966	107.611	117.464	111.859	102.491	.104	.175	.955
400.000	92.479	112.128	103.800	113.572	107.869	99.250	.105	.180	1.007
450.000	90.117	108.587	100.396	109.972	104.284	96.350	.106	.184	1.062
500.000	88.011	105.325	97.354	106.656	101.063	93.754	.107	.189	1.119

CENTERLINE TEMPERATURES AT DOWNCOMER LOCATIONS

TIME = 500.000

HEIGHT FROM CL CENTER TEMPERATURE

.000	88.011
.940	93.754
1.410	94.235
1.880	94.714
2.350	95.194
2.820	95.431
3.227	95.636

DIMENSIONLESS THICKNESS TEMPERATURE

.000	100.848
.100	110.839
.200	118.893
.300	125.046
.400	129.395
.500	132.064
.600	133.192
.700	132.907
.800	131.332
.900	128.576
1.000	124.740

Table A.3 Sample listing of the F02.DAT output file (Cont'd)

TIME	TC	TMU	TMD	THU	THD	T JUMP	DCU	DCD	FR HPI
550.000	86.132	102.331	94.634	103.602	98.172	91.430	.108	.193	1.178
600.000	84.456	99.588	92.200	100.798	95.574	89.348	.109	.198	1.240
650.000	82.959	97.079	90.021	98.230	93.239	87.482	.110	.202	1.304
700.000	81.623	94.788	88.067	95.881	91.135	85.808	.111	.207	1.371
750.000	80.430	92.698	86.316	93.734	89.241	84.307	.112	.211	1.441
800.000	79.361	90.791	84.744	91.773	87.536	82.958	.113	.216	1.513
850.000	78.405	89.053	83.331	89.984	85.998	81.746	.115	.220	1.588
900.000	77.549	87.468	82.061	88.350	84.608	80.655	.116	.225	1.666
950.000	76.816	86.027	80.927	86.861	83.355	79.693	.117	.230	1.742
1000.000	76.126	84.713	79.904	85.502	82.229	78.811	.118	.234	1.825

CENTERLINE TEMPERATURES AT DOWNCOMER LOCATIONS

TIME = 1000.000

HEIGHT FROM CL CENTER TEMPERATURE

.000	76.126
.940	78.811
1.410	78.957
1.880	79.103
2.350	79.248
2.820	79.320
3.227	79.382

DIMENSIONLESS THICKNESS TEMPERATURE

.000	81.232
.100	88.366
.200	94.689
.300	100.064
.400	104.395
.500	107.621
.600	109.716
.700	110.683
.800	110.550
.900	109.364
1.000	107.191

Appendix A

Table A.3 Sample listing of the F02.DAT output file (Cont'd)

TIME	TC	TMU	TMD	THU	THD	T JUMP	DCU	DCD	FR HPI
1050.000	75.506	83.514	78.980	84.261	81.208	78.015	.119	.239	1.911
1100.000	74.949	82.419	78.145	83.127	80.281	77.295	.120	.244	2.000
1150.000	74.448	81.419	77.391	82.089	79.441	76.645	.121	.249	2.092
1200.000	73.997	80.505	76.708	81.140	78.677	76.056	.123	.253	2.187
1250.000	73.590	79.669	76.091	80.271	77.992	75.523	.124	.258	2.285
1300.000	73.224	78.905	75.532	79.475	77.340	75.035	.125	.263	2.386
1350.000	72.890	78.204	75.024	78.745	76.769	74.596	.126	.268	2.489
1400.000	72.591	77.562	74.564	78.075	76.247	74.200	.127	.273	2.596
1450.000	72.318	76.975	74.145	77.451	75.773	73.838	.128	.279	2.705
1500.000	72.074	76.436	73.765	76.888	75.340	73.511	.130	.284	2.818

CENTERLINE TEMPERATURES AT DOWNCOMER LOCATIONS

TIME = 1500.000

HEIGHT FROM CL CENTER TEMPERATURE

.000	72.074
.940	73.511
1.410	73.545
1.880	73.579
2.350	73.613
2.820	73.629
3.227	73.644

DIMENSIONLESS THICKNESS TEMPERATURE

.000	74.328
.100	78.764
.200	82.841
.300	86.450
.400	89.502
.500	91.927
.600	93.678
.700	94.727
.800	95.067
.900	94.714
1.000	93.699

Table A.3 Sample listing of the F02.DAT output file (Cont'd)

TIME	TC	TMU	TMD	THU	THD	T JUMP	DCU	DCD	FR HPI
1550.000	71.853	75.941	73.420	76.371	74.944	73.213	.131	.289	2.934
1600.000	71.652	75.486	73.106	75.895	74.582	72.941	.132	.295	3.053
1650.000	71.470	75.067	72.820	75.456	74.254	72.695	.133	.300	3.176
1700.000	71.305	74.682	72.560	75.052	73.954	72.470	.134	.306	3.301
1750.000	71.155	74.327	72.322	74.679	73.680	72.266	.135	.312	3.430
1800.000	71.018	74.000	72.106	74.336	73.432	72.080	.137	.318	3.561